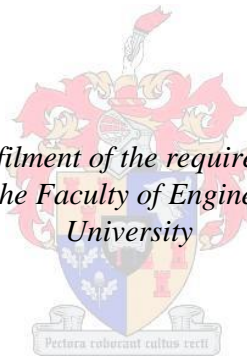


Inflatable weir hydraulics

by

Dayton Tagwi

*Thesis presented in fulfilment of the requirements for the degree of
MScEng (Water) in the Faculty of Engineering at Stellenbosch
University*



Supervisor: Prof. G.R. Basson

March 2015

DECLARATION

Herewith I declare that I know the meaning of plagiarism and that all the text, calculations, results, drawings, and graphs in this thesis are primarily my own work. All other work has been cited as appropriate in accordance with the prescribed referencing method.

Name: Dayton Tagwi

Signed:

Date: 2015 /02 / 05

SYNOPSIS

General objective of the study

This thesis aims to evaluate the hydraulics of an inflatable weir in its fully inflated position to the almost fully deflated position using different diameter circular weirs with varying discharges, by considering the change in the weir radius and the dynamic pressures on the weir. In the evaluation, three cylindrical weirs were installed in a 2m wide flume and tested over various discharges.

Methodology

The three weirs, one with a 300mm diameter, another with a 250mm diameter, and the last one with a 100mm diameter, were used to determine the effects of over flow water on the weir as seen in the different stages of the normal operation of an inflatable weir. Simulation involved measurement of the upstream and downstream water levels with the weir height involved at stable over flow conditions. Measurement of pressure variations was done on the weir faces with different water inflow rates to the test flume with three pressure sensors installed on each weir at 0° , 11.25° and 22.5° from the crest to the downstream. Additionally a single 0.15m radius weir was tested for pressures 67.5° , 78.75° and 90° from weir crest. Water level variation on the downstream of the weir was created by means of a variable tail gate to observe its effects.

Results of the investigation

The effects of upstream arches, stage, radius of curvature, discharge, pressure, energy losses over the weir and the downstream hydraulic jump were investigated in the inflation and deflation of the inflatable weir. The findings were as follows:

- Based on literature by Chanson and Montes (1998), Shabanlou et al. (2013), Schmocker et al. (2011) and Bahzad et al. (2010), upstream arches have insignificant influence on the performance of the inflatable weir. There is rather reduced afflux due to the shape of the upstream of the weir from the Bernoulli's equation. This shape of the upstream of the weir also contributes to the transport of sediments Gebhardt et al. (2012).
- Investigation of the discharge coefficient and factors influencing showed that:

-
- As the weir radius is reduced during the deflation, the unit discharge over each weir increased with increase in head above the crest.
 - Discharge coefficient of the inflatable weir increases with the increase in head above weir crest, and the discharge coefficient is inversely proportional to the radius of curvature of the weir.

 - Investigation of pressures on the downstream face of the weir models showed that:
 - The negative (suction) pressure acting on the downstream face of the weir becomes increasingly negative with increase in H/R values.
 - Point of separation of nappe was seen with pulsations of pressure of the record pressure.

Generally, energy dissipation over the weir decreases with the decrease in the weir radius and the jump is more stable with the smallest circular weir and can be more accurately determined in the case of a small weir.

Conclusions and Recommendations

The inflatable weir has a high discharge at its fully inflated position. Its hydraulic performance is largely influenced by inflow head and is inversely proportional to the radius of curvature. Nappe pulsation as seen in the nappe vibrations can cause the vibration of weir.

Future research on inflatable weirs should aim to monitor the negative pressure on measuring pressures further down the face of the weir because larger negative pressures are expected to develop after 90° as with this study.

LIST OF ABBREVIATIONS

U.S.	University of Stellenbosch
WSD	Water Supplies Department of Hong Kong

NOMENCLATURE

b_c	effective width of the weir
C_d	discharge coefficient
D	the drop height or the weir height
d_{crest}	flow depth at crest
d_c	critical flow depth
d_{crest}/d_c	dimensionless flow depth at crest
E	the specific energy
E/R	relative head
F_r	Froude number
g	acceleration due to gravity
H_0	total energy head for free surface streamline
H_1	upstream total head
H_w	total energy head for a free surface streamline
R	circular weir radius
H_w/R	dimensionless upstream head on crest
L_j	length of the jump
L_d	length of the drop
q	discharge per unit width of weir
V	velocity of the free surface streamline
y	flow depth
y_1	flow depth just downstream of weir

y_2	sequent jump flow depth
y_c	critical flow depth
Z	effective step height

ACKNOWLEDGEMENTS

“For it is not by might nor by power but by the Spirit” (Zechariah 4:6).

Special thanks go to all the University staff who supported and supplied the material for the construction of the circular weirs and the testing of the weir models.

I would also like to express my sincere gratitude to my dedicated supervisor, Professor G.R. Basson, for his support and guidance.

I would like to appreciate and thank my wife for her perseverance and faith.

I would like to thank the guardian angel sent from above, all Glory and Honour to GOD.

TABLE OF CONTENTS

DECLARATION	i
SYNOPSIS	ii
LIST OF ABBREVIATIONS	iv
NOMENCLATURE	v
ACKNOWLEDGEMENTS	vii
TABLE OF CONTENTS	viii
LIST OF FIGURES	xi
LIST OF TABLES	xiv
CHAPTER 1: INTRODUCTION	1
1.1 Background	1
1.1.1 Use of inflatable weirs	2
1.1.2 Disadvantages of weirs in the river systems	3
1.1.3 Conditions to which an inflatable weir in operation is subjected to.....	4
1.2 Problem statement	4
1.3 Justification of the study	5
1.4 Objectives of the study	5
1.4.1 Main objective	5
1.4.2 Specific objectives.....	5
CHAPTER 2: LITERATURE REVIEW	7
2.1 Background	7
2.2 Present day use of inflatable weirs	9
2.3 Operation of the inflatable weir	10
2.4 Hydraulic and structural performance of the inflatable weir	11
2.4.1 Variation of internal pressure and overflow.....	11
2.4.2 Vibrations and their effects on the water filled weir	13
2.4.3 Nappe aeration	17
2.5 Flow over circular a crested weir	20
2.5.1 Flow in open channels.....	21

2.5.2 Effect of upstream weir face on weir performance.....	24
2.5.3 Back water effects of weir	27
2.5.3 Discharge coefficient on circular crested weirs	29
2.5.4 Summary of C_d values of circular weirs from literature	46
2.5.4 Pressure distribution over weir	48
2.5.5 Flow depth at the crest and critical flow over weir.....	53
2.5.6 Energy loss over weir crest	57
2.5.7 Energy dissipation and jump length on the downstream of weir	58
CHAPTER 3: METHODOLOGY FOR EXPERIMENTAL STUDY	62
3.1 Introduction.....	62
3.2 Schematization of deflation stages of the inflatable weir	62
3.3 Experimental configuration and physical model construction	63
3.4 Instrumentation, data acquisition and analysis.....	69
3.4.1 Inflow measurement.....	69
3.4.2 Depth gauge measurements	70
3.4.3 Pressure measurement on weir model	71
3.4.4 Jump length	75
3.5 Accuracy of measurements during experiment	76
3.6 Effects of viscosity and surface tension and model scaling.....	78
CHAPTER 4: RESULTS AND DISCUSSION	81
4.1 Introduction.....	81
4.2 Stage-discharge relationships of the weir models	81
4.2.1 Relationship between unit discharge (q) and stage (H)	81
4.2.2 Relationship between coefficient of discharge, C_d with total head, H_w and radius of curvature, R	82
4.3 Pressure distribution over the weir.....	86
4.4 Crest depth and critical flow at crest	94
4.5 Energy dissipation over of weir	95
4.5 Energy dissipation downstream of weir.....	97
4.6 Hydraulic jump length	98

CHAPTER 5: CONCLUSIONS AND RECOMMENDATIONS	100
REFERENCE LIST	102
APPENDIX A: Over flow over weir models	I
APPENDIX B: Experimental data on discharge measurement.....	IV
APPENDIX C: Experimental data and literature studies on C_d.....	VII
APPENDIX D: Experimental data on pressures in meters.....	VIII
APPENDIX D: Real life inflatable weir	X

LIST OF FIGURES

Figure 1.1 Schematic diagram of an inflatable weir (Wittler JR, 2004).....	1
Figure 2.1 Increasing overflow head with constant internal pressure (Alhamati <i>et al</i> , 2005)	12
Figure 2.2 Increasing internal pressure with constant overflow head (Alhamati <i>et al</i> , 2005)	12
Figure 2.3 Flow over air-inflated weir (Alhamati <i>et al.</i> , 2005)	13
Figure 2.4 Serrations and deflectors on inflatable weir (Brussels, 2006)	14
Figure 2.5 Vibrations of the partly deflated dam type B and type C (Chervet, 1984).....	15
Figure 2.6 Vibration modes of weir (Chervet, 1984)	16
Figure 2.7 Wake regions downstream the deflated weir (Chervet, 1984).....	17
Figure 2.8 V-notch behavior of air filled weir partially filled (Alwan, 1979)	19
Figure 2.9 Circular face on downstream of inflatable weir (arcon-aquapro.com, 2013).....	19
Figure 2.10 Flow over circular crested weir (viewed from US Laboratory)	20
Figure 2.11 Flow transition in open channel (Chadwick, 2004).....	22
Figure 2.12 Variation of the discharge and specific energy with depth (Chadwick, 2004).....	23
Figure 2.13 Specific energy due to slope (Chanson, 2004)	23
Figure 2.14 Upstream arches at crest on a circular crested weir (Shabanlou, 2013)	24
Figure 2.16 Upstream crest arch effect on the head and velocity (Shabanlou, 2013)	25
Figure 2.17 Configuration of the flow geometry for free overflow (Schmocker <i>et al.</i> , 2011)	26
Figure 2.18 C_d (H_o/R) for $\alpha_o = 90^\circ$ with $\alpha_d = 20^\circ, 30^\circ, 45^\circ, 90^\circ$ and $\alpha_d = 90^\circ$ with $\alpha_o = 20^\circ, 30^\circ, 45^\circ, 90^\circ$ (Schmocker <i>et al.</i> , 2011).....	26
Figure 2.19 Different weir crests tested (Bahzad <i>et al.</i> , 2010)	27
Figure 2.20 Optimal upstream radius of curvature (Gebhardt <i>et a.l</i> , 2012)	28
Figure 2.21 Design chart for estimating afflux $\Delta y/y_2$ against y_2/w and Fr (Gebhardt <i>et al.</i> , 2012)	29
Figure 2.22 Definition of circular rounded weir by Bos (1987)	30
Figure 2.23 Circular crested weir discharge coefficient results Bos (1978).....	31
Figure 2.24 Overflow characteristics of circular weirs (Chanson <i>et al</i> , 1998).....	32
Figure 2.25 Fully and partially-developed inflow theoretical conditions on circular cylinders compared to the experimental results (Chanson <i>et al</i> , 1998).....	33
Figure 2.26 Circular cylinders compared to the experimental results (Chanson <i>et al.</i> , 1998).....	33
Figure 2.27 Comparison of present study to previous studies by Chanson <i>et al.</i> (1998).....	35
Figure 2.28 Over flow in the on circular weir (Chanson, 1997)	36
Figure 2.29 Flow past a circular crested weir assumed (Haghiabi, 2012)	37
Figure 2.30 Good agreement of the experimental results with empirical equation.	38
Figure 2.31 C_d against H_1/R (Heidarpour, 2010; 2013).....	39
Figure 2.32 Experimental configuration, water surface profile and discharge coefficient (Emad, 2011)	40
Figure 2.33 Cylindrical weir and circular crested weirs investigated (Shabanlou <i>et al.</i> , 2013)....	41
Figure 2.34 Variation of Cd with the ratio $H1R$ for cylindrical weirs and half-shaped cylindrical weirs respectively.....	42
Figure 2.35 Effect of height on weir discharge (Shabanlou <i>et al.</i> , 2013).....	43

Figure 2.36 C_d with the ratio H/D_h for study by Alhamati <i>et al.</i> (2005) and a comparison with the earlier studies (Alhamati <i>et al.</i> , 2005)	44
Figure 2.37 Experimental set up during investigation Abdul-latif <i>et al.</i> (2010).....	45
Figure 2.38 C_d against H/R (Abdul-latif <i>et al.</i> , 2010)	45
Figure 2.39 Summary of C_d values for rounded / circular crested weirs from literature.....	47
Figure 2.40 Convex flow pressure distributions (Abdul-latif <i>et al.</i> , 2010).....	48
Figure 2.41 Flow-net schematic diagram for weir (Abdul-latif <i>et al.</i> , 2010).....	49
Figure 2.42 Pressure distribution for a 1:1 sloping downstream face Bos (1978)	50
Figure 2.43 Decreasing ratio y against $P\gamma y$ (Haghiabi, 2012).....	51
Figure 2.44 Decreasing ratio y against $P\gamma y$ (Haghiabi, 2012).....	51
Figure 2.45 Over flow on the inflatable dam membrane (Chanson, 1997)	52
Figure 2.46 Pressure on the downstream face of weir from weir crest (Chanson, 1997)	53
Figure 2.47 Dimensionless flow depth at circular weir crest (Chanson, 1998)	54
Figure 2.48 Critical flow for curvilinear flows (Orgaz <i>et al.</i> , 2008)	55
Figure 2.49 Dimensionless critical weir depth (left Figure) and discharge at crest (right Figure) (Orgaz <i>et al.</i> , 2008)	56
Figure 2.50 Equivalent drop structure and the comparison to the circular weir (Chanson 1998).....	57
Figure 2.51 Energy loss over weir crest Chanson (1998)	58
Figure 2.52 Hydraulic jump definition (Chanson, 2004)	58
Figure 2.53 Cases of the formation of a hydraulic jump (Cruise, 2007)	59
Figure 2.54 L_j/y_2 against Froude number (Cruise, 2007)	59
Figure 3.1 Simulation of different stages of the inflatable weir (viewed from US laboratory)	63
Figure 3.2 Schematic set up of the whole system used for the experiments (viewed from US laboratory).....	64
Figure 3.3 Flume with weir and measuring apparatus (viewed from US laboratory)	65
Figure 3.4 Side view of flume (viewed from US laboratory)	66
Figure 3.5 Measuring equipment in the middle of the flume (viewed from US laboratory)	67
Figure 3.6 Submerged jumps at 53.028l/s (left) and 143.43l/s (right) (viewed from US laboratory)	68
Figure 3.7 Schematic section through weir during overflow (viewed from US laboratory)	68
Figure 3.8 SAFMAG electromagnetic flow meter.....	69
Figure 3.9 Depth gauge (viewed from US laboratory).....	70
Figure 3.10 Corrected depth (viewed from US laboratory)	71
Figure 3.11 Position of the pressure sensors on a quadrant downstream of the weir model during the test (viewed from US laboratory)	72
Figure 3.12 Zero flow measurement of pressure by the first three pressure sensors during test of the $R = 0.15\text{m}$ weir model (Viewed in US laboratory)	73
Figure 3.13 Pressure reading at $0.0236\text{ m}^3/\text{s}$ during test of the $R = 0.15\text{m}$ weir model (Viewed in US laboratory).....	73
Figure 3.14 Pressure at $0.039389\text{ m}^3/\text{s}$ during test of the $R = 0.15\text{m}$ weir model (Viewed in US laboratory).....	74
Figure 3.15 Measurement of the jump length (Viewed in US laboratory)	76
Figure 3.16 Accuracy versus precision (Rothman, 1998)	77
Figure 4.1 Relationship between unit discharge and stage	82

Figure 4.2 Relationship between C_d with H_w/R	83
Figure 4.3 Relationship between C_d with H_w/R for the measured results and literature studies.....	85
Figure 4.4 Pressures on surface of weir 1: R 0.15m.....	86
Figure 4.5 Pressures on surface of weir 2: R 0.125m.....	87
Figure 4.6 Pressures on surface of weir 3: R 0.05m.....	87
Figure 4.7 Pressures on surface of weir 1: R 0.15m.....	88
Figure 4.8 Measured average pressure against angle from weir crest for the R = 0.15m weir at 0 °, 11.25° and 22.5° for different flows.....	89
Figure 4.9 Measured average pressure against angle from weir crest for the R = 0.125m weir at 0 °, 11.25° and 22.5° for different flows.....	89
Figure 4.10 Measured average pressure against angle from weir crest for the R = 0.05m weir at 0 °, 11.25° and 22.5° for different flows.....	90
Figure 4.11 Pressure against angle for the R = 0.15 weir at different flows for the lower three pressure sensors after turning the R = 0.15m model.....	90
Figure 4.12 Comparison of Chanson (1997) motion equation and the first pressures at 0 °, 11.25° and 22.5° on the R=0.15m	91
Figure 4.13 Comparison of Chanson (1997) motion equation and the first pressures at 0 °, 11.25° and 22.5° on the R=0.125m	92
Figure 4.14 Comparison of Chanson (1997) motion equation and the first pressures at 0 °, 11.25° and 22.5° on the R=0.05m	92
Figure 4.15 Comparison of Chanson (1997) motion equation and the experimental data after turning the R = 0.15m model.....	93
Figure 4.16 d_{crest}/d_c against H_w/R , a measure of discharge	94
Figure 4.17 d_{crest} against q , a measure of discharge.....	95
Figure 4.18 Energy line over weir and hydraulic jump (Viewed in the US laboratory)	96
Figure 4.19 $\Delta H/H_1$ versus H_w/R a, measure of energy loss over weir	96
Figure 4.20 $\Delta H/d_{crest}$ versus, a measure of energy loss over weir.....	97
Figure 4.21 Variation of energy dissipation	98
Figure 4.22 Relationship between L_j/Y_2 and Froude number	99

LIST OF TABLES

Table 2.1 Empirical of discharge coefficients formulae for circular-crested weirs (Chanson, 1998)	34
Table 2.2 Concepts for curvilinear flow over rounded crest weirs	56
Table 2.3 Types of Hydraulic Jumps (Finnemore, 2002)	60
Table 5.1 Range of pressure measured from weir face during experiments on weir models ...	101
Table 5.2 Range of pressure weir face on a prototype weir 3m high	101

CHAPTER 1: INTRODUCTION

This chapter highlights the research area of interest, the main objectives and specific objectives of the study. The basic need for the research undertaken is also highlighted.

1.1 Background

Diverse hydraulic structures have been built for the flow of water in river channels. These include rubber dams often called inflatable weirs, which were developed and put to use in the 1950s. The first inflatable weir was built in Los Angeles River, California for flood mitigation (Plaut *et al.*, 1998). Technological improvement of the structure has always been continuous. The simplicity of the inflatable weir concept is largely due to the ease of placement and its flexibility. A unique characteristic of the inflatable weir, as investigated in this study, is its ability to adjust weir height, offering a control system which meets different needs. For example, during flood conditions, it could either be in the fully inflated or deflated position. This offers protection to the weir during floods while reducing damming and allowing sediment removal from the dam basin. The hydraulic structure can be inflated with air or water as seen in Figure 1.1. This Figure shows the inflatable weir with fins for aeration of the nappe in the inflated and deflated positions.

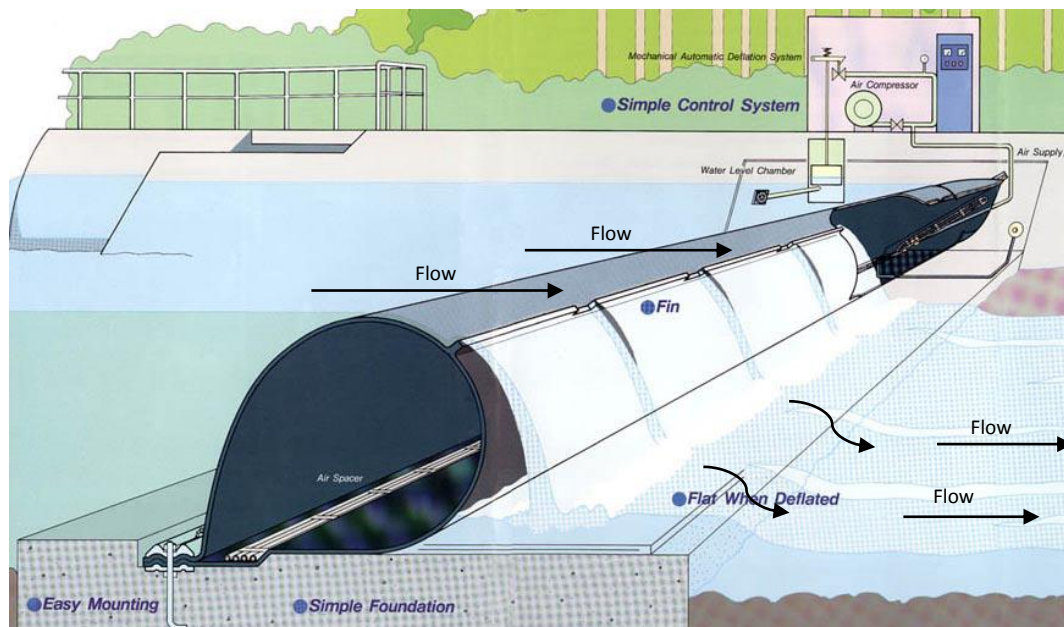


Figure 1.1 Schematic diagram of an inflatable weir (Wittler JR, 2004)

The inflatable weir, sometimes called a rubber dam or fabridam that spans the whole river width. The inflatable weir often comprises of a rubber mounted on a concrete sill with plates, bolts and nuts embedded in the concrete floor, as shown in Figure 1.1. This configuration facilitates the sealing of air and/or water in the dam body for operation of the inflatable weir (Tam, 1994). When installing a weir or rubber dam on an existing concrete dam wall crest, a light foundation of 100mm to 150mm is often required to enable a firm anchoring of the weir. This is much simpler in contrast to the use of steel gates on an existing concrete dam wall crest wherein a 500mm to 800mm foundation is needed (Bridgestone, 1997a).

1.1.1 Use of inflatable weirs

In some instances the inflatable weir is used for controlling flood waters and raising the height of existing spillways, while allowing some water to flow over the top of the dam and to continue downstream. In other applications, inflatable weirs are used as tidal barriers to protect rivers from salt contamination, to prevent beach erosion and also to divert water in order to form brine lakes and to prevent chloride pollution or chemical dispersion downstream of water courses. Inflatable weirs are also used for storing additional water for supply needs, power generation, diversion of the upstream water, impounding water for recreation and even groundwater recharge.

In agriculture, weirs are largely used for creating additional storage of water and diversion of water into an irrigation canal. In some cases, it is used to raise river water levels, in order to reduce the available net positive suction head of river abstraction pumps used for irrigation purposes. Abstracting water for irrigation from rivers is often difficult because of the high alluvial and, at times, low water levels in the river. From the above described applications, it is evident that the inflatable type weir has a relative wide application in rivers. Due to the need of water storage, weirs have been put in place in river channels. As the weir blocks the river course, water rises, forming a storage point. With this storage, enough abstraction of the water resource is made available for agriculture. Despite the achievement made due to such an intervention, the water course is also affected. Flowing water is retarded and this has an impact on the environment and river flow patterns.

1.1.2 Disadvantages of weirs in the river systems

Agricultural weirs have been built, mainly, to provide irrigation water. However, due to erosion, coupled with various land uses, many weirs have been rendered obsolete. The resultant low flow velocities and low vortices by the weir in a river regime are, however, ideal at pump intakes. However, they also tend to cause accumulation of sediments and suspended loads, and this stops them passing down the river. Despite the abstraction process by pumps, sediments can continue to be deposited on the pump suction side before they are drawn in by pumps. This is undesirable in normal pumping.

Sediments are capable of causing much damage to pumps due to abrasion resulting from high suction velocities involved in pumping. Loss of habitat due to salt accumulation also eliminates plant species along with silt deposits from upstream. In a single flood event, small intakes have been seen to be about 80% covered with sediments in rivers as compared to the rivers without weirs. Gravel and sometimes cobbles were observed to be transported in a similar fashion, thus forming the root cause of sedimentation (Rooseboom, 2011).

Damage to the dam body is also caused by vandalism (puncturing and cutting) of the weir by people (Tam, 1997). With the overflow water on the weir, it often appears relatively calm, but overflow water in weirs can be dangerous places for boating, swimming or wading. These are capable of submerging a person indefinitely, posing a risk. This phenomenon is described as the white-water effect.

Cleaning and desilting of weirs are necessary as this maintains the original storage capacity of water by the weir (dam membrane), as well as cleans the intake or diversion area. This promotes a much cleaner intake of water by pumps, thus reducing the chances of damage to the pumps. Surveys conducted on weirs show that many agricultural weirs need to be replaced (Charles *et al.*, 2004). Unless large gates are provided on permanent weirs, concentration of pollutants and a large proportion of the original depth and storage capacity of weirs are likely to be lost. With the introduction of the inflatable weir, low flow velocity water can be directed to intakes. This can also provide the necessary head required to flush and scour sediments, pollutants and debris from the weir storage.

1.1.3 Conditions to which an inflatable weir in operation is subjected to

While in operation, inflatable weirs, inevitably, experience some damage as a result of the flowing water and suspended materials. In the process of flushing, sand tends to pile up on the weir when it lies flat, but partial inflation is normally done so as to stop the weir from being completely buried by the sand, which would make it difficult to inflate. Abrasion of the weir also takes place but is minimal because the inflatable weir is made of abrasion resistant material, such as Linatex rubber.

Vibrations of the inflatable weir structure have also been noted to be one of the causes of abrasion, which could cause leaks on the dam body (Gebhardt, 2006). The various practical problems encountered in the operation of inflatable weirs require information about the upstream, over-flow and downstream flow conditions, in order to achieve the best operation practice. A practical understanding is often necessary for the ideal operation of air and/or water-filled inflatable weirs.

1.2 Problem statement

Concrete weirs have been in place in river systems for some time. They, however, could pose some challenges in the river systems as they could impede the flow in the river channel, causing the settling of sediments in the weir basin and debris collection upstream of the weir. This normally results in the alteration of the bed slope and, at times, a change in the river course, which could also have a detrimental impact on the ecology at large with stagnated waters.

Permanent weirs also give rise to the problem of eutrophication as a result of collection of the runoff water with little flushing at the point of the weir. At times, the river course is altered, thus, affecting the immediate land use that is nearby or next to the river. With permanent weirs, periodic cleaning of the weir basin is often employed. This is costly and may disturb the uptake of river water for its proposed use.

In an effort to eliminate these problems encountered with fixed weirs, gates have been used but are however expensive to construct and to maintain. The introduction of the inflatable weir has been considered for eliminating the problems encountered with fixed weirs and gates. However, managing the rise and fall of the inflatable type weir to create flushing of sediments and

debris/scum from the weir basin at the appropriate times while maintaining its usual function of retaining/diverting the required water for use, is critical. Flushing, though, has the effect of releasing large volumes of sediments at once and consideration of the seasons for spawning and emerging of juvenile fish should be taken into account to reduce potential sediment pollution downstream of the weir.

1.3 Justification of the study

Though vandalism (puncturing and cutting) is possible with air-filled and or water-filled weirs, there is an increasing interest in their use because of the ease of placement and the relatively stable overflow. In the case of a permanent weir, the weir becomes relatively unstable at high overflow due to the fixed weir height. In the case of an inflatable weir, deflation and inflation of the structure can be done to compensate for the corresponding stage fluctuations. Managing the rise and fall of the weir at the appropriate time, allows flushing of sediments and scum, creating a clean river system, as well as retaining the required water for use. It is, therefore, important to examine the dynamic behaviour and stability of an inflatable weir under different overflow conditions, in relation to the rise and fall of the water levels during operation. Much of the research on inflatable weirs has been restricted to cases with no overflow and, in most cases, attention has been focused on the equilibrium shape of the dam body and the vibrations or dynamic response.

1.4 Objectives of the study

1.4.1 Main objective

To evaluate the performance of an inflatable weir in its normal operation using circular weir models.

1.4.2 Specific objectives

Evaluation of the inflatable weir constituted assessment of parameters within the region before the weir, over the weir and downstream of the weir model. These include:

- ❖ Assessment of the upstream conditions that influencing the performance of the weir;
- ❖ Investigation of the discharge coefficient and factors influencing it;
- ❖ Investigation of pressures on the downstream face of the weir models and;

- ❖ Investigation of energy dissipation over the weir and characteristics of the downstream hydraulic jump.

CHAPTER 2: LITERATURE REVIEW

This chapter presents information from literature which is relevant to the focus area of this study. It gives some background on inflatable weirs and its physical operation and performance. Subsequently relevant research information from literature on inflatable, circular crested and cylindrical weirs are presented. The relevant research information include discharge coefficients, pressure on the weir faces, energy dissipation over the weir and the hydraulic characteristics of the downstream hydraulic jump.

2.1 Background

Many rivers transport organic and inorganic matter resulting from erosion in distant and nearby catchments along the river course. The organic and inorganic matter being transported include materials such as agricultural waste, decaying vegetative matter and sediments. These form a principal source of constituents and are often carried by traction, saltation, suspension and solution in the river regime. Rivers have been, at times, used for the refuse by poultry and pig breeders, and the pollutants in solution, submerged or in suspension are often eyesores when they collect at weirs. This animal waste gathered at the weir is often unhygienic (Tam, 1997). Permanent weirs also act as effective sediment traps when put in high alluvial rivers, promoting the accumulation of sand. If sediments are allowed to accumulate behind the weir, the depth of the pool/storage is likely to decrease and the available freeboard would also be reduced (Stuart, 2012).

Weirs, though, still remain a necessity when water is needed mainly for agricultural purposes. Inflatable weirs do not only serve to direct low flows towards intakes, but they also provide the necessary head required to flush and scour sediments from the intake area and from the general reserve retained by the dam body. Adoption of the inflatable weir in Hong Kong, China, led to the removal of obsolete weirs. Some were replaced with a more effective and better designed weir and, in some cases, inflatable weirs. (Tam, 1994).

The design of inflatable weirs can be very simple. It does not include any mechanical moving parts (hinges, bearings) as in the case of flap gates. There are no problems owing to corrosion and rusting noted in the use of inflatable weirs. Painting and the use of lubricants are not needed as these could be harmful to the nearby environment. Inflatable weirs also have an

additional advantage compared to the permanent concrete weirs because they are not easily affected by settlements or earthquakes. These are some of the advantages of the inflatable weirs compared to the concrete weirs and metal gates.

Inflatable weirs also have an additional advantage of a lower initial and maintenance cost compared to the metal gates. Maintenance on inflatable weirs is necessary, though, and the serviceable life could be 20 years and more. In addition to the considered advantages of inflatable weirs, one can also choose the fluid of operation of the weir.

Types of inflatable weirs

In practice, there are three types of inflatable weirs in use, namely the water-filled, air-filled, and air and water-filled weir. By and large, the air-filled inflatable weir is preferred and, quite often, the design and construction of an air-filled weir is simpler compared to that of a water-filled weir. The water-filled weir is also more expensive to construct since the foundation requires a wider concrete sill to cater for its relatively larger squat shape, weight and a much more expensive water pump set and pipelines. For an air-filled weir system of the same height, larger pipe diameters are required for the flow of water than smaller diameter pipes. In contrast, in an air-filled weir, air blowers create pressures inside the weir of up to 0.25 bars when inflated, forming the shape of a circle. It is also shorter, which is why a narrower concrete sill is necessary (Zhang et al., 2002). For the water-filled weir, the entire height of the weir rises or lowers evenly, thus also reducing the chances of the formation of a v-notch (warping of weir downstream with the flow) on weir. The average length of inflatable weirs in use is up to 100m and, in some cases, is made up of a specially made membrane of up to 200m in length, which makes it suitable for weirs to span across most rivers. Despite the differences in the fluid of operation, weirs offer relatively low capital and operating costs, and there are also more advantages on the river system (Charles et al., 2005). The inflatable weir can be made in one piece at a factory and rolled up for easy transportation to the dam site and then constructed (Bridgestone, 1997a). Weir heights are usually less than 5m, and some up to 10m are achieved (ec21, 2013). In a normal operation, the weir or dam body is deflated in times of high overflows. A little spill-over is allowed in low overflow with a fully inflated weir.

2.2 Present day use of inflatable weirs

Thousands of inflatable hydraulic structures have been placed along river systems for many uses. Inflatable weirs are one such intervention that have been in use since 40 years ago. Furthermore, these have been used in cold areas where the temperatures are as low as - 40°C. In the USA, a 4.6m high, 67m long inflatable dam is used to regulate water levels for a reservoir at a 9.8MW hydroelectric plant at Highgate Falls. The air-filled weir in its fully inflated configuration minimizes ice problems allowing normal operation of the weir (U.S. Army, 2011).

When flow in the river system is substantially high, take off for irrigation purposes is readily available and excess water is allowed to continue downstream, as well as flush and clean up the river bed of deposits and pollutants. In this instance, the weir is in a deflated position. As the flow recedes, the weir is inflated, holding back water for later use. This ideology can be characterized by a flat topography as in the Cape Coral located in Southwest Florida close to seawater elevations, where, in order to develop the area for residential and commercial use, a canal system was created to drain excess water to avoid overflow into the nearby surrounding settlement. When the water receded, a need to dam the water arose, in order to supply people with water. This water was to be used by a population of approximately 400,000 from the inflatable weir system placed in the canal. Before the water was supplied by private well with little withdrawal from the city's freshwater canal system since the water could not be stored by use of a permanent weir due to the potential flooding hazard (George, 2004).

In the proposed use, the only challenge was the need for an automation to flush sediments and debris, as well as stop possible flooding which could render the weir useless. This was achieved by providing a rapid response to changes in the water levels. Operation of the weir was done manually to offer a secure and continuous supply of water, cleaning the canal and avoiding flooding. This was labour intensive. Automation and manual operation of the inflatable weir would, however, require one to know at what stage the weir should rise and fall with the effects on membrane or dam body. Some studies had to be undertaken to enable full operation of the weir.

Most of the research carried out on inflatable weirs or dam membranes looked at the effects of overflow situations of the inflated structure. In some instances, as will be discussed in section 2.3, a laid out procedure without a basis is used for the operation of the weir. In this study, the

use of the inflatable weir is mainly used to provide potable water and, in essence, irrigation water. Simulation of the assumed different positions of operation were done in the research. This could shed light on the hydraulics of the rise and fall in the weir, thus giving a better understanding of the weir.

2.3 Operation of the inflatable weir

According to Zhang *et al.* (2002), weir inflation and deflation is controlled by devices installed in a control room with an air blower or water needed to inflate and deflate the weir system. There are three kinds of systems identified for use to date. These are the bucket, float, and electrical system. With the bucket type system, flowing water is allowed to collect in a bucket, which will, in turn, mechanically tip the opening and exhaust valve to deflate the weir at desired upstream water levels. In the case of an electrical system, sensors monitor the rise and fall of the water level, opening the exhaust valve automatically with desired water levels. For the float type system, a float fluctuates up and down with the water level on the upstream side of weir, opening and closing the exhaust valve. In the operation described by Zhang and Zheng's procedure, there is no justified analysis on the chosen level of deflation of system.

Based on Bridgestone (1994), procedures recommended for the inflation or deflation of an air-filled weir are as stated:

Inflation

1. One is to inspect the upstream side to ensure people's safety;
2. Debris, (especially sharp objects) adjacent to the rubber weir should be removed;
3. The air exhaust valve should be closed;
4. Opening of The air supply valve should be opened;
5. The air compressor should be started; and
6. While monitoring the air inflation, the pressure should be checked according to the headwater level at the time. If the headwater level is less than 1/2 of the weir height, the air pressure should be approximately 60% of the design pressure. Then switch off the air compressor and close the air supply valve.

Deflation

1. The downstream side should be inspected for safety reasons;

2. It is important that there are no sharp objects downstream;
- 3 The drainpipe to drain the condensed water should be opened; and
4. The air exhaust valve to deflate the dam should be opened.

2.4 Hydraulic and structural performance of the inflatable weir

Studies on the inflatable weir show structural instabilities during over flow, contributing to membrane vibrations and structural responses. Despite an increasing interest in the inflatable weir, there is insufficient information of the performance of inflatable weirs at overflow periods. These overflow periods occur in the inflated, partially inflated, and deflated position of the dam body.

2.4.1 Variation of internal pressure and overflow

Knowledge of the variation of pressure in the operation of the inflatable weir was found to be particularly important in its design. This is mainly due to the susceptibility of dam body to vibrations and warping with the changing shape during deflation and inflation. This has an influence of the performance of the weir. Anwar (1967) found that the variables that are likely to affect the discharge per unit width, 'q', over the weir are the overflow head H, dam height D_h , internal air pressure p, perimeter length of rubber material l, the acceleration due to gravity g, dam base width b and modulus of elasticity of the rubber material E. Then a relationship for the weir, $q = f(H, D_h, l, b, g, p, E)$ was obtained based on the sharp crested weir formula. In the study, the coefficient of discharge C_d was such that $C_d = \phi(H/D_h)$ where in ϕ is the pi dimensionless groups which are; $\phi = f(\Pi_1, \Pi_2, \Pi_3, \Pi_4, \Pi_5) = 0$, indicating that C_d is a function of (H/D_h) . Figures 2.1 and 2.2 show the variation of the cross-section shape of the inflatable weir due to overflow head, H and how it affects C_d values for selected internal air pressure in kN/m^2 .

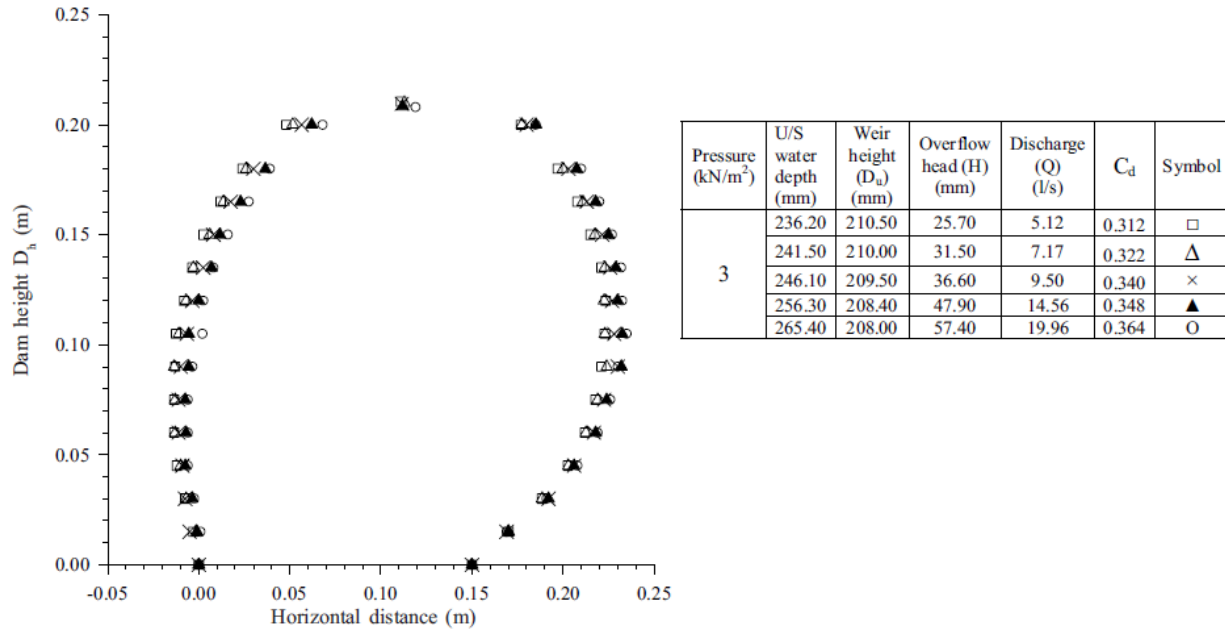


Figure 2.1 Increasing overflow head with constant internal pressure (Alhamati *et al*, 2005)

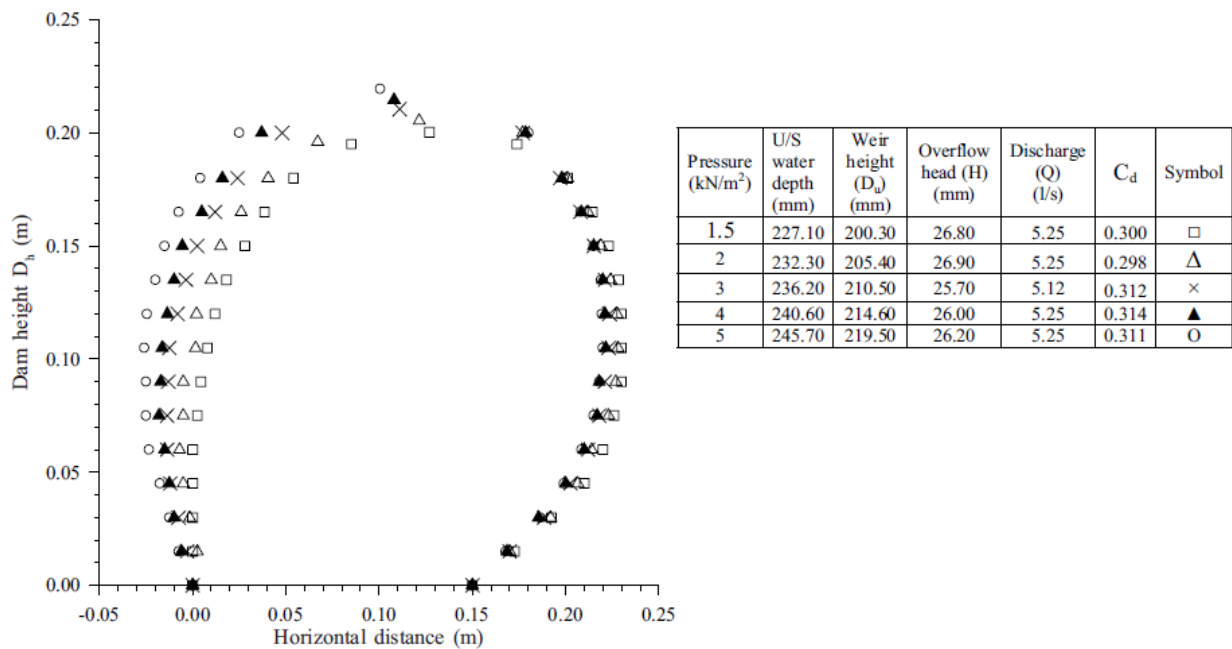


Figure 2.2 Increasing internal pressure with constant overflow head (Alhamati *et al*, 2005)

With the experiments conducted, it was observed that the internal pressure had a strong effect on the deformation of the weir cross-section. It was more significant compared to the overflow head, but unclear on how much it affected the C_d values for the conditions as shown. Alhamati *et al.* (2005) observed that air inflatable weirs are not suitable for high overflows because high

levels of vibration occur in the body when the ratio of H/D_h was approximately greater than 0.2 and where D_h and H are as shown in Figure 2.3.

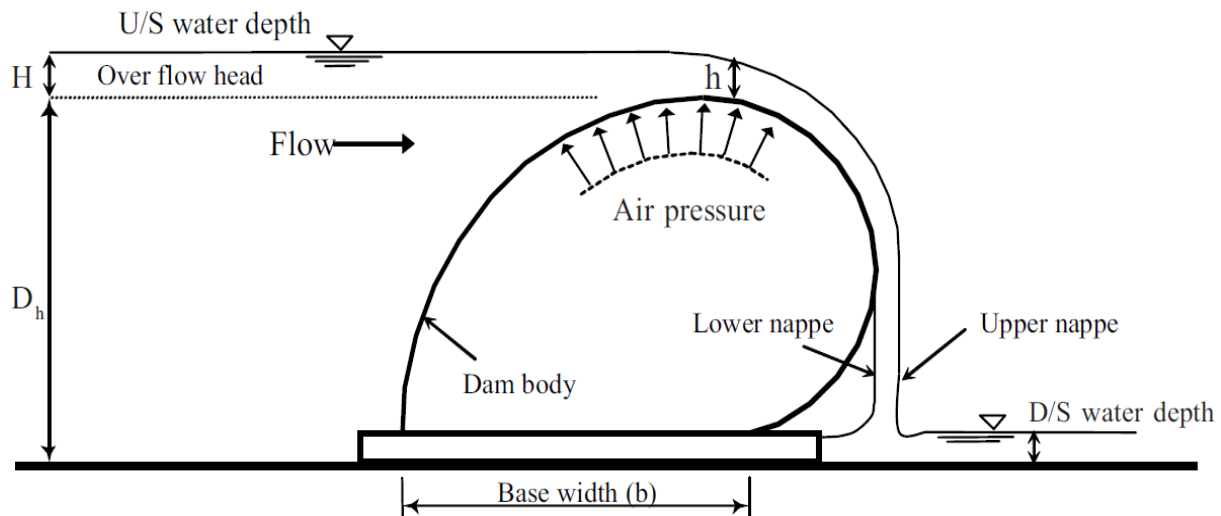


Figure 2.3 Flow over air-inflated weir (Alhamati *et al.*, 2005)

Water-inflated weirs were found to be more stable compared to the air-inflated weirs. Vibrations in water filled weirs occurred when the ratio H/D_h was approximately 0.5 and greater. Anwar (1967) also found that the dam body of air and water-inflated weirs starts to vibrate when the ratios of H/D_h are greater than 0.25 and 0.6 respectively. These vibrations have been identified as the link to the failure of the dam membrane. Vibration also causes the flow over the weir crest to fluctuate, propagating waves in the flowing water, which promotes downstream erosion. It was also discovered that debris erosion occurred on the weir at overflow conditions, adding to one of the root causes of damage to the inflatable weir. Chanson (1998) investigated the overflow characteristics of the inflatable weir. He found that overflow waters may impart some form of fluid-structure interactions on the dam body. These cause vibrations of the membrane, which, in turn, lead to damage or destruction of the weir and the river bed.

2.4.2 Vibrations and their effects on the water filled weir

When the dam body is deflated completely, the water flows over the weir lying flat on the river bed. In some cases, a special design might include provision for partially-inflated operation. In operation, the head losses associated with the deflated membrane must be quite low to optimize the hydraulic performances of the channel, some hydrodynamic processes often occur. These form part of the erosion and damage factors on the weir or dam body as a result of the

hydraulic jump induced vibrations, near-critical flow induced vibrations, and wake induced vibrations (vortex shedding) and debris erosion.

In the operation, Chanson (2005) noted that the deflated membrane could sustain large positive pressure, but cannot sustain high negative pressures. These vibrations could cause abrasions of the inflatable weirs, resulting in leaks, as shown in some past studies. To reduce the vibrations on the weir, breakers/fins and serrations are sometimes used. Serrations and the addition of fins to the downstream side of the weir (see Figure 2.4) are used to improve the dynamic stability of the weir.



Figure 2.4 Serrations and deflectors on inflatable weir (Brussels, 2006)

Since the geometry is independent of the pressure distribution on the surface of the inflatable weirs changes vibrations occur with different characteristic shape modes, amplitudes and frequencies (Gebhardt, 2006). Generally, the following types of vibrations could be identified:

Type A: Vibrations of the nappe;

Type B: Vibrations due to pressure fluctuations;

Type C: Vibrations dam due to uplift forces; and

Type D: Vibrations of the deflated membrane.

Type A vibrations arise in inflatable dams with deflectors. This observed occurrence is known as flap gates and can be seen at small overflow depths with low tail water levels. Due to insufficient aeration of the nappe, free-surface undulations and the motion made by flapping up and down instabilities known as Kelvin-Helmholtz, instabilities occur in some instances. Nappe ventilation and breakers, as described by Minor (1975) and Chanson (1996), were discovered to be the

solution to this problem. As vibrations of the nappe result only in small deformations of the dam body compared with the other vibration types, the vibrations were considered of less contribution to the damage of the weir.

Type B vibrations were described by Chanson (1997), their root cause was identified as an unstable nappe separation on the downstream face of the weir as seen in Figure 2.5.

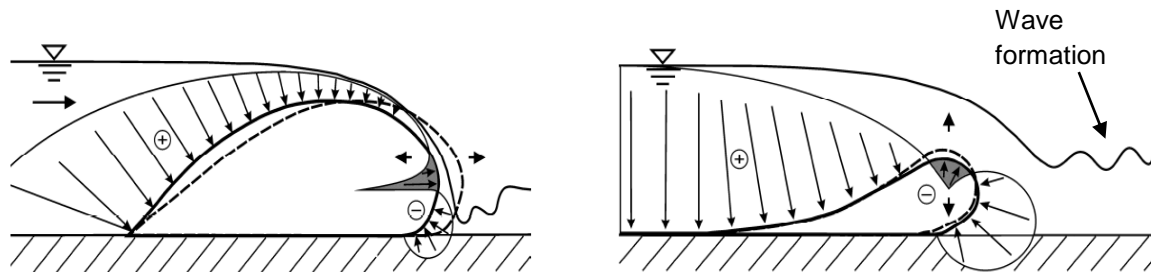


Figure 2.5 Vibrations of the partly deflated dam type B and type C (Chervet, 1984)

As a result of these pressure differentials, the dam body undergoes a series of vibrations with deformations taking place. Wave formation also occurs downstream and causes abrasion and erosion of the river bed (Ogihara *et al.*, 1985). The incorporation and use of a deflector ensures a stable nappe separation and forms an air cavity which stops adhesion of the nappe to the weir. It was noted, though, that the effectiveness of the deflectors is limited and the nappe eventually adheres to the dam body again as overflow increases. The investigations conducted show that the air-filled weir was readily used because the water-filled weirs are more stable. The air-filled weir gives little vibration of the weir.

Type C vibrations occur due to uplift forces as seen at high submergence of the weir on to the weir membrane. In this case, the upstream and downstream water levels are fairly high in relation to the inflatable dam as seen above in Figure 2.5. With the variation in pressure and the flexibility of the rubber, a wave propagating action similar to that seen in pressure fluctuation vibrations, is observed. These are, however, of significantly lower frequencies compared to Type B.

When the weir or dam body is fully deflated, type D vibrations start acting. The relatively low pressure on the weir or dam body cause wake action and shear stresses on membrane, thus damaging the weir. Though the anchoring of the system is part to play in the formation of the wake vibrations, vibrations seem to occur at super critical and near critical conditions in the

operation such that the wake effect is limited to turbulent flow river systems. It was discovered that the deflated weir can sustain large positive pressures, but that it cannot sustain the negative pressure and bottom shear stresses in the direction normal or opposite to the flow. Chervet (1984) sheds light on the abrasion taking place within a short period of time of the inflatable dam which is a result of a flow condition when the Froude number is between 0.3 and 3 as seen in Figure 2.6.

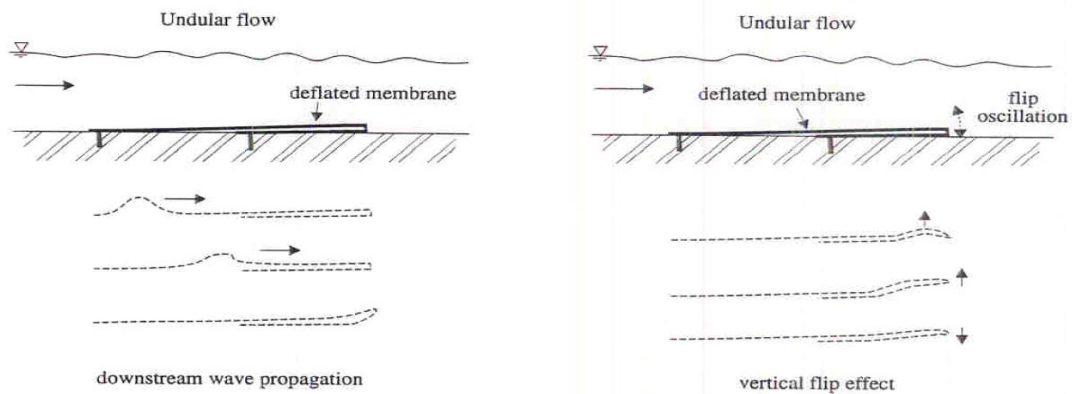


Figure 2.6 Vibration modes of weir (Chervet, 1984)

Of the two different modes discovered, Chervet proposed that the weir should be left slightly inflated to prevent supercritical flow conditions. Figure 2.7 shows the wake regions downstream the deflated weir.

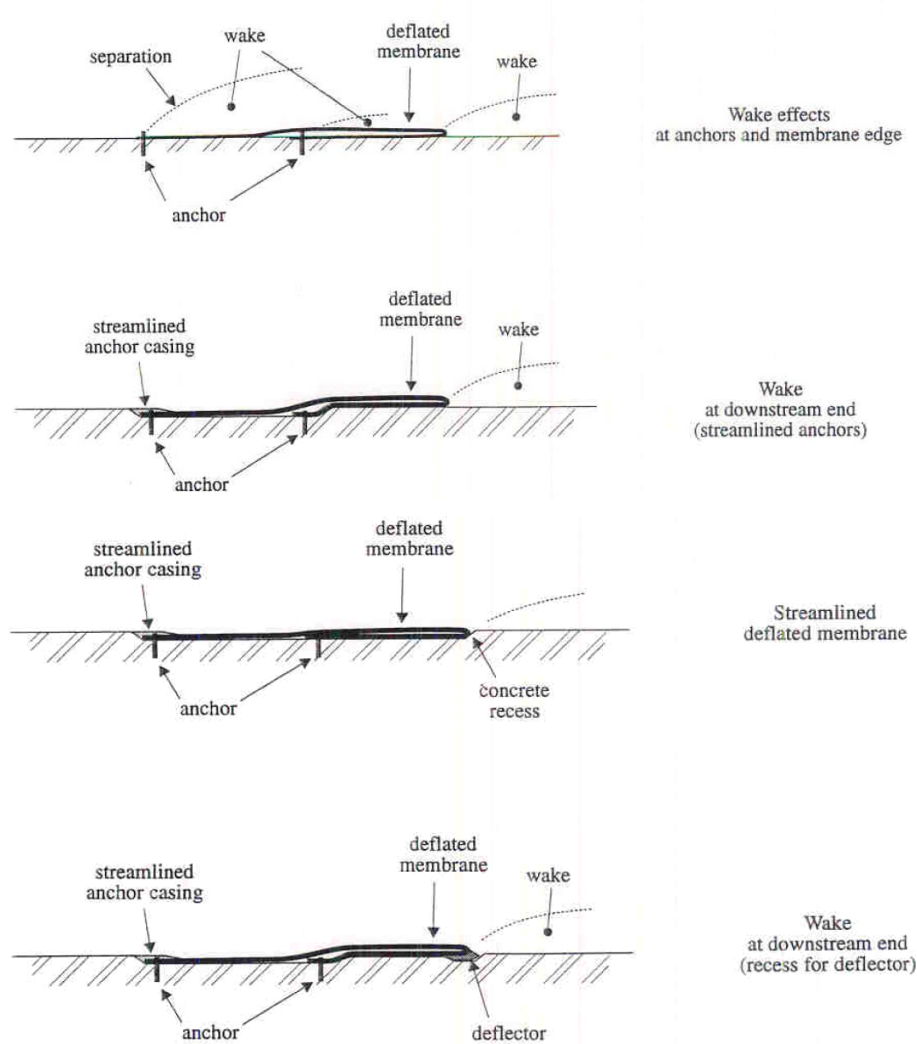


Figure 2.7 Wake regions downstream the deflated weir (Chervet, 1984)

An example of a damaged inflatable weir occurred in the Lahn River in Germany. This weir was damaged owing to vibrations of the deflated dam body which had occurred over a few years (Gebhardt, 2006). When deflated, the weir lies flat on the floor and usually anchors, and casings are streamlined on the floor as well.

2.4.3 Nappe aeration

Nappe aeration plays a very important contribution to the weir over flow. As water flows over the weir, the gravitational forces and the energy in the flowing water tend to pull the nappe straight and perpendicular to the floor bed. Without nappe aeration, the nappe tends to adhere to the weir face, creating a vacuum because of the rounding of the weir. It also prevents nappe

separation. Rouve *et al.* (1974) studied nappe suction and nappe ventilation and found a similar understanding. They also discovered that nappe suction and nappe ventilation increase the discharge coefficient by up to 15% to 20% when the weir is in operation. Nappe ventilation in the inflatable weir operation is largely responsible for the vibrations of the weir. During low overflow periods of an air-filled weir, the nappe was seen to adhere to the weir until it formed the downstream flow. When flow was increased, the nappe was seen to separate, forming a series of nappes. The falling water, adhering to the weir, caused negative pressure as it separated from the weir at the anchoring (Alhamati *et al.*, 2005). Chow (1959) described the effects of the drop in pressure under the nappe to have adverse effects which could lead to the following:

- A change in the shape of the nappe;
- Unstable performance of the weir;
- An increase in pressure differentials on the crest of the dam; and
- An increase in discharge, which is accompanied by pulsating of the nappe.

In his research on aeration of the nappe, Alhamati *et al.* (2005) introduced atmospheric pressure under the nappe by inserting pipes underneath the falling nappe on the downstream side of his test model. This allowed atmospheric pressure to be created underneath the nappe to ensure free separation. The inflatable weir would at one time collapse at the abutments and the center. Collapse at the center gave rise to the formation of a v-notch which caused the weir to overflow at one point. The downstream river bed was then subjected to local scouring. Stationary vortexes also developed in the tail-water and this had the potential to erode the sloped banks. Practical experience has shown that this does not adversely affect the regulation of the headwater level. The V-notch behaviour was also observed in the air filled rubber dams when the dam body deflated or under conditions of low pressure (Alhamati, 2002). This behaviour was also perceived by other scholars such as Alwan (1979) and Al-shami (1983) as shown in Figure 2.8.



Figure 2.8 V-notch behavior of air filled weir partially filled (Alwan, 1979)

However, in this research, simulations were carried out with the assumption that the weir would retain its circular sausage shape and would not experience any V-Notch behaviour. In the process of inflation and deflation of the inflatable weir, the downstream weir face tends to be a half ellipse, but the circular weir is however a very close representation of the downstream weir face shape. Figure 2.9 shows the inflatable weir in its successive positions while in operation.

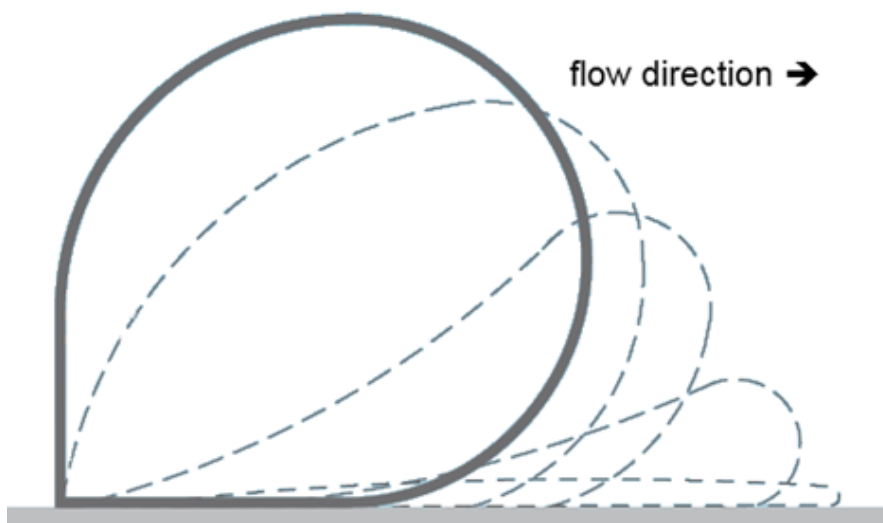


Figure 2.9 Circular face on downstream of inflatable weir (arcon-aquapro.com, 2013)

Little over-flow was allowed with no weir deflation and it was noted by Anwar (1967) and Chanson (1996) that the over-flow characteristics on inflatable weirs were similar to that of a circular crested weir. The research undertaken is based on this reason of similarity.

2.5 Flow over circular a crested weir

The stage discharge over the inflatable weir is more complex compared to that of a permanent weir structure. This is because the shape of the weir is varied due to the change in the internal pressure, overflow head above the crest, and downstream water depth while in operation. However, at each stage, there is a corresponding coefficient of discharge on the weir as with a permanent weir structure. Just like all other weirs, water flowing towards the circular weir eventually goes over the weir, and passes onto the downstream side. Figure 2.10 shows the regimes of flow over the weir under discussion.

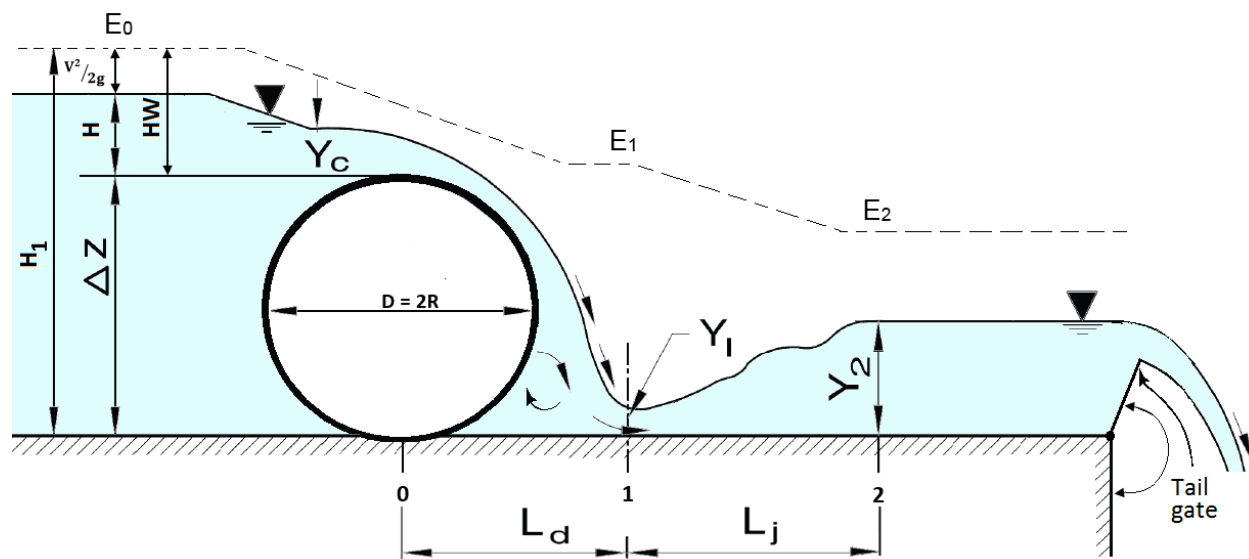


Figure 2.10 Flow over circular crested weir (viewed from US Laboratory)

The tail gate was raised and lowered to introduce the hydraulic jump for assessment of the downstream water conditions. In this study of the hydraulics of the inflatable weir, the overflow water conditions and pressure on the face of the weir are looked at closely, in order to gain more understanding on the performance of the inflatable weir.

2.5.1 Flow in open channels

As flow enters the flume, it is characteristic of the open channel flow which is either steady or unsteady in its flow, and uniform or non-uniform in its flow. In steady flow, depth is constant with time and distance, and gravity forces in balance with resistive forces in the fluid. Steady non-uniform flow has a depth varying with distance not with time, and flow may be gradually varied (Chadwick, 2004).

In open channel flow, there exists a free water surface constituting the boundary with the atmosphere, with negligible shear forces and more frictional losses occur on the wall and bed of the flume. For the purposes of analysis, energy is conserved for the water in the open channel flow as it moves along the flume, and frictional losses due to the flume are neglected. Bernoulli's equation best describes the open channel flow with the application of Newton's second law on open channel flow. Figure 2.11 describes the transition in the fluid flow with regards to the specific energy when there is a rise in the channel bed. As the water flows in the flume, it exhibits specific energy as a result of the potential and kinetic energy within the flowing water (Chanson, 2006) such that:

$$E = y + \frac{v^2}{2g} \dots\dots\dots 2.1$$

Where

E - is the specific energy (m) y - is the depth from the bottom of the channel (m)

V - is the velocity of flow and (ms⁻¹) g - is the acceleration due to gravity (ms⁻²)

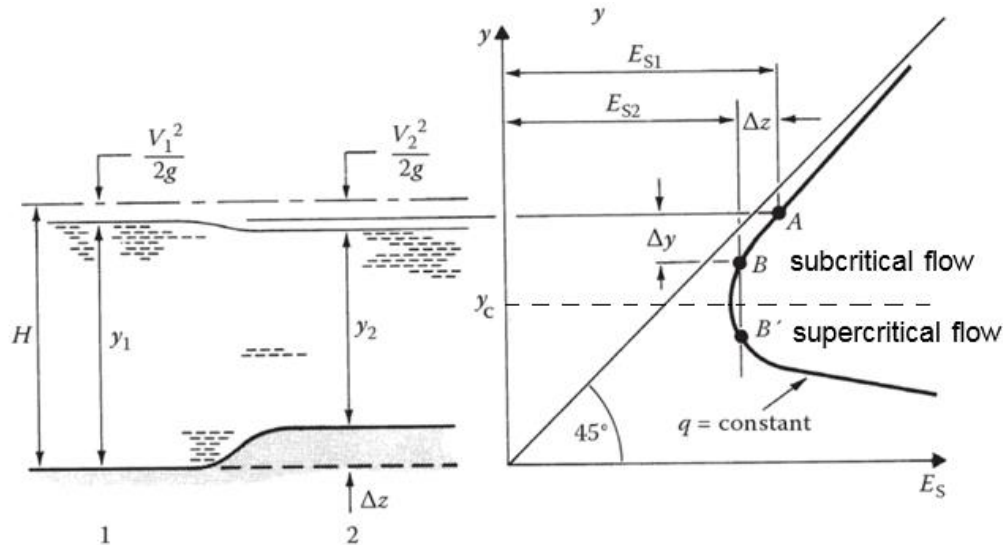


Figure 2.11 Flow transition in open channel (Chadwick, 2004)

Steady non-uniform flow can also be rapidly varied, calling for the application of the energy and momentum principles with the change in the geometry of the channel. As the water flows over the weir, fluid undergoes a change in speed due to the energy in the flowing water and the gravitational force.

According to the Froude's number, flow is classified as critical flow when Froude number = 1, supercritical flow or fast and rapid flow when Froude number > 1, and subcritical flow or slow and calm flow when Froude number < 1. The transition point of flow from supercritical to critical flow occurs at a point realized as the critical point. This condition is normally influenced by parallel stream line flow as the water flowing over the weir models slopes and inclines at a critical point. The critical flow condition is often unstable and causes the formation of standing waves between the two flows, supercritical flow and subcritical flow (Hager, 1985). As an identifier for a specific level of flow, there exists a level of flow below or above critical flow in which fluid is in a higher or low energy state compared to energy at critical depth. Figure 2.12 explains the variation of the discharge and specific energy with depth.

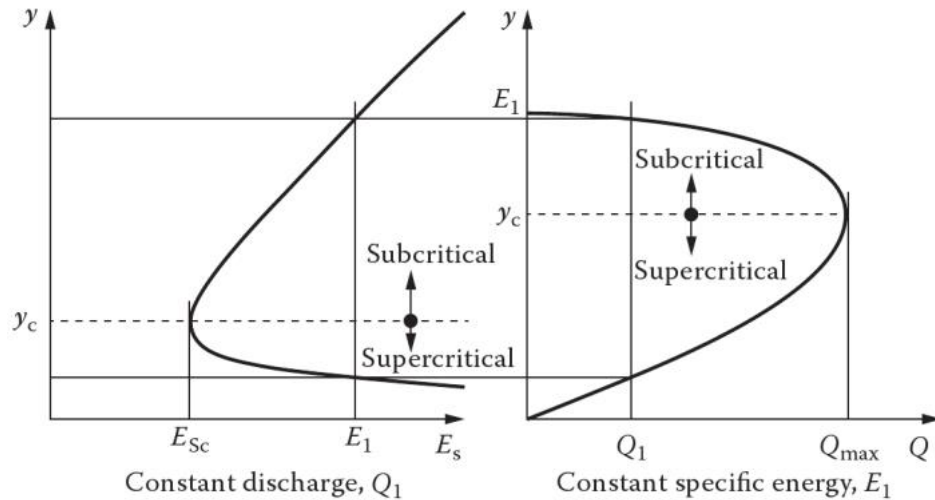


Figure 2.12 Variation of the discharge and specific energy with depth (Chadwick, 2004)

The supercritical flow is characterized by high flow velocities and shallow depths compared to the critical flow, while the subcritical forms low velocities and depths larger than critical flow. As the water flows over the weir model, it is in one of these states and cannot exhibit both with the critical flow forming the dividing flow condition. Due to the slope of the flume bed, the specific energy over the flume is altered due to elevation and frictional loss. Figure 2.13 shows the change in energy due to slope.

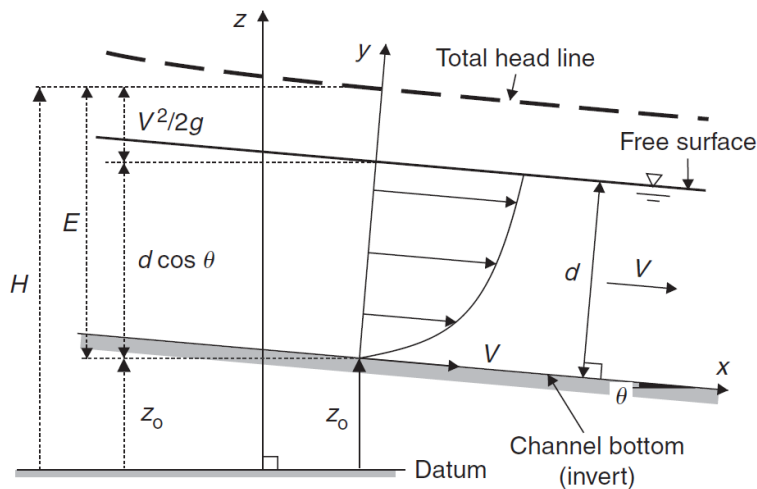


Figure 2.13 Specific energy due to slope (Chanson, 2004)

The piezometric head contributing to the flow field is presented as $d \cos \theta$ in Figure 2.13.

2.5.2 Effect of upstream weir face on weir performance

Chanson and Montes (1998) investigated and found that the upstream channel conditions are to a very little extent influential to the development of the discharge coefficient. Different studies on the effects of upstream arches on circular crested weirs confirm this finding.

2.5.2.1 Shabanlou *et al.* (2013)

Shabanlou *et al.* (2013), using the sharp crested weir formula, found that the crest arch on the upstream side of the weir had negligible influence on the discharge coefficient at all angles in the experiments performed except at 90° . In his study, he varied the upstream arch angle from 0° , 30° , 45° , 60° , to 90° , keeping the downstream angle and crest fixed. Figure 2.14 shows the arch of the crests during the experiment conducted.

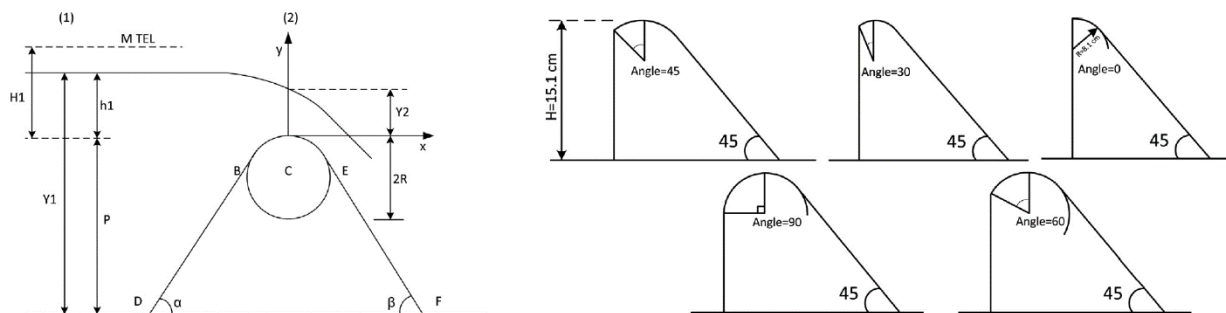


Figure 2.14 Upstream arches at crest on a circular crested weir (Shabanlou, 2013)

For H_1/R ranging from 0.8 to 0.84 and a consequent C_d of 0.53 to 0.7, variation of the C_d was up to 3% as measured in the experiment. The crest arch on the upstream also had an insignificant contribution to the energy losses and there was no certain trend in the variation of the energy losses as seen in the results below in Figure 2.15

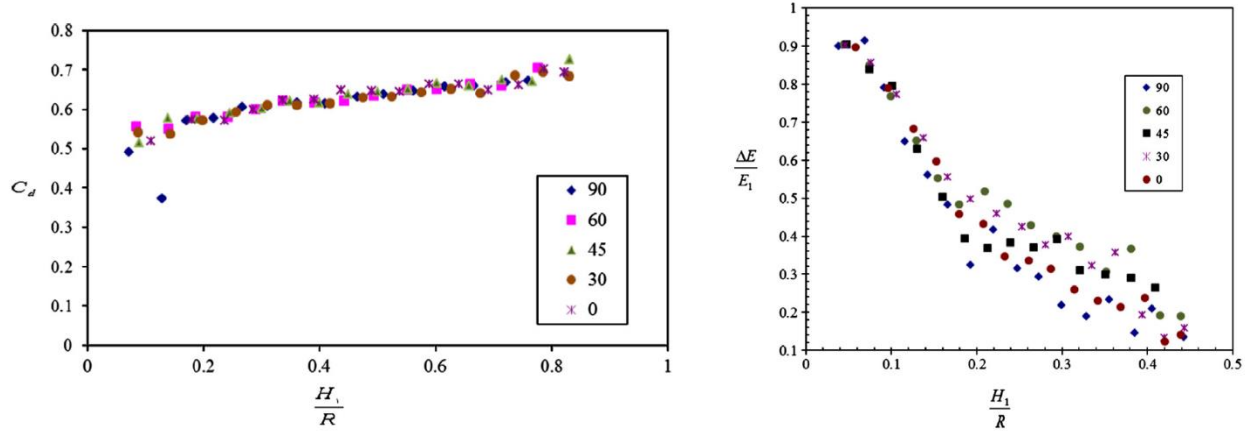


Figure 2.15 Upstream crest arch effect on the discharge coefficient and energy losses (Shabanlou, 2013)

The situation of having a varying upstream crest arch is similar to what is experienced in the use of the inflatable weir. Shabanlou *et al.* (2013) discovered that, despite the negligible effects of the crest arch on the C_d , energy losses, depth of flow, the velocity distribution over the weir crest at all angles, at 0° , there was some significant influence on the depth of flow and velocity distribution. Figure 2.16 shows the observed trend.

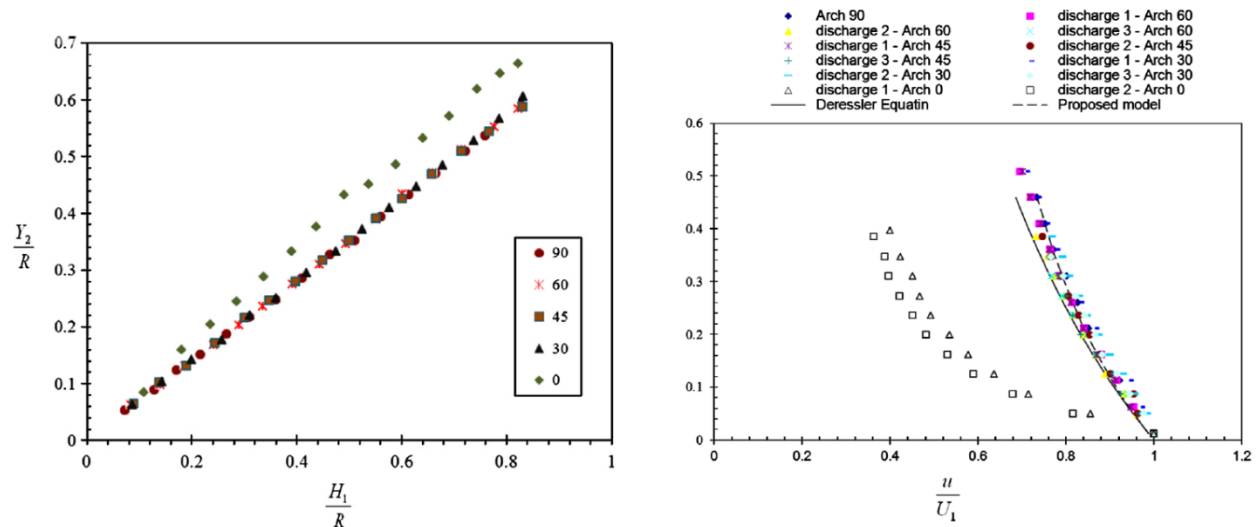


Figure 2.16 Upstream crest arch effect on the head and velocity (Shabanlou, 2013)

At 0° , the depth of flow over the weir crest raised significantly as inflow to arch was increased. This was accompanied by a corresponding decrease in the velocity profile as inflow to the arch was increased.

2.5.2.2 Schmocker *et al.* (2011)

Schmocker *et al.* (2011) also investigated the various combinations of upstream and downstream angles. In his research he conducted tests on ten circular-crested weir configurations almost similar to Shabanlou's configuration. Figure 2.17 shows the experimental configuration used.

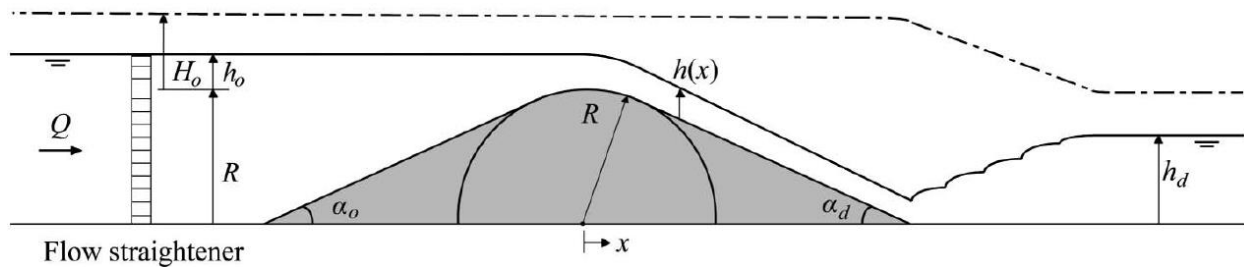


Figure 2.17 Configuration of the flow geometry for free overflow (Schmocker *et al.*, 2011)

Using the sharp crested weir formula, he found that the angles upstream and downstream of the weir have a degree of contribution on the C_d such that $C_d = \frac{2}{\sqrt[3]{3}} \left(1 + \frac{3\rho_k}{11 + \Omega\rho_k} \right)$ where $\rho_k = H_o/R$ is the relative crest curvature and $\Omega = 4.5$, the downstream angle, α_d , increases the C_d and upstream angles α_o has insignificant contribution on the C_d . This is seen graphically in Figure 2.18.

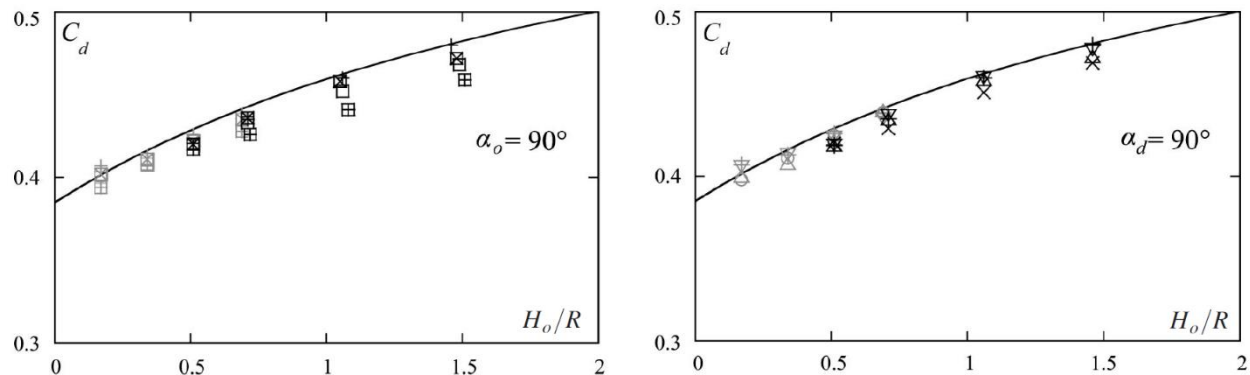


Figure 2.18 C_d (H_o/R) for $\alpha_o = 90^\circ$ with $\alpha_d = 20^\circ, 30^\circ, 45^\circ, 90^\circ$ and $\alpha_d = 90^\circ$ with $\alpha_o = 20^\circ, 30^\circ, 45^\circ, 90^\circ$ (Schmocker *et al.*, 2011)

2.5.2.3 Bahzad *et al.* (2010)

Bahzad *et al.* (2010) investigated the hydraulic influence of the geometric properties of the rounded crest weir (shape on weir) on the weir performance. In the investigations, the sharp

crest, inside semi-circular, outside semi-circular and circular crest shape weirs were tested. Figure 2.19 shows the weir shapes experimented on. Rounding the weir crest is expected to increase performance of the weir which in turn increases the C_d .

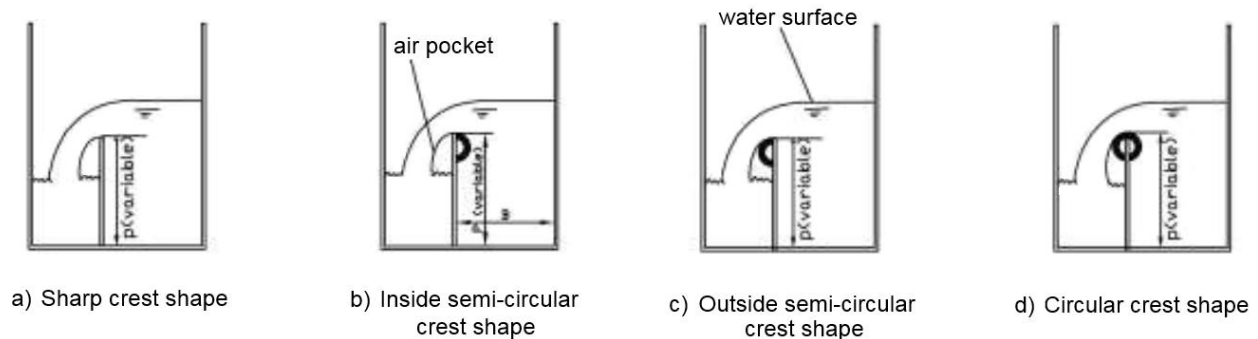


Figure 2.19 Different weir crests tested (Bahzad *et al.*, 2010)

For all the test configurations used, there was an energy difference of 1% between the two ends of the weirs which could be ignored. C_d was proportional to the upstream Froude number and also proportional to the increase of upstream water depth to weir height (h_1/p). Bahzad *et al.* (2010) obtained empirical power equations for comparing the data sets and found that the hydraulic performance of the weir was higher for small weir heights for all crest shapes. The highest performance was for an inside semi-circular crest weir at crest radius of 3.15cm and 3.75cm for an outside semi-circular crest. The highest performance on a circular crest weir was also obtained with a radius of 2.5cm and a radius to weir height (r/p) of 0.25. Honar *et al.* (2008) also concluded that the rounded edge weir discharge is 10% more than that of the squared edge weirs.

2.5.3 Back water effects of weir

In the design of hydraulic structures, design criteria focuses on the ease with which water can pass over hydraulic structure. This reduces the risk of weakening and collapse of the hydraulic structure, mainly due to the unexpected or expected floods. In the use of the inflatable weir, the water level, immediately upstream of the structure, is expected to rise due to the weir obstruction (afflux). Gebhardt *et al.* (2012) conducted a research on the backwater effects of a Jambor weir sill and compared it to the traditional weirs. In his study, he defined the Jambor weir sills as ground sills, a flap gate, inflatable dam and a sector gate. His study focused on the assessment of the headwater with the respective tail-water conditions and the resultant discharge of the hydraulic structure. In the investigation upstream of the weir shape, he found

that there is an increased or reduced afflux due to the shape of the upstream of the weir from the Bernoulli's equation. The shape of the upstream of the weir also contributes to the transport of sediments. Gebhardt *et al.* (2012) deduced an optimum radius of curvature of the upstream of a weir using hydraulic modelling. An S-shaped ramp, with respect to the radii of the changing sill height, was found to be ideal. Figure 2.20 gives the realized idea upstream radius.

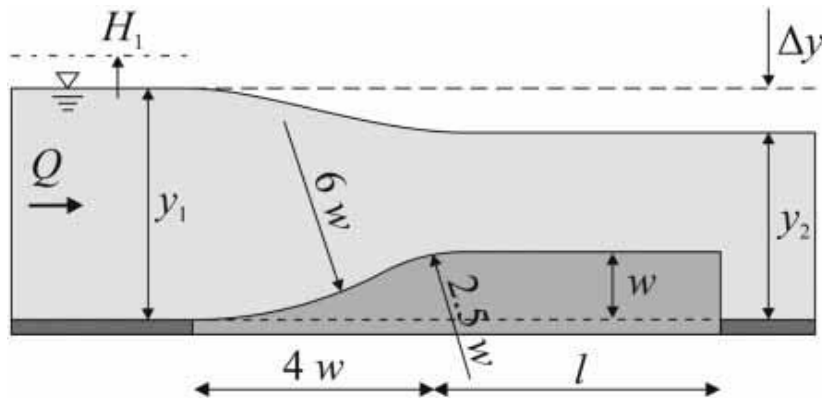


Figure 2.20 Optimal upstream radius of curvature (Gebhardt *et al.*, 2012)

This shape is closely exhibited by the use of the inflatable weir. In the study conducted, it was found that there is an advantage of reduced afflux due to the hydraulically optimized shape of the weirs as with the Jambor sill. As a result of this study, the identical discharge capacity for a traditional weir compared to an inflatable weir required a lower weir height for the discharge capacity to be maintained. This reduces the cost of the hydraulic structure significantly, introducing a saving on the construction of the hydraulic structure with the reduced weir height. The research also led to the development of a useful chart for the estimating afflux as seen in Figure 2.21.

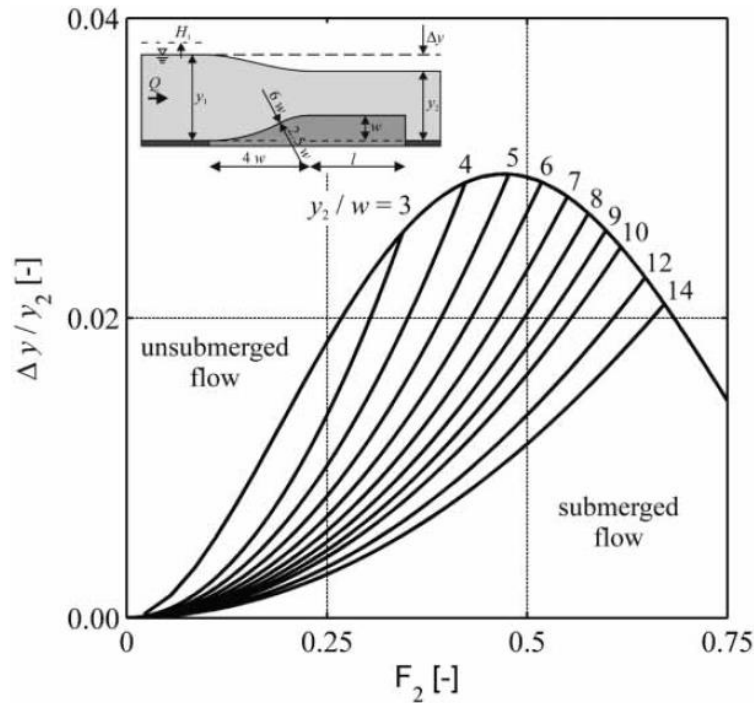


Figure 2.21 Design chart for estimating afflux $\Delta y/y_2$ against y_2/w and Fr (Gebhardt *et al.*, 2012)

2.5.3 Discharge coefficient on circular crested weirs

Data from literature on discharge coefficients of circular/cylindrical crested weirs are either based in the discharge formula for broad crested weirs ($Q = C_{wb} b \sqrt{g} \left(\frac{2}{3}\right)^{\frac{3}{2}} H^{1.5}$) or the discharge formula for sharp crested weirs ($Q = C_{wr} b \frac{2}{3} \sqrt{2g} H^{1.5}$). In this study the broad crested weir discharge formula is considered the more appropriate formula for inflatable weirs as used by Chanson. The discharge coefficients on circular crested weirs are presented in this section as they were published but to enable a comparison of all circular crested weir discharge coefficients, a summary at the end of this subsection is presented with all discharge coefficients transformed to discharge coefficients based on the broad crested weir discharge formula. The discharge coefficients based on the sharp crested weir formula are therefore transformed by multiplying these coefficients with 1.732 (i.e. $\{\frac{2}{3} \sqrt{2g}\} / \{(\frac{2}{3})^{\frac{3}{2}} \sqrt{g}\}$).

Previous studies on the circular and cylindrical crested weirs, as obtained from literature, include:

1. Bos (1978) experimental

The cylindrical weir, as studied by Bos (1978), is a high C_d hydraulic structure, mainly used as a spillway. He considered a vertical upstream structure with the rounding at the crest to avoid nappe separation. Figure 2.22 gives the hydraulic design of a circular weir as explained by Bos (1978) and his findings.

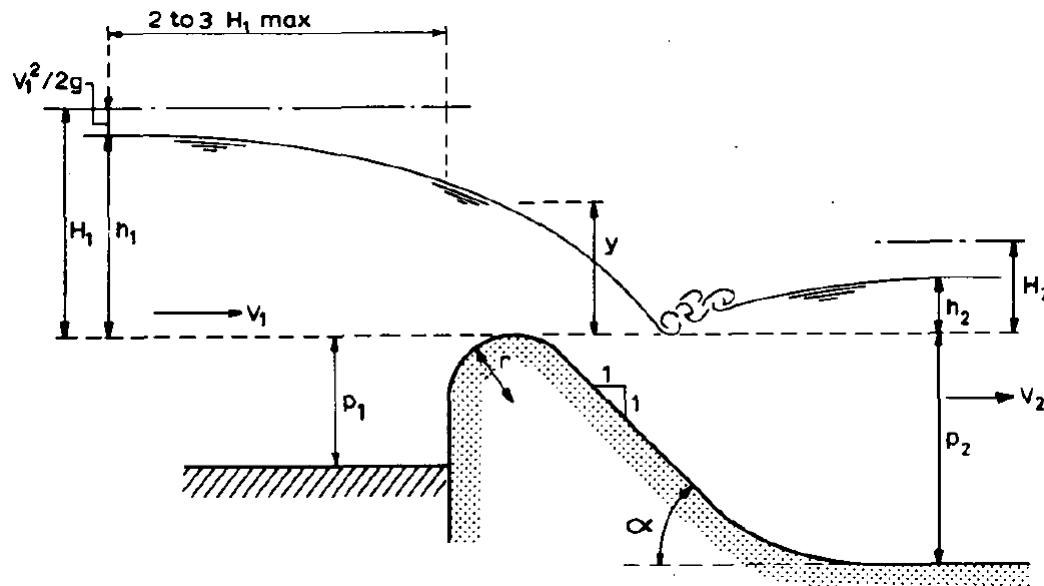


Figure 2.22 Definition of circular rounded weir by Bos (1987)

In his findings, he concluded that the C_d based on the broad crested weir equation was equivalent to that of a broad crested weir such that:

$$Q = C_e \frac{2}{3} \sqrt{\left(\frac{2}{3}g\right)} b_c H_1^{1.5} \dots\dots\dots 2.2$$

Where C_e - effective discharge coefficient and;

$$C_e = C_0 C_1 C_2 \quad \text{with} \quad C_0 = f\left(\frac{H_1}{r}\right)$$

$$C_1 = f\left(\frac{p_1}{H_1}\right)$$

$$C_2 = f\left(\frac{p_1}{H_1} \text{ and slope of the upstream weir face}\right)$$

$$C_e = f\left(\frac{H_1}{r}\right) \text{ with } C_0 (\text{maximum}) = 1.49 \text{ if } H_1 \text{ exceeds } 5$$

Bos also conducted experiments on the measurement of C_d and obtained the results that were very close the theoretical equation 2.2. Figure 2.23 illustrates the findings from the experimental data.

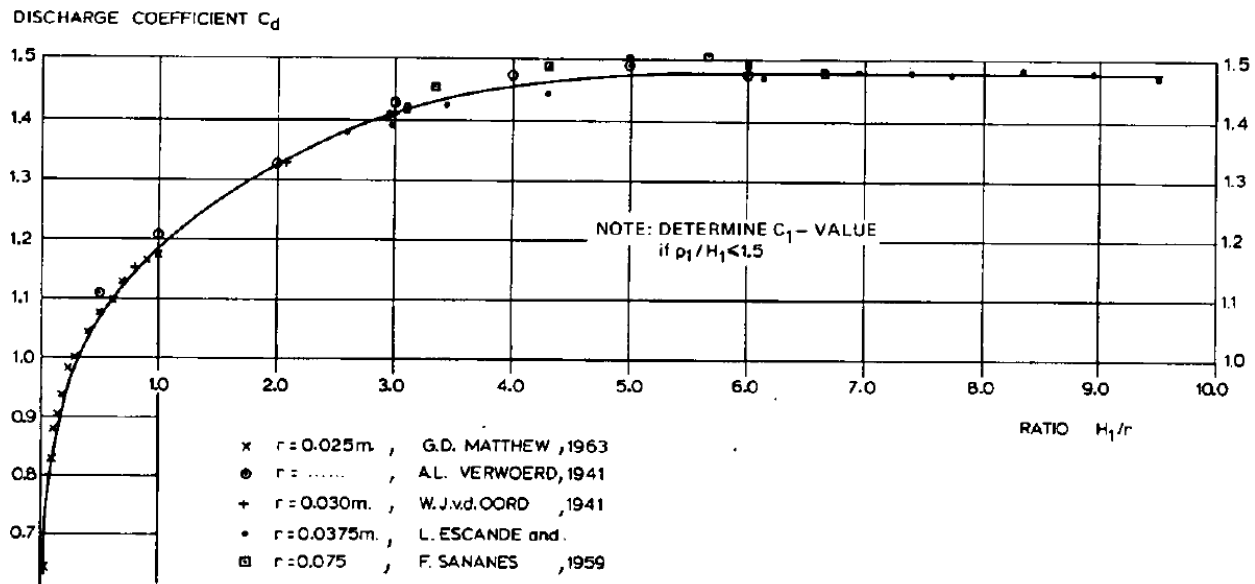


Figure 2.23 Circular crested weir discharge coefficient results Bos (1978)

The experimental data observed by Bos (1978) also compared reasonably well with the earlier studies as seen above.

2. Chanson *et al.* (1998; 2006)

Chanson *et al.* (1998), investigated the effect of a fully-developed inflow and the inclusion of an upstream ramp at 30° in the experiments. Investigations show that the size of the circular weir, the ratio of weir height from the crest to bed with the radius of the weir and the introduction of an upstream ramp had no influence on the discharge coefficient, crest depth and the energy dissipation. Figure 2.24 shows the experimental configuration for the tests explained and conducted.

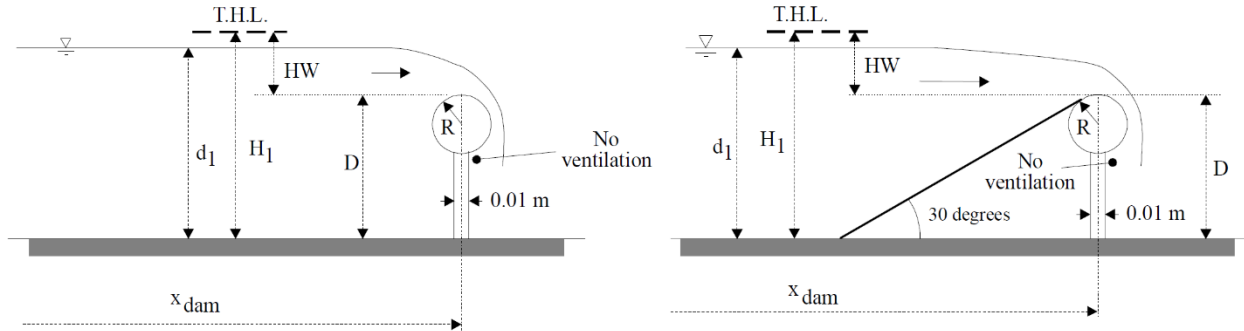


Figure 2.24 Overflow characteristics of circular weirs (Chanson *et al*, 1998)

The inflow conditions were found to be very influential on the weir crest depth and C_d as the inflow into the flume changed. Equations based on the broad-crested weir equation for the fully developed inflow and the partially developed inflow were developed respectively such that:

$$C_d = 1.185 \left(\frac{H_w}{R} \right)^{0.136} \dots\dots\dots 2.3$$

for the fully developed inflow ($0.45 < H_w < 1.9$)

$$C_d = 1.1268 \left(\frac{H_w}{R} \right)^{0.181} \dots\dots\dots 2.4$$

for the partially developed inflow ($0.35 < H_w < 3.5$)

Experimental investigations show that the C_d values are fairly larger for the fully developed flow as compared to the partially developed flow. Results of the different inflow conditions on the circular cylinders were compared to above equations for the studied scenarios and are shown in Figure 2.25.

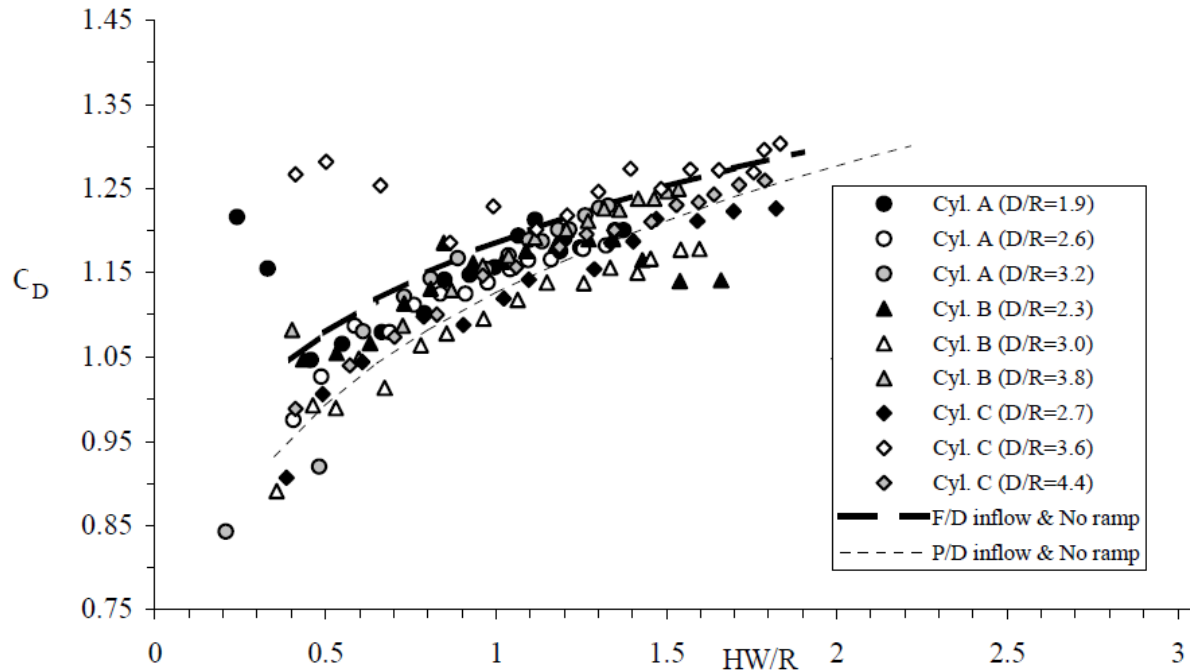


Figure 2.25 Fully and partially-developed inflow theoretical conditions on circular cylinders compared to the experimental results (Chanson *et al*, 1998)

Chanson *et al.* (1998) findings on the effect of having a ramp support the studies on the upstream arches previously explained in literature on upstream arches. Figure 2.26 show the experimental findings.

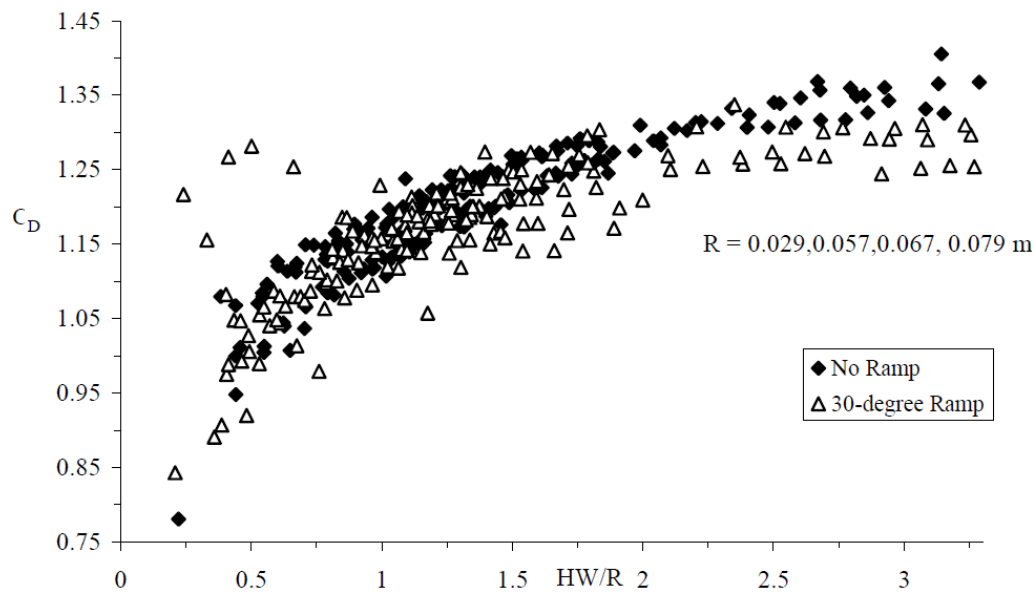


Figure 2.26 Circular cylinders compared to the experimental results (Chanson *et al*, 1998)

Chanson *et al.* (1998) also looked at earlier studies on based on the broad crested weir equations. These are tabulated is table 2.1.

Table 2.1 Empirical of discharge coefficients formulae for circular-crested weirs (Chanson, 1998)

Reference	C_d	Comments
REHBOCK (1929)	$0.552 + 0.177 \sqrt{30 - \left(5 - \frac{HW}{R}\right)^2}$	Model data as given in SARGINSON (1972).
FAWER (1937)	$1 + 0.221 \frac{HW}{R} - 0.0260 \left(\frac{HW}{R}\right)^2$	Model data. $W = 0.303$ m. $R = 0.0325$ m. $0.5 \leq HW/R \leq 3$. $0 \leq D-R \leq 0.3325$ m.
JAEGER (1956)	$\frac{3}{2} \left(\frac{R}{HW} + \frac{4}{3} - \sqrt{\left(\frac{R}{HW}\right)^2 + \frac{4}{3} \cdot \frac{R}{HW}} \right)$	Theoretical result validated with model data.
MATTHEW (1963)	$1 + 0.230 \frac{HW}{R} - 0.010 \left(\frac{HW}{R}\right)^2 - 0.0154 \frac{R}{HW}$	Model data. Vertical upstream face. $R = 0.0254$ m. $0.1 \leq HW/R \leq 1$.
	$1 + 0.240 \frac{HW}{R} - 0.028 \left(\frac{HW}{R}\right)^2 - 0.0184 \frac{R}{HW}$	Upstream face with 45-degree slope. $R = 0.0254$ m. $0.1 \leq HW/R \leq 1$.
	$1 + 0.240 \frac{HW}{R} - 0.026 \left(\frac{HW}{R}\right)^2 - 0.0181 \frac{R}{HW}$	Upstream face with 45-degree slope. $R = 0.0254$ m. $0.1 \leq HW/R \leq 1$. $D=2 \cdot R$.
MONTES (1964)	$1.169 \left(\frac{HW}{R}\right)^{1/8}$	Re-analysis of data. $0.05 < HW/R < 1.2$
SARGINSON (1972)	$0.702 + 0.145 \sqrt{33 - \left(5.5 - \frac{HW}{R}\right)^2} - 3.146 \frac{\sigma}{\rho_w \cdot g \cdot HW} \left(1 - \left(1 + 1.2 \frac{HW}{R}\right)^{-4/9}\right) + 0.160 \frac{HW}{D}$	Model data. Ventilated nappes. Liquids : water, water + Lissapol N ($0.034 < \sigma < 0.059$ N/m). $R = 0.00315$ to 0.068 m. $HW/R < 2$ to 4
ROUVE and INDLEKOFER (1974)	$0.94440 + 0.35497 \frac{HW}{R} - 0.10791 \left(\frac{HW}{R}\right)^2 + 0.010309 \left(\frac{HW}{R}\right)^3$	Model data. Semicircular crest with ventilated nappe. $W = 0.599$ m. $0.0102 \leq R \leq 0.148$ m. $0.21 \leq D-R \leq 0.96$ m. for $HW/R < 4.0$
	1.299	for $HW/R > 4.0$
PRESENT STUDY	$C_D = 1.2676 \left(\frac{HW}{R}\right)^{0.1811}$	Model data. Un-ventilated nappes. $W = 0.25$ to 0.3 m. Horizontal channels. Partially-developed inflow. $0.35 < HW/R < 3.5$
	$C_D = 1.1854 \left(\frac{HW}{R}\right)^{0.1358}$	Fully-developed inflow. $0.45 < HW/R < 1.9$

Despite the aeration conditions in previous researchers, further comparison was expressed graphically as seen in Figure 2.27 for the circular weir due to the similar nappe adherence observed in the test. Nappe observations, though not recorded by Chanson (1997) were similar to what was observed by Sarginson (1972) with the ventilated nappe giving basis of comparison.

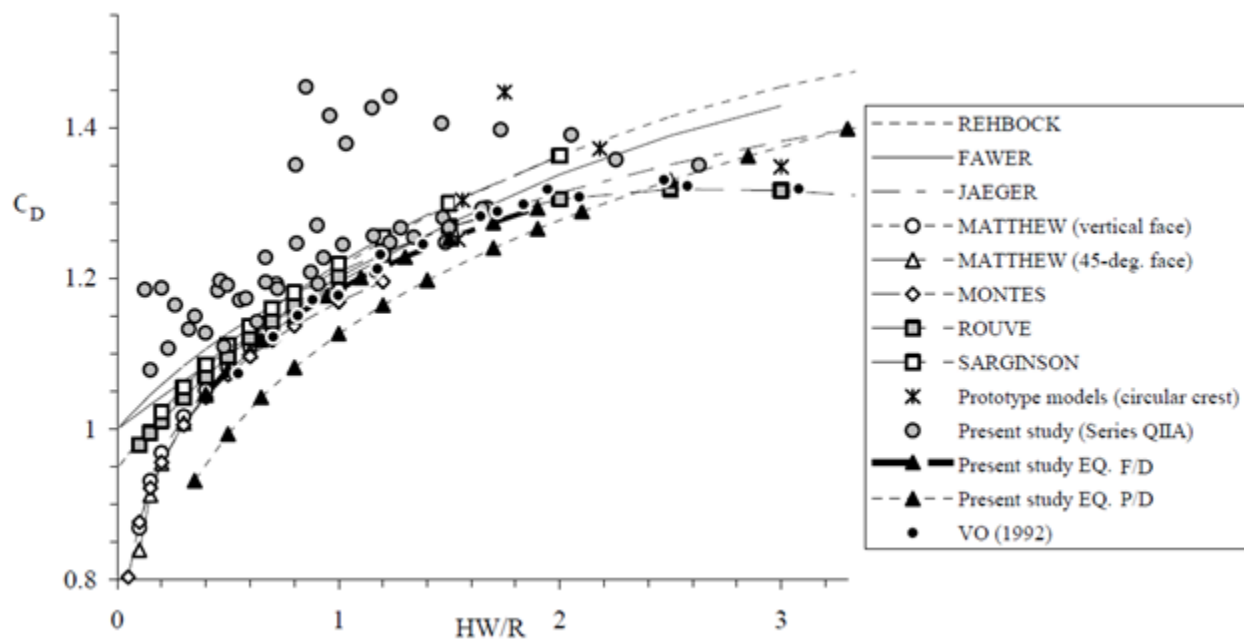


Figure 2.27 Comparison of present study to previous studies by Chanson *et al.* (1998)

Cylindrical weirs have a high coefficient of discharge as a result of the shape of the weir. Studies have shown that the weir coefficient is largely influenced by the head, weir radius, and suction and nappe aeration. C_d was also found to be normally greater than one based on the broad crested weir equation by 15% - 20% due to absence of nappe aeration (Chanson *et al.*, 1998). Figure 2.28 shows the phenomenon of nappe adherence to the circular weir as demonstrated in the experiments conducted.

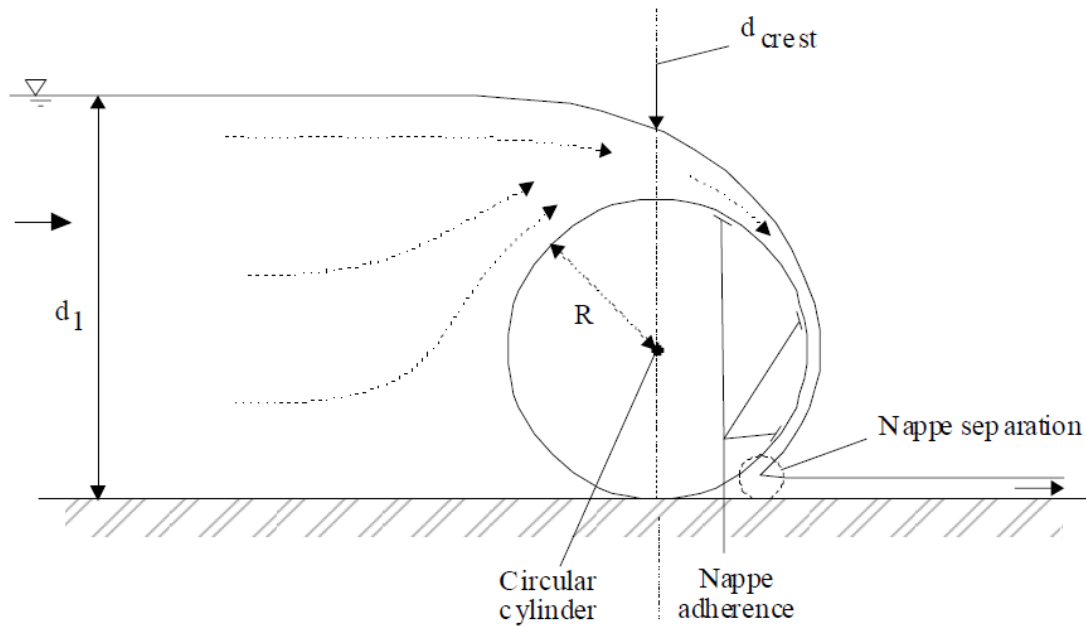


Figure 2.28 Over flow in the on circular weir (Chanson, 1997)

Due to the shape of the weir, stream lines passing over the weir crest have more curvature and this has a direct contribution to the discharge coefficient C_d (Bagheri *et al.*, 2010).

3. Amir H. Haghiabi (2012)

Haghiabi (2012) conducted experiments to validate the experimental finding using the Dressler theory. He applied a velocity correction factor at the weir crest, developing empirical equations for C_d , velocity and pressure profile with the observed experimental results. His experimental results showed a good agreement validating his empirical equations. Figure 2.29 is a schematic diagram of the flow past a circular crested weir assumed.

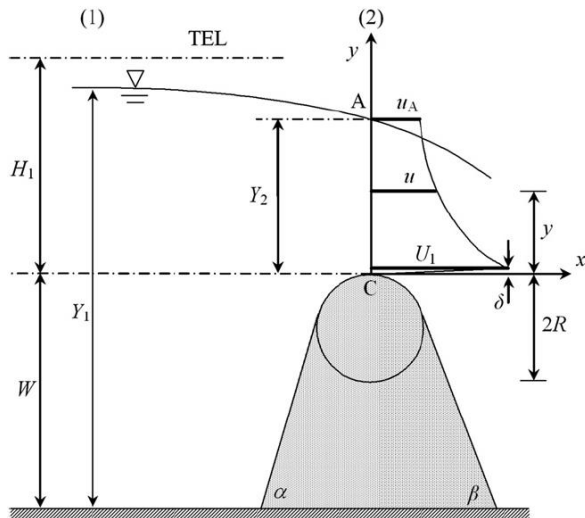


Figure 2.29 Flow past a circular crested weir assumed (Haghiabi, 2012)

In generating the equations, some assumptions were made, which were:

- Steady, subcritical inflow to the weir crest;
- Viscosity and surface tension were negligible and;
- Boundary layer thickness at crest was also negligible for accelerating flow on nappe.

Equation 2.5 developed based on the broad crested weir formula is given by (Haghiabi, 2012):

$$C_d = 2.787 \frac{z^2 [\ln(z)]^{\frac{5}{2}}}{\left(\frac{z-1}{0.71}\right)^2 (z^2-1)^{\frac{1}{2}}} \dots\dots\dots 2.5$$

Where $z = 1 + 0.71 \frac{H_1}{R}$ with an assumption the $y_2 = 0.71H_1$. This is validated by the experimental results in the study. Figure 2.30 shows the experimental results compared to the empirical equation developed from the Dressler theory validating the assumption made.

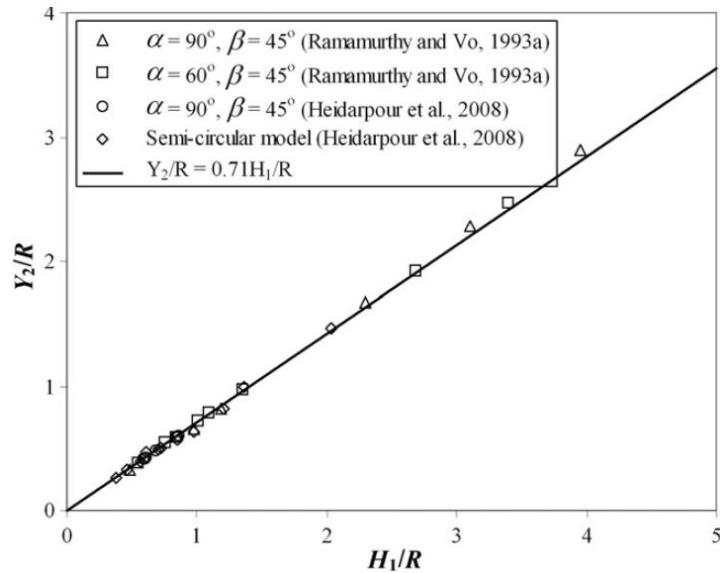


Figure 2.30 Good agreement of the experimental results with empirical equation.

4. Heidarpour (2010)

Similar to Haghiabi (2012), Heidarpour (2010; 2013) used the potential flow theory in velocity distribution over cylindrical weirs to predict the velocity distribution, and expressed C_d based on the experimental broad crested weir equation:

$$C_d = 1.1757 \left(\frac{H_1}{R}\right)^{0.1469} \dots\dots\dots 2.6$$

And the theoretical broad crested weir equation:

$$C_d = \frac{3\sqrt{3}}{2} \left(\frac{H_1}{R}\right)^{-1} + \frac{1}{k-1} \sqrt{\left(1 - \frac{d}{H_1}\right)} \left[\left(1 + \frac{kd}{R}\right) - \left(1 + \frac{kd}{R}\right)^{1/k} \right] \dots\dots\dots 2.7$$

Where is $k = 2$

The experimental recorded velocities for the different cylinder sizes were compared and found to be very close to the prediction method within $\pm 5\%$. Figure 2.31 shows the experimental results and the predictions for the 2010 and 2013 experiments.

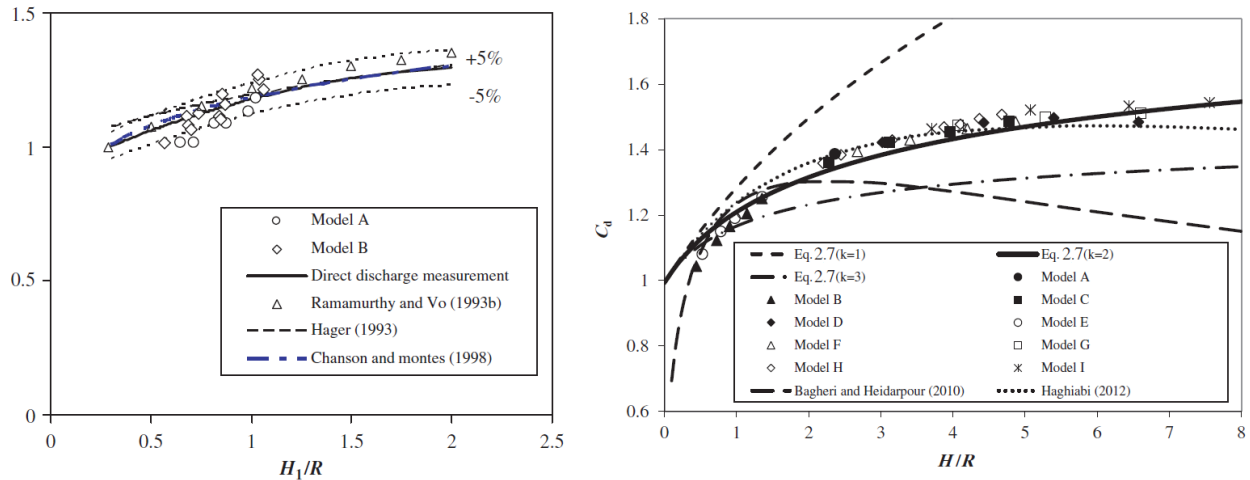


Figure 2.31 C_d against H_1/R (Heidarpour, 2010; 2013)

5. Emad Abdul Gabbar Al Babely (2011; 2012)

Emad *et al.* (2011) also investigated the overflow characteristics of three circular weirs 114mm, 90mm and 63mm in size. His findings showed that the increase in the ratio of depth of flow over the weir crest to cylinder radius resulted in a proportional increase in the C_d . He assumed a hydrostatic pressure distribution at the weir crest and a uniform velocity distribution. However, in practice, the pressure distribution is not hydrostatic and the velocity distribution is not uniform over the weir crest. The bottom geometry of the channel was also seen to affect the discharge coefficient, giving the equation below based on the broad crested weir. The maximum discharge per unit width at a weir crest for ideal fluid flow derived from the Bernoulli equation was used by Emad (2011) as expressed below. The unit discharge was also related to the total energy above the crest and discharge as seen by Bos (1978):

$$q = C_d \sqrt{g} \times \left(\frac{2}{3} \times (H - D) \right)^{3/2} \dots\dots\dots 2.8$$

Figure 2.32 shows the experimental set up and the relationship between the C_d and the ratio of $\left(\frac{H_w}{R} \right)$ as found by Emad *et al.* (2011) in the experiments conducted.

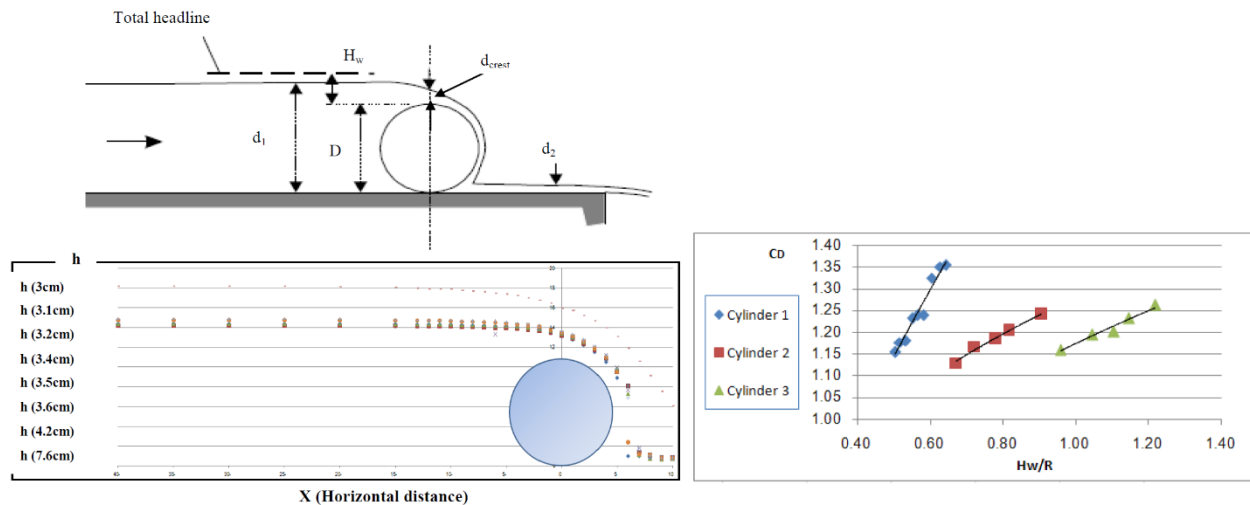


Figure 2.32 Experimental configuration, water surface profile and discharge coefficient (Emad, 2011)

Emad (2012) also studied the effect of the geometrical characteristics of an oblique cylindrical weir C_d . In his study, he discovered that the geometrical characteristics and inclination of the oblique cylindrical weir decreased the C_d as the weir radius increased. The oblique weir resulted in an increase in the C_d compared to that of a normal weir of the same size.

6. Shabanlou *et al.* (2013)

The study results of Shabanlou *et al.* (2013) on the crest arch on the upstream side of a cylindrical weir are partially presented in Section 2.5.2.1 above. They found that the upstream crest arch had an insignificant contribution to the C_d , energy losses, head and velocity for upstream arch angles of 0° , 30° , 45° , 60° , to 90° . However, at arch angle of 0° , head and velocity are increased significantly. In a more recent study conducted the same year, Shabanlou *et al.* (2013) further investigated the effect on both cylindrical and circular crested weirs based on the broad crested weir. Figure 2.33 shows the two types of weir investigated.

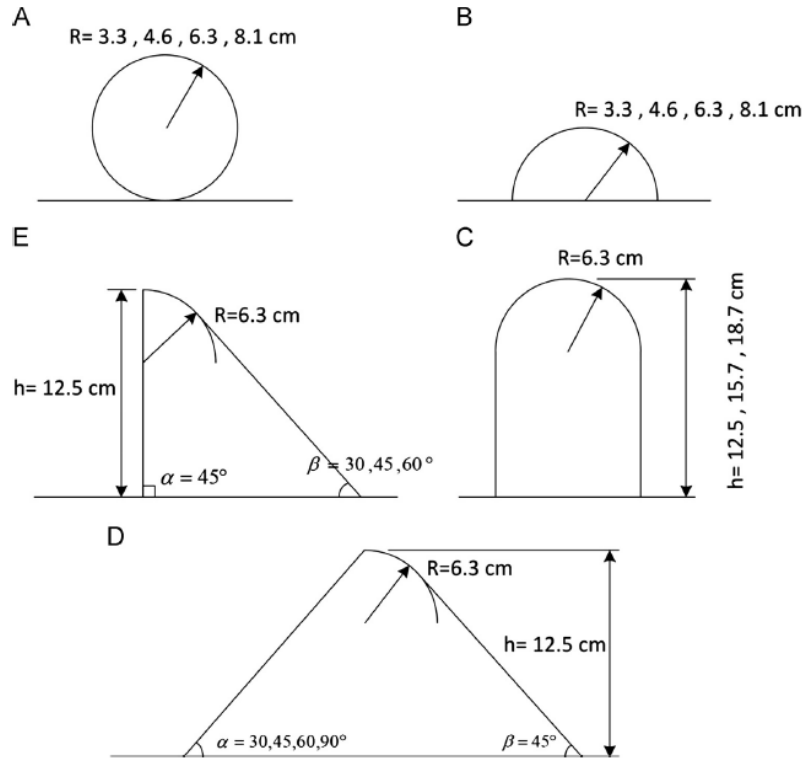


Figure 2.33 Cylindrical weir and circular crested weirs investigated (Shabanlou *et al.*, 2013)

In the study undertaken, both cylindrical and circular crested C_d increased with an increase in head. The upstream slope also has no influence on the C_d in both cases and partial energy loss occurs on both weirs, however it was noted that the energy loss was greater for the cylindrical weirs. Increasing the downstream slope on the weirs, consequently increases the energy losses. The study also conclude that in both cases, cylindrical and circular crested weir, the crest flow depth is equal to 0.7. However, increasing the upstream slope increased the partial crest flow depth at values greater than 0.6 marginally. The downstream slope angle only affected the flow depth and did not affect the crest flow depth. Shabanlou *et al.* (2013) in the study of the weirs used the C_d for a sharp crested weir equation 2.9:

$$C_d = \frac{q}{(2/3)\sqrt{(2/3)gH_1^2}} = f\left(\frac{H_1}{R}\right) \dots\dots\dots 2.9$$

Figure 2.34 show the variation of the C_d with the ratio $\frac{H_1}{R}$ of both the cylindrical and circular crested weir.

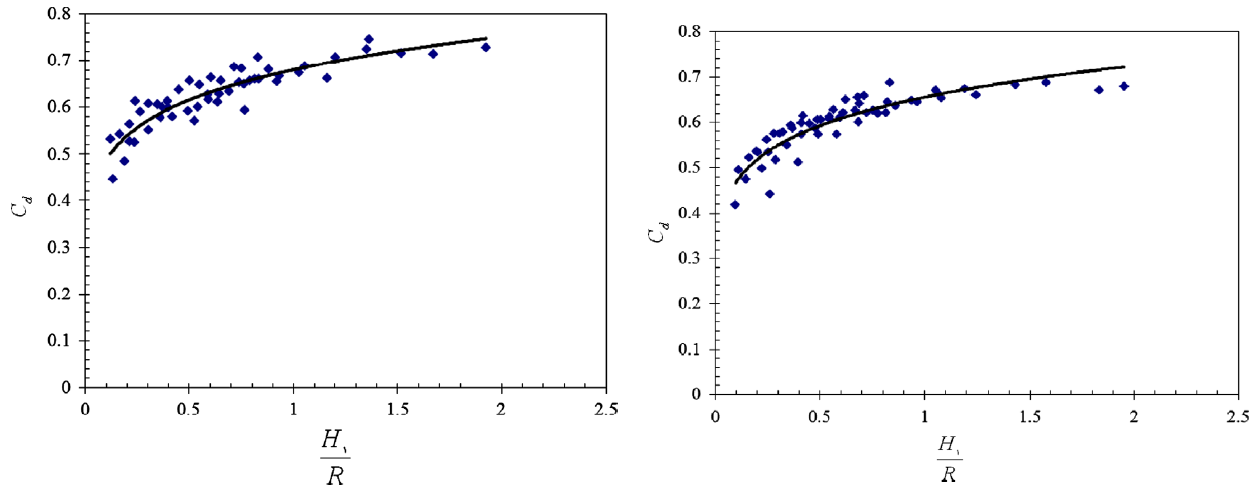


Figure 2.34 Variation of C_d with the ratio $\frac{H_1}{R}$ for cylindrical weirs and half-shaped cylindrical weirs respectively

The experimental data was fitted to give the two relations respectively with $R^2 = 0.8$ in both cases are were given by equation 2.10 and 2.11:

$$C_d = 1.185 \left(\frac{H_1}{R}\right)^{0.146} \dots\dots\dots 2.10$$

$$C_d = 1.135 \left(\frac{H_1}{R}\right)^{0.146} \dots\dots\dots 2.11$$

Shabanlou *et al.* (2013) also concluded that the height of the weir marginally increases the C_d for the group C weir (shown in Figure 2.33) heights of 187mm, 156.7mm and 125mm and for cylindrical and half-cylindrical weirs height of 63mm as seen in Figure 2.35.

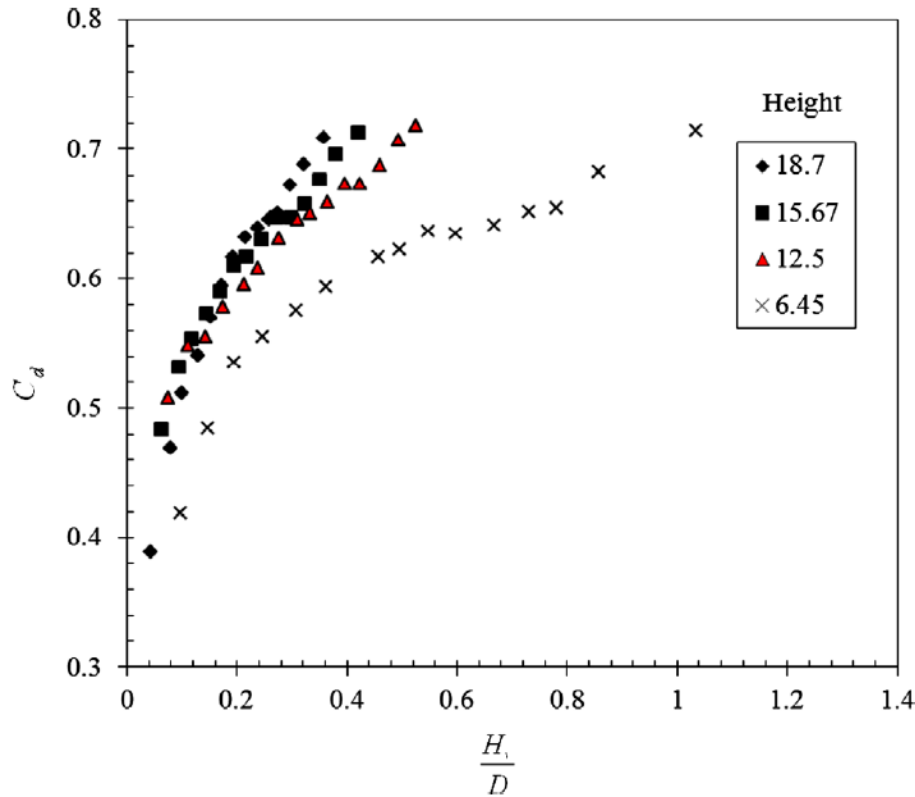


Figure 2.35 Effect of height on weir discharge (Shabanlou *et al.*, 2013)

7. Alhamati *et al.* (2005)

Alhamati *et al.* (2005) conducted an experiment on an air inflated and water-filled inflatable weir with different internal pressures with a fixed head and the converse. Discharge over the inflatable weirs was measured using a rectangular sharp crested weir and the C_d was calculated based on Anwar (1967) sharp crested weir equation, $C_d = \frac{q}{\sqrt{2gH^{1.5}}}$ considering $H \approx H_w$. On plotting C_d against H/D_h from the experimental data, a best fit was obtained from the data giving an empirical equation for $R = 0.94$ for the air inflated weir:

$$C_d = 0.5066 (H/D_h)^{0.2447} \dots\dots\dots 2.12$$

In an earlier study by Anwar (1967) similarly developing an empirical equation, he found that, $C_d = 0.4866(H/D_h)^{0.11}$ and $C_d = 0.4338(H/D_h)^{0.0649}$ from the experimental data obtained for an air and water inflated dam respectively. Alhamati *et al.* (2005) found that the data obtained from the tests conducted was similar to that of Anwar (1967) and this was explained by the fact that

an inflatable weir at low pressure acts like a broad crested weir compared to the same inflatable weir at a high internal pressure with the same overflow conditions. Figure 2.36 shows a graphical representation of study by Alhamati *et al.* (2005) and the other, comparing earlier studies for an air inflated weir.

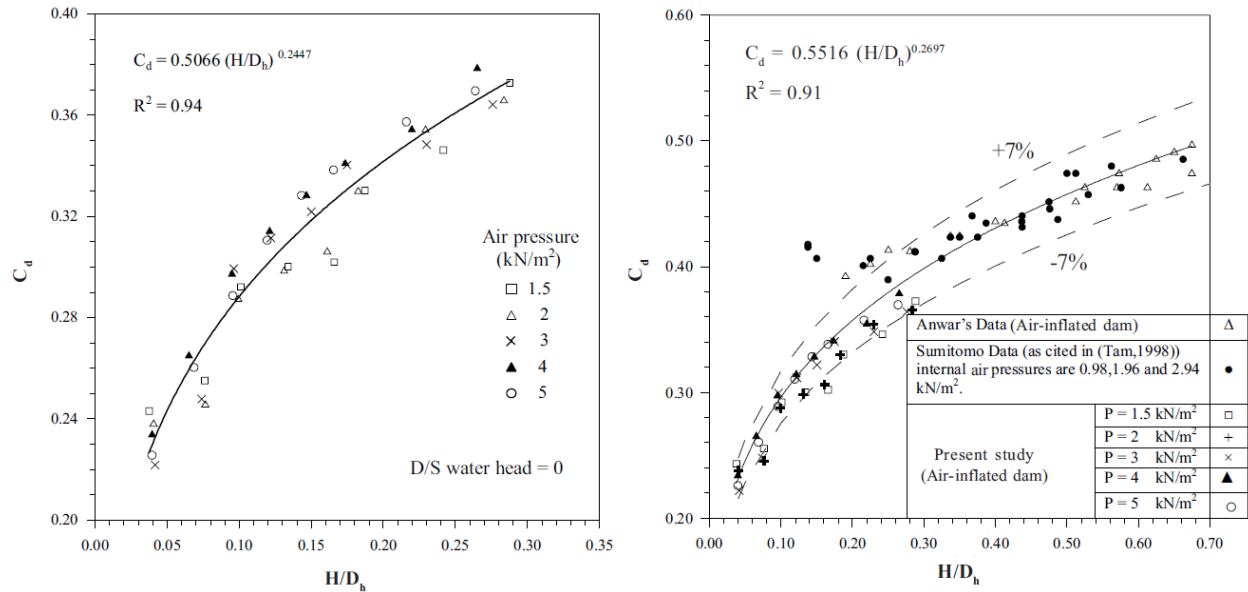


Figure 2.36 C_d with the ratio H/D_h for study by Alhamati *et al.* (2005) and a comparison with the earlier studies (Alhamati *et al.*, 2005)

Data sets by Alhamati *et al.* (2005) covered a smaller range as compared to the earlier studies and all the combined studies gave another empirical equation, $R^2 = 0.91$:

$$C_d = 0.5516 (H/D_h)^{0.2697} \dots\dots\dots 2.13$$

8. Abdul-latif *et al.* (2010)

Abdul-latif *et al.* (2010) conducted an experiment on the evaluation of the C_d for three different weir radii, 40mm, 600mm and 70mm, for a semicircle shape as shown in Figure 2.37.

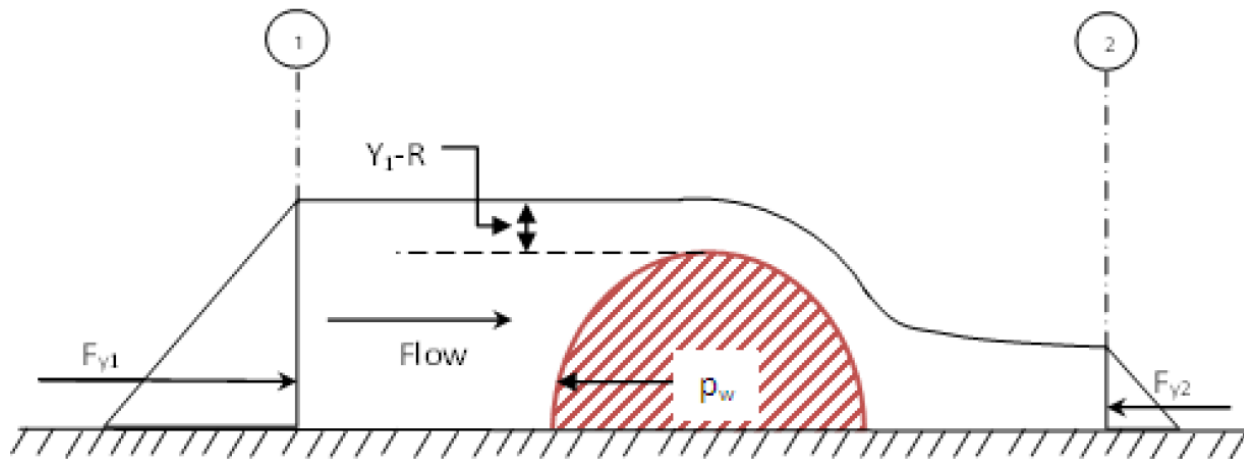


Figure 2.37 Experimental set up during investigation Abdul-latif *et al.* (2010)

For each weir radii tested, there was an empirical equation developed from the measured data approximating $H \approx H_w$, fixing the exponential term giving $q = 1.7468H^{1.5}$, for the 400mm radius of curvature, $q = 2.189H^{1.5}$ for the 600mm radius of curvature and $q = 2.1747H^{1.5}$ for the 700mm radius of curvature. From the study conducted, it was conclusive that the C_d was proportional to head above the crest and inversely proportional to the radius of curvature. Figure 2.38 show the findings of the test conducted.

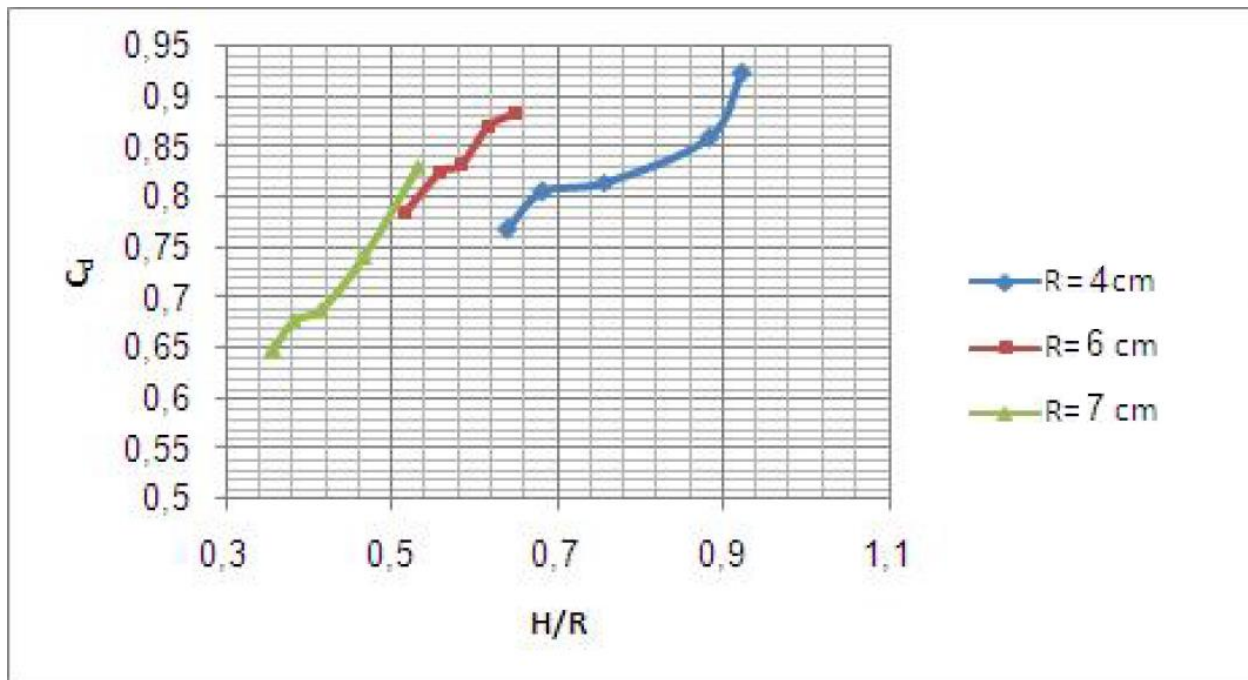


Figure 2.38 C_d against H/R (Abdul-latif *et al.*, 2010)

2.5.4 Summary of C_d values of circular weirs from literature

A summary of the experimental and theoretical C_d values of circular/cylindrical weirs as obtained from literature (all based on the broad crested weir formula) versus $\frac{H_w}{R}$ is presented in Figure 2.39.

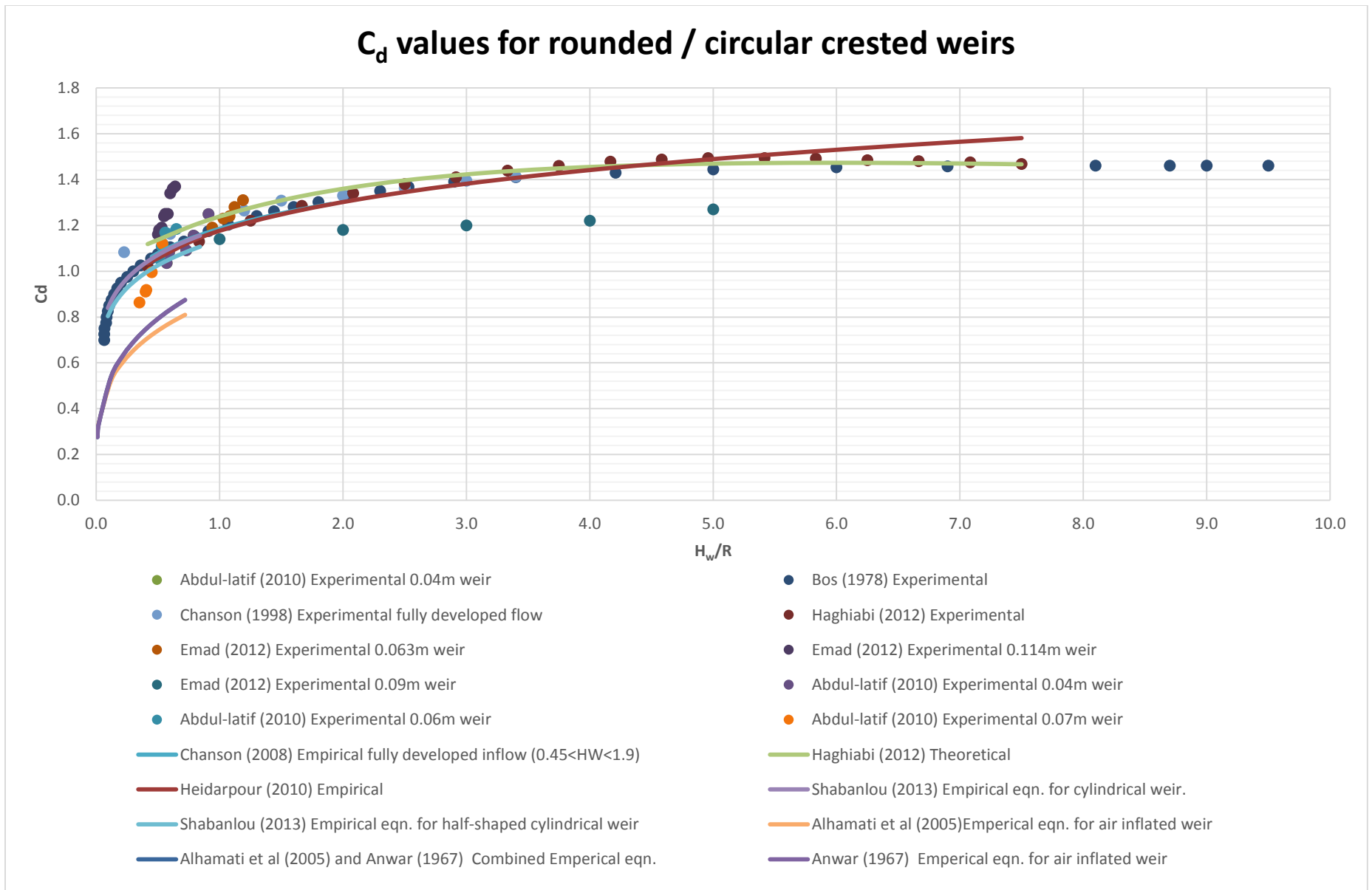


Figure 2.39 Summary of C_d values for rounded / circular crested weirs from literature

2.5.4 Pressure distribution over weir

In the study of pressure acting on circular weirs during overflow, most studies are centered on the pressure right at the weir crest ($\theta = 0^\circ$). A study by Chanson (1997) has considered the pressure on the weir crest and the downstream weir face. These studies by different authors are delineated below.

2.5.4.1 Abdul-latif *et al*, 2010

Since there are significant pressure differentials that are experienced on the face of hydraulic structures of a curved nature due to the overflow water and forces induced by constituents of the over flow waters, there is need for knowledge in the variation of the pressure on the weir crests in the design process. When considering the vertical plane of the effect of the stream line curvature, there is an incremental decrease in pressure distribution as the water flows past the hydraulic structure. Due to the convex shape involved, there is a tendency to have a fall in pressure to that below the hydrostatic pressure (Abdul-latif *et al.*, 2010). This pressure differential could be found analytically or experimentally with sensors, as used in this study. In Abdul-latif's study in which he used net analysis, he discovered that the ratio between forces acting on the downstream weir surface that counteracts the pressure force acting on upstream weir surface has a resultant force of approximately 0.5. Figure 2.40 shows the pressure over a rounded crest weir.

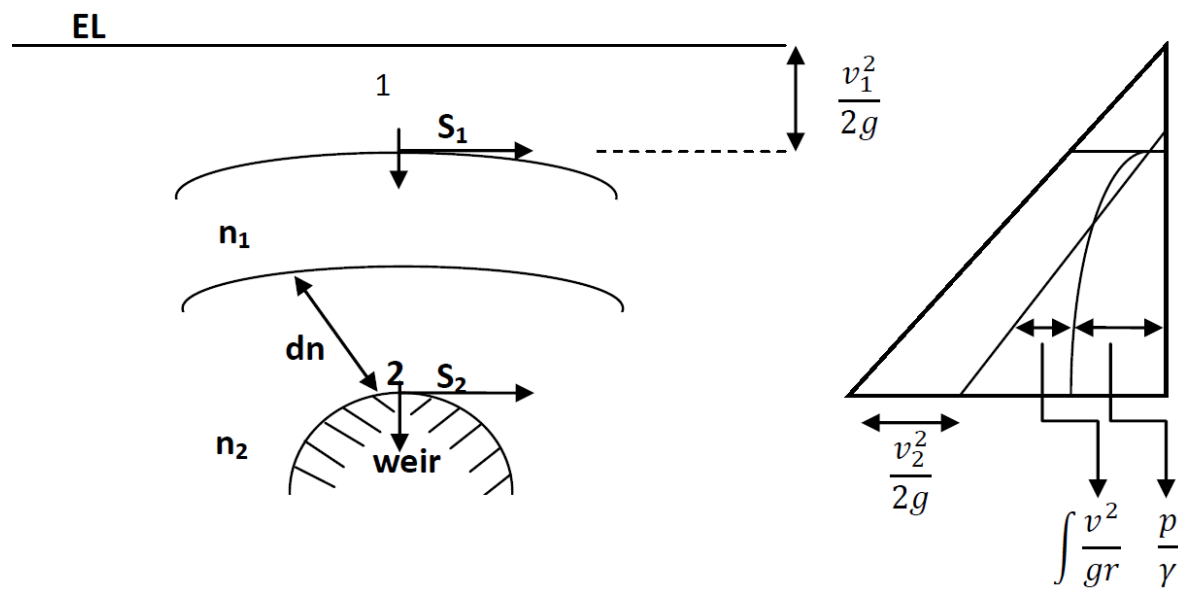


Figure 2.40 Convex flow pressure distributions (Abdul-latif *et al.*, 2010)

In effect, the upstream forces were twice the downstream forces in all the tests undergone with weir models. Abdul-latif *et al.* (2010) concluded that the pressure acting force per unit width acting on the weir surface which is in the equal and opposite direction to force exerted by weir on block of water is calculated as $P_w = \frac{1}{2}\gamma(y_1 - R + y_1)\frac{R}{2} = \frac{\gamma R}{4}(2y_1 - R)$, where y_1 is upstream flow depth and γ water specific weight. The absence of hydrostatic pressure and the nappe adherence on the weir surface makes the C_d for weirs to be more than one as a result of the shape which offers velocity distributions and pressure differentials. Abdul-latif *et al.* (2010) concluded that when considering a flow path in the center of the weir, in the vertical plane, flow is subject to normal acceleration and, in addition, to tangential acceleration owing to the curved surface. As a result, the flow velocity close to the weir is faster than that on the outer part of the flow along the same plane, and this causes a decrease in the discharge coefficient and an increase in the radius of curvature as seen in Figure 2.41.

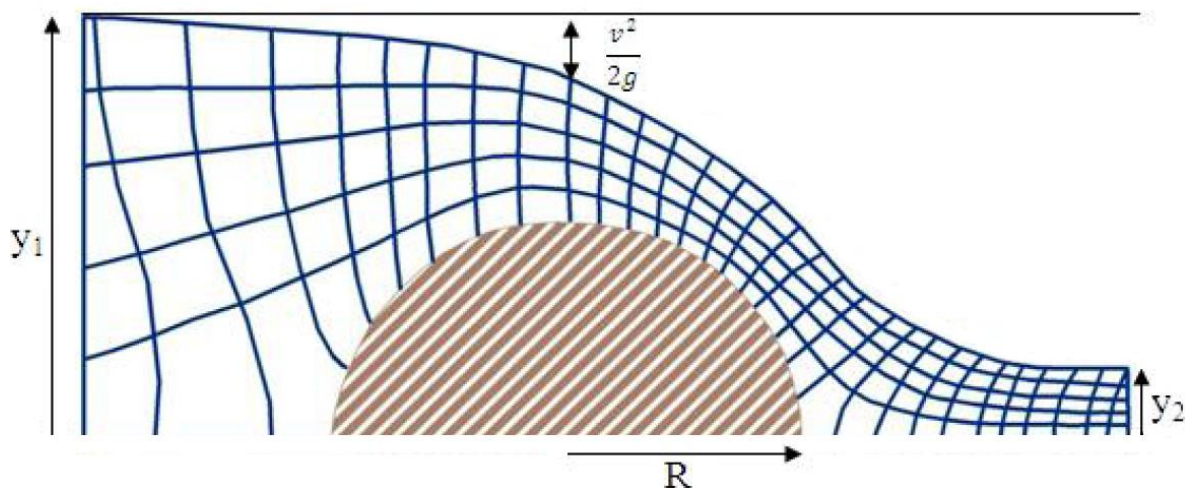


Figure 2.41 Flow-net schematic diagram for weir (Abdul-latif *et al.*, 2010)

In effect, for a vertical plane in the center of the weir crest with a radius R , there will be a component of acceleration in respect of the curvature of the form V^2/R . This will exhibit a maximum at the point close to the surface of the weir and a minimum on the outer surface of the flowing water.

2.5.4.2 Bos (1978)

Bos (1978) in his studies concluded that if the ratio H_w/R is small, the pressure on the weir crest is maintained positive. As the ratio H_w/R increases, the pressure on the weir face decreases

until it becomes negative but consequently increases the C_d . The minimum pressure on the weir face was determined as $\frac{P}{\rho g} = H_1 - (H_1 - y) \left(\frac{r + ny}{r} \right)^{\frac{2}{n}}$ where $n = 1.6 \cdot 0.35 \cot \alpha$ with y being the crest depth approximated $0.7H_1$ at negligible approach velocity. Figure 2.42 shows the minimum pressure experienced at a weir, with the approximation by former equation.

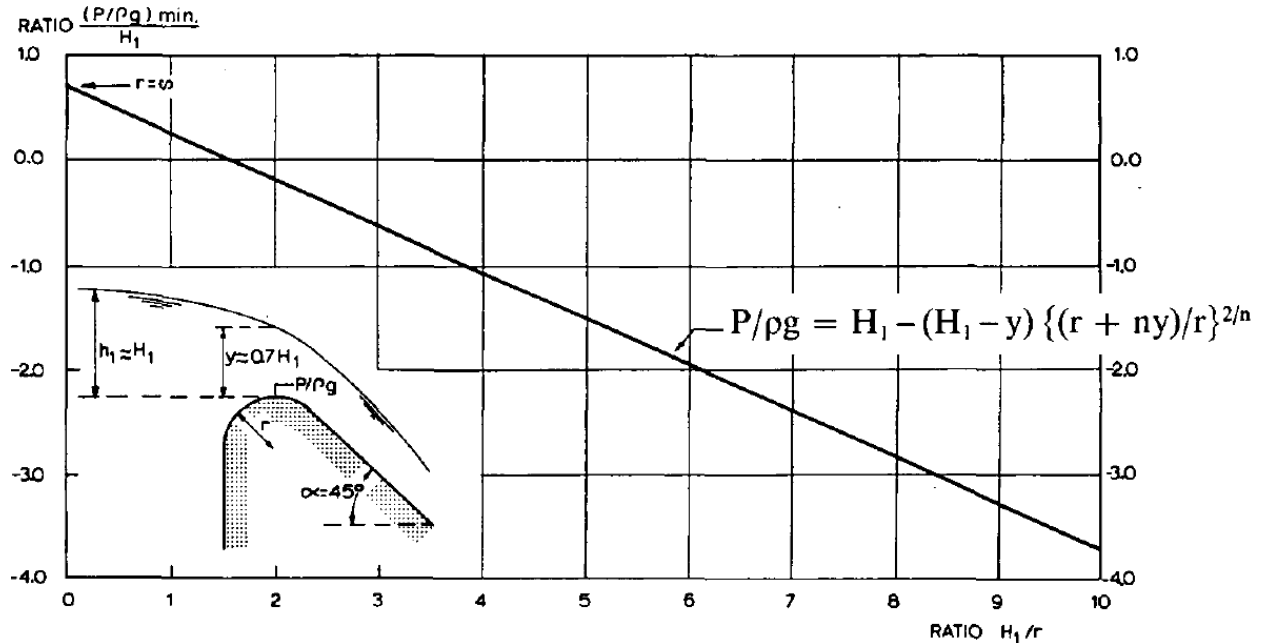


Figure 2.42 Pressure distribution for a 1:1 sloping downstream face Bos (1978)

2.5.4.3 Haghiabi (2012)

Haghiabi (2012) in the use of the Dressler theory obtained the pressure profiles on the circular weir. He defined pressure over the weir crest as:

$$\left(\frac{P}{\gamma}\right)_y = H_1 - y - 0.29H_1 \frac{\left(\frac{y}{R}\right)^2 \left[1 + \frac{y}{R} - 1\right]}{\left(1 + \frac{y}{R}\right)^4 \left[\ln\left(1 + \frac{y}{R}\right)\right]^3} \frac{Z^4 [\ln(Z)]^3}{(z-1)^2 (Z^2 - 1)} \dots\dots\dots 2.14$$

Where $z = 1 + 0.71 \frac{H_1}{R}$

In a series of test in the conducted experiments, Haghiabi (2012) clearly shows the ratio of y against $\left(\frac{P}{\gamma}\right)_y$ as seen graphically in Figure 2.43

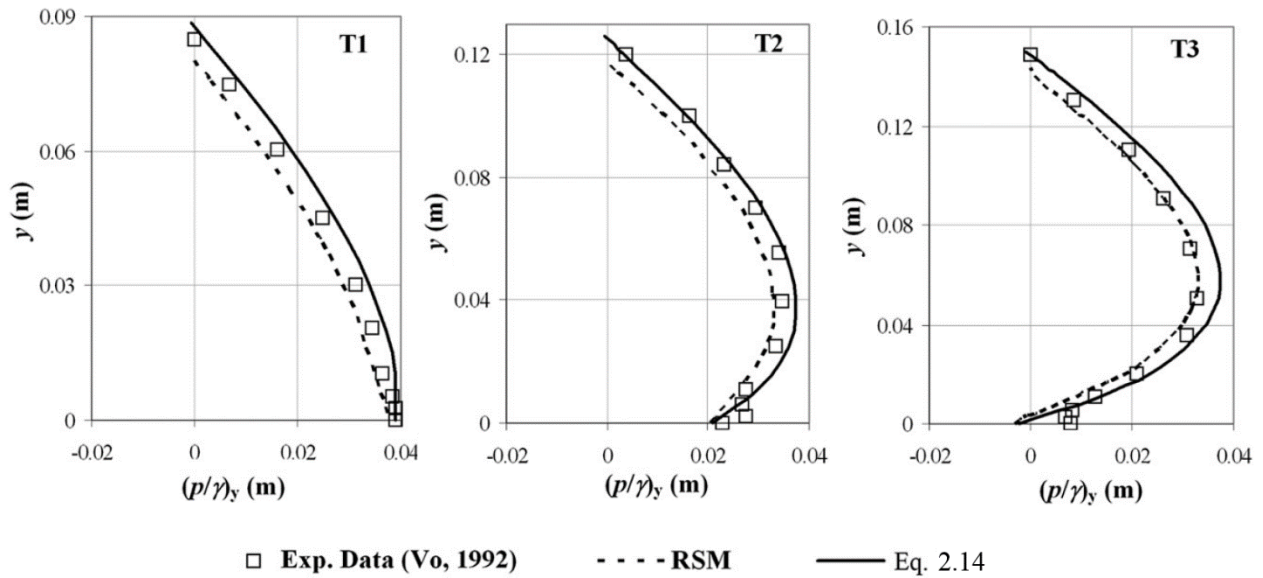


Figure 2.43 Decreasing ratio y against $\left(\frac{P}{\gamma}\right)_y$ (Haghiabi, 2012)

The plotted experimental data showed agreed with the prediction equation developed for the crest profile. Ramamurthy *et al.*, (1992) as cited by also showed that ratio y against $\left(\frac{P}{\gamma}\right)_y$ as seen in Figure 2.44.

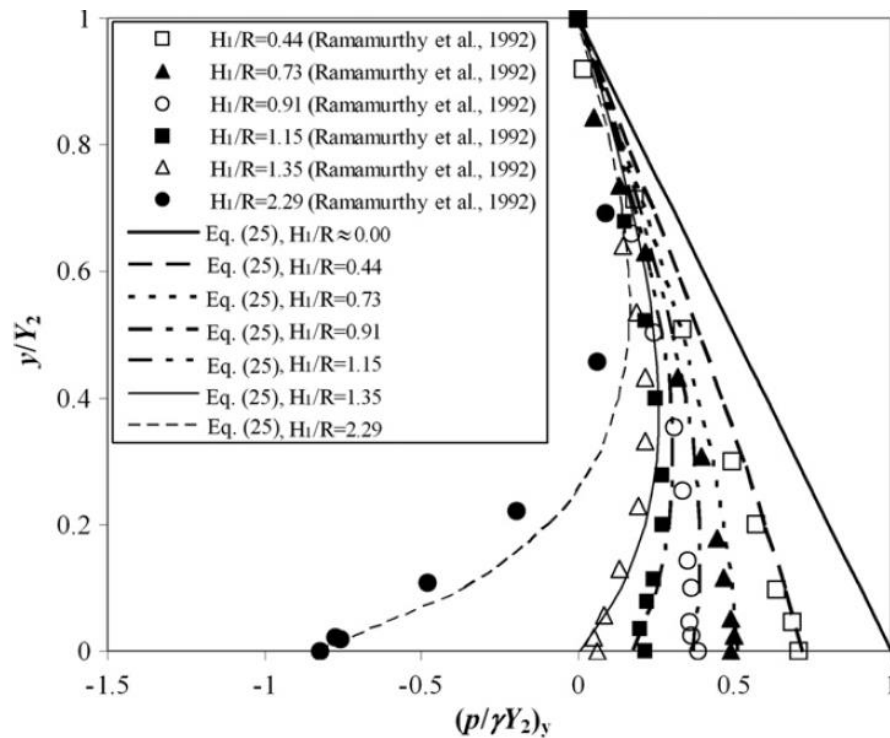


Figure 2.44 Decreasing ratio y against $\left(\frac{P}{\gamma}\right)_y$ (Haghiabi, 2012)

2.5.4.4 Chanson (1997)

Chanson (1997) deduced the overflow pressure above the inflatable dam membrane from the motion equation. This equation best describes the pressure over the downstream of the weir faces of the circular weir, is given by:

$$\frac{P_{atm}-P_s}{\rho_w g R} = \frac{d}{R} \left(F^2 \cos \Phi \left(1 + \frac{d}{2R} \right) \right) \dots\dots\dots 2.15$$

where P_{atm} – atmospheric pressure (kg. m. s⁻²)

P_s – cylinder surface absolute pressure and (kg. m. s⁻²);

d – nappe thickness (m)

Equation 2.15 gives the theoretical sub atmospheric wall pressure as investigated when the centrifugal forces become larger than the gravity component, such that $P_s < P_{atm}$. Figure 2.45 explains the over flow on the inflatable dam membrane as described in equation above.

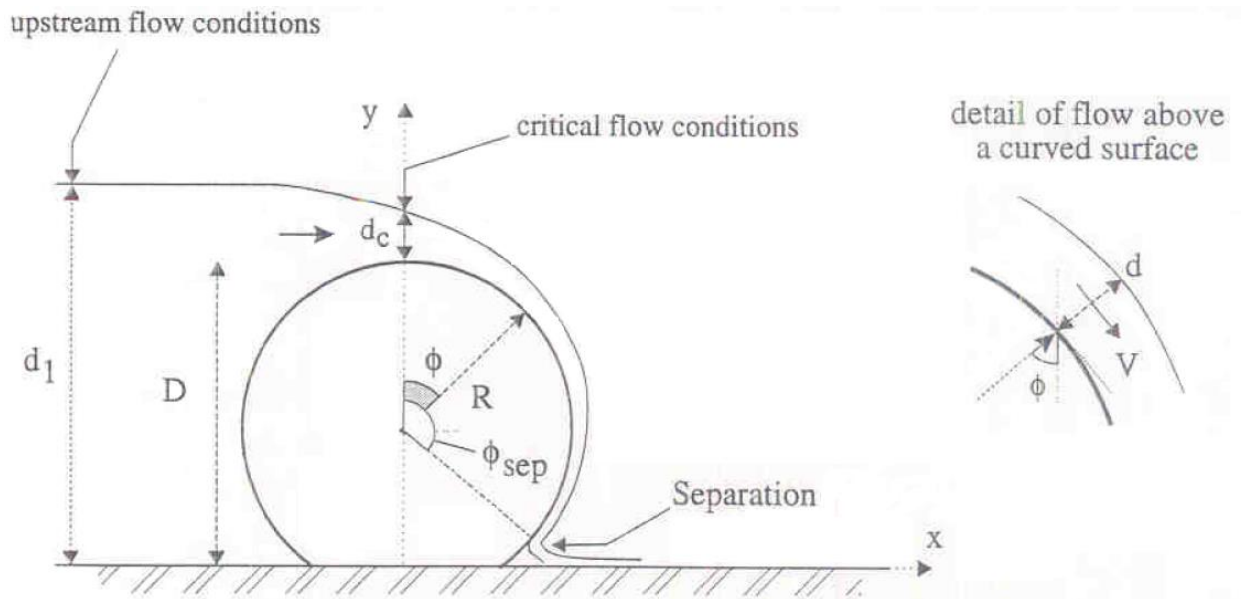


Figure 2.45 Over flow on the inflatable dam membrane (Chanson, 1997)

In the lower quadrant $90^\circ < \phi < 180^\circ$ the gravitational force adds to the component of the centrifugal force of the curvature of the weir. Chanson (1997) in his study noted that the in process of deflation, the dam membrane must not be located in the region of low mean and

instantaneous mean pressure resulting in the up lift of the membrane. Stability of the weir is achieved by installing it in a region of pressure larger than the hydrostatic. Figure 2.46 shows the pressure distribution on weir as investigated by Chanson from equation 2.15.

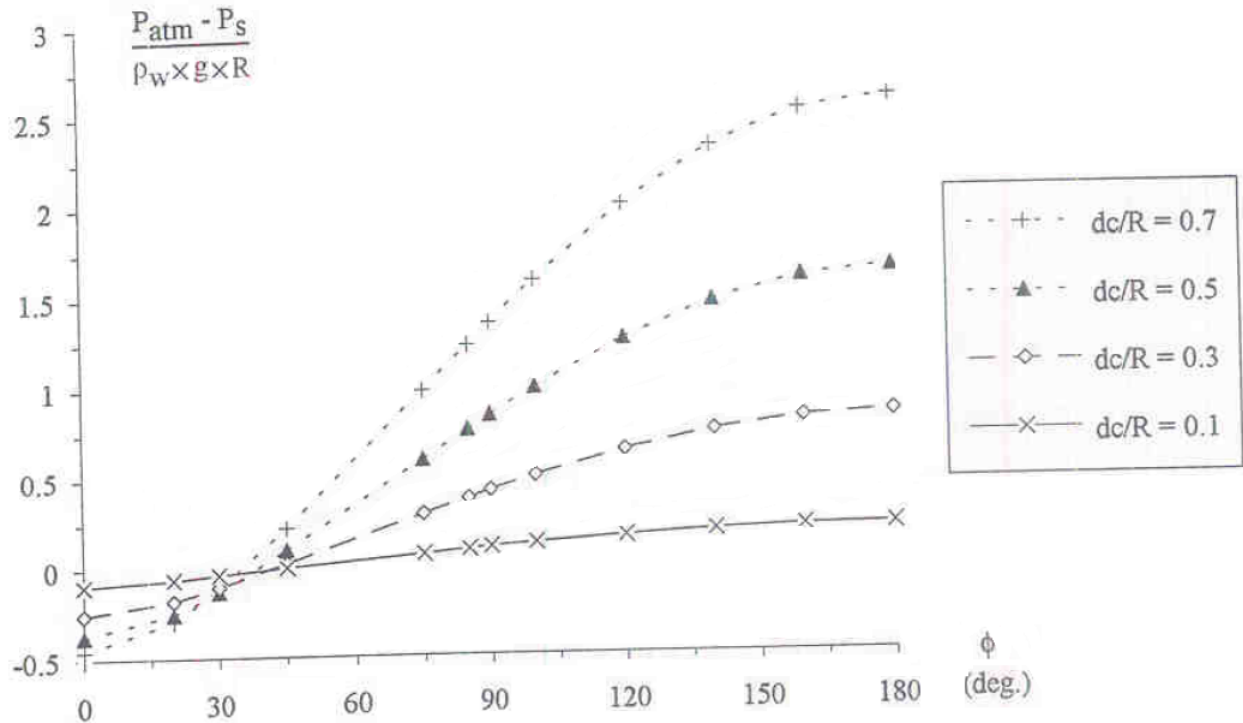


Figure 2.46 Pressure on the downstream face of weir from weir crest (Chanson, 1997)

2.5.5 Flow depth at the crest and critical flow over weir

The influence on the C_d done by the channel geometry and force causing flow patterns is measured by the dimensionless ratios that can be obtained from the measured experimental data. The crest flow depth at critical conditions under hydrostatic pressure distribution was expressed by Chanson (1998) as $d_c = \sqrt[3]{\frac{2q^2}{g}}$. Due to the curvature of the weir crest, the pressure is less than hydrostatic pressure and velocity is varied over the crest weir as the water flows over the weir. Using different cylinder sizes in his experiments, he showed that there is a decrease in the ratio d_{crest}/d_c against H_w/R as seen graphically below. In this experiment, the data was correlated by equation 2.16 and a normalised correlation coefficient of 0.844 was found.

$$d_{crest}/d_c = \frac{0.85}{1 - 0.31 \times e^{(-2 \times H_w/R)}} \dots\dots\dots 2.16$$

Where

$$0.02 \leq H_w/R \leq 2.63m \text{ and } 0.042 \leq R \leq 0.117 m$$

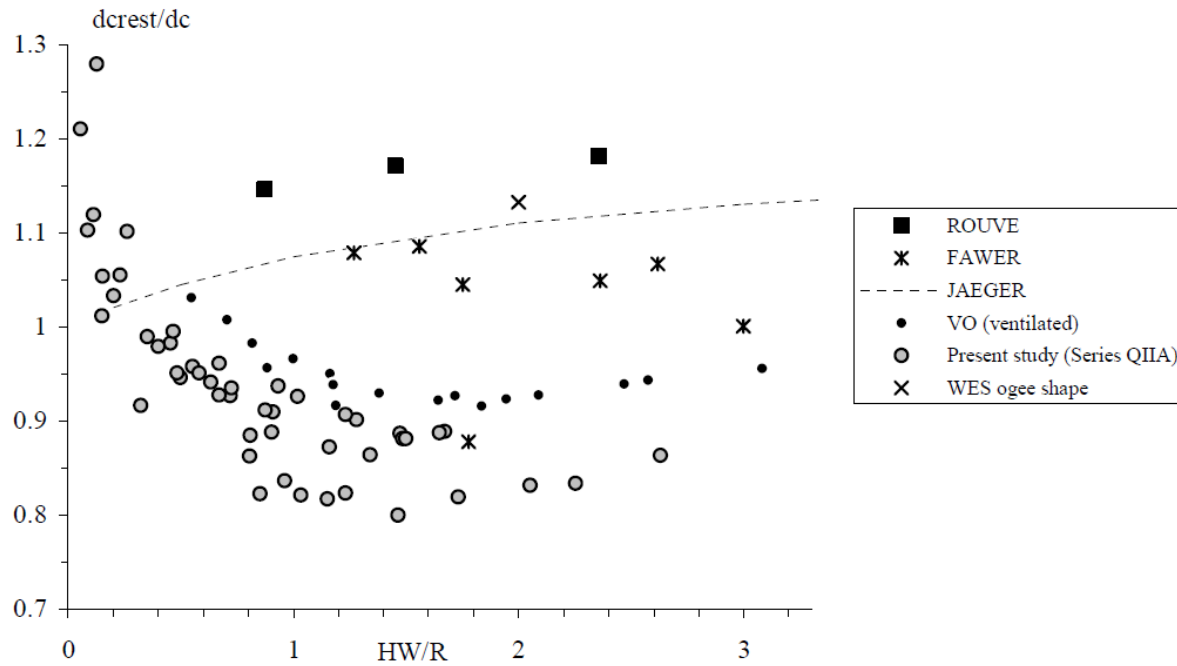


Figure 2.47 Dimensionless flow depth at circular weir crest (Chanson, 1998)

In the experiments conducted, the weir radius had an influence on the flow depth with the fully developed inflow only.

Critical flow over circular weir

Orgaz *et al.*, (2008) found that the critical flow principle was useful in the analysis of the overflow on the circular crested weirs. He analysed the stream line curvature over the weir by comparing the experimental data with the approximations deduced. The study concluded showed that as the water flows over the weir, C_d increases with the increase in the relative head (E/R) due to the rounded weir crest. At the same time the increase in the flow velocities results in the consequent decrease in relative depth as E/R increases. The rounded crest weir flow is critical when the normalized specific energy E/R is within the range 0.5 and 0.6 and, at large heads, flow becomes supercritical. Total energy head was described by Orgaz *et al.*, (2008) as given by $H_0 = z + y + \frac{V^2}{2g} = z + E$. Figure 2.48, shows the critical flow over the weir.

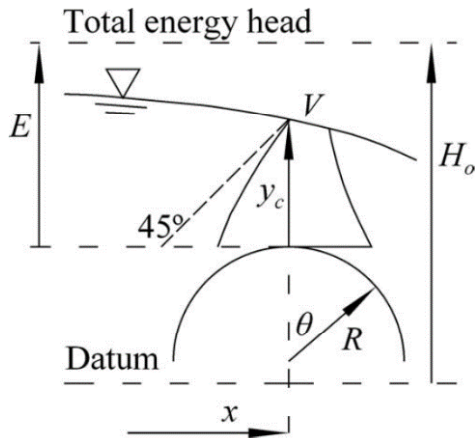


Figure 2.48 Critical flow for curvilinear flows (Orgaz *et al.*, 2008)

Due to potential and kinetic energy in the flow, the head remains constant anywhere inside the flow field. Then the differential energy yields zero such that $\frac{dz}{dx} + \frac{dy}{dx} + \frac{v dv}{g dx} = 0$. With unit weir discharge being given by $q = VH$ and taking into account the correction coefficient for curvilinear flow and backwater equation, Orgaz *et al.* (2008) defined the specific energy for critical flow as follows:

$$E = y_c + \frac{q^2}{2gH_c^2} = y_c \left[1 + \frac{1}{2C} y_c H_c \right] = \delta y_c \dots \dots \dots 2.17$$

and $\delta = \frac{E}{y_c}$

with $q = C_d (gE^3)^{\frac{1}{2}} \dots \dots \dots 2.18$

Curvilinear flow theories from former studies gave good fits for the described equations where $n = 2$ and $k = 0.6$ are parameters in the Fawer theory and $m = 2$ is also a parameter in the Jaeger theory. These are shown in table 2.2

Table 2.2 Concepts for curvilinear flow over rounded crest weirs

Author	Hypotheses	Equations
Fawer (1937)	Irrotational flow. Potential variation of curvature of streamlines.	$H=y\left[1+\frac{y}{2R}-\frac{n}{2+k}\frac{(y/R)^2}{1+n(y/R)}\right]$
Jaeger (1956)	Irrotational flow. Linear variation of radius of curvature of streamlines.	$H=\frac{R}{m-1}\left(1+\frac{my}{R}\right)^{1/m}\left[\left(1+\frac{my}{R}\right)^{1-1/m}-1\right]$
Dressler (1978)	Irrotational flow. Perturbation expansion to first order of Euler equations. Equivalent to free vortex.	$H=(R+y)\ln\left(1+\frac{y}{R}\right)$
SCM, Chanson (2002)	Uniform horizontal velocity. Constant centrifugal acceleration.	$E=y+\frac{q^2}{2gy^2}\left(1-\frac{2y}{R}\right)$
Matthew (1963), Hager (1985)	Irrotational flow. Linear variation of curvature and inclination of streamlines.	$C=1-\frac{y_c}{R}E=y_c+\frac{q^2}{2gy_c^2}\left(1-\frac{22y_c}{27R}\right)$
Matthew (1991)	Irrotational flow. Iterative expansion of Picard of the stream function to third order.	$\delta=\frac{E}{y_c}=\left(\frac{2}{3}+\frac{34}{1029}\frac{E}{R}\right)^{-1}C_d=0.5443\left[1+\frac{E}{R}\left(0.2716-0.0453\frac{E}{R}\right)\right]$

Note: SCM=simple centrifugal model.

Orgaz *et al.* (2008) also established a relationship of C_d of the circular weir and Froude number at the weir crest with the critical depth for uniform velocity, $y_{cu} = \left(\frac{q^2}{g}\right)^{\frac{1}{3}}$, with hydrostatic pressure distribution. $y_{cu} = y_c$ for parallel flow lines where $R = 0$ and $\alpha = \frac{y}{H}$ for the dimensionless critical depth. Below are some equations on theories of the approximated curvilinear flow and the results obtained by Orgaz *et al.* (2008) on dimensionless critical weir depth and discharge at crest.

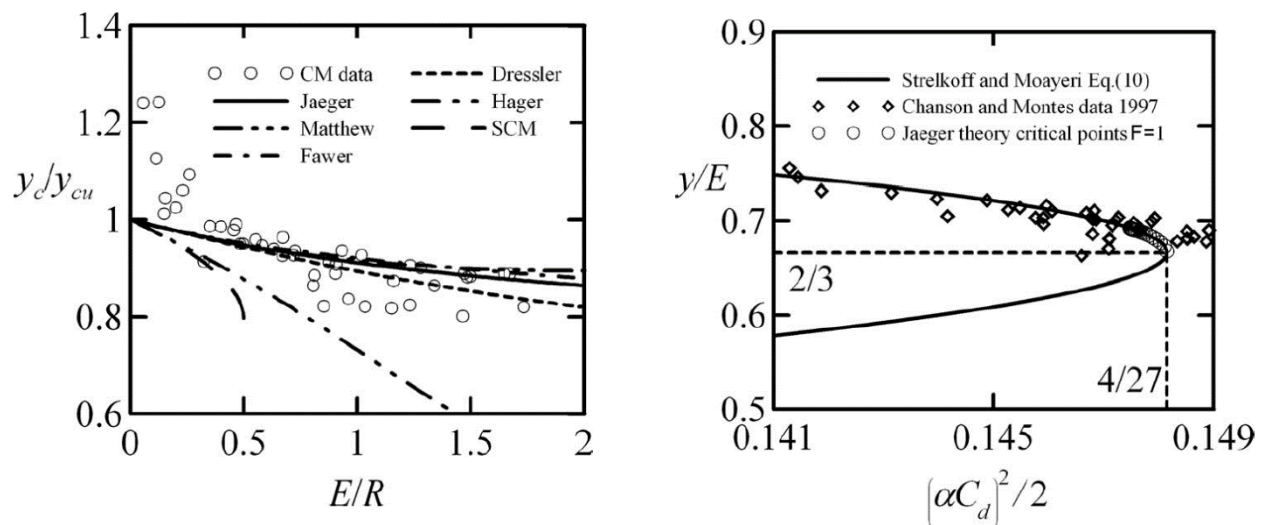


Figure 2.49 Dimensionless critical weir depth (left Figure) and discharge at crest (right Figure) (Orgaz *et al.*, 2008)

2.5.6 Energy loss over weir crest

Shabanlou *et al.* (2013) found that in the studies conducted, generally, the energy loss over the weir decreased with the increase in the head water. With the experiments conducted, it was found that increasing the downstream face slope of the weir increases the head loss. In these two scenarios, head loss is mainly attributed to the shear stresses in the stream lines of the flowing water due to its viscosity. This phenomenon was also seen by Kang (2014) in the study of flow characteristics in sloping weirs. Chanson (1998), also concluded that the flow over a circular weir could be considered to be similar to that of a drop structure with the same height. Other researchers, like Rand (1955), validated this argument for a range $0.045 < \frac{d_c}{D} < 1$ for the equivalent drop structure with the comparison of tests as seen in Figure 2.50, and expressed the estimation of the dimensionless head loss as

$$\frac{\Delta H}{H_1} = 1 - \left(\frac{0.54 \times \left(\frac{d_c}{D}\right)^{0.275} + 1.71 \left(\frac{d_c}{D}\right)^{-0.55}}{1.5 + \frac{D}{d_c}} \right) \dots\dots\dots 2.19$$

Where $\Delta H = H_1 - H_2$

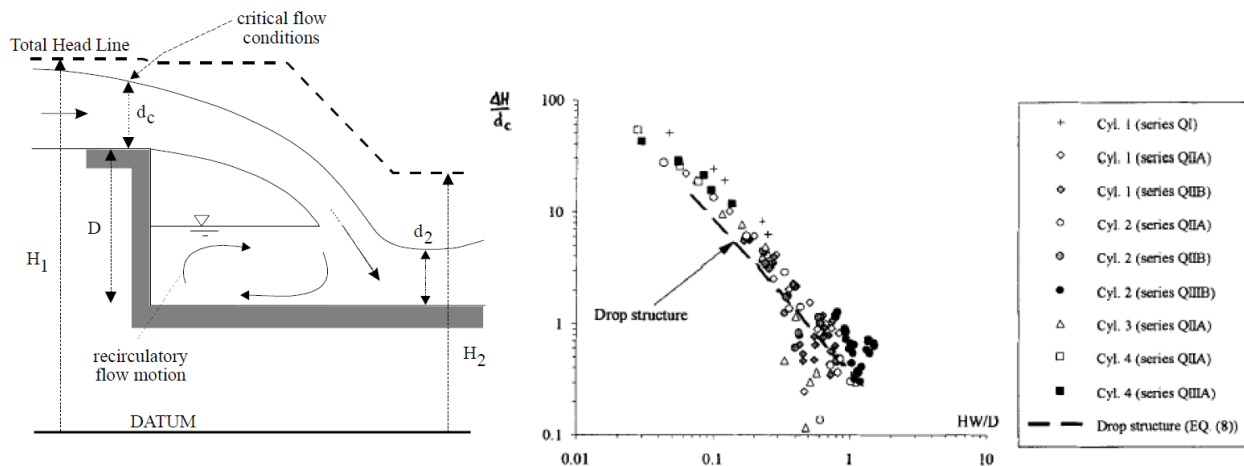


Figure 2.50 Equivalent drop structure and the comparison to the circular weir (Chanson 1998)

The graphical comparison by Chanson (1998) showed that the energy dissipation was increasingly low with increasing weir crest head. The energy loss over weir crest by Chanson (1998) is shown in Figure 2.51.

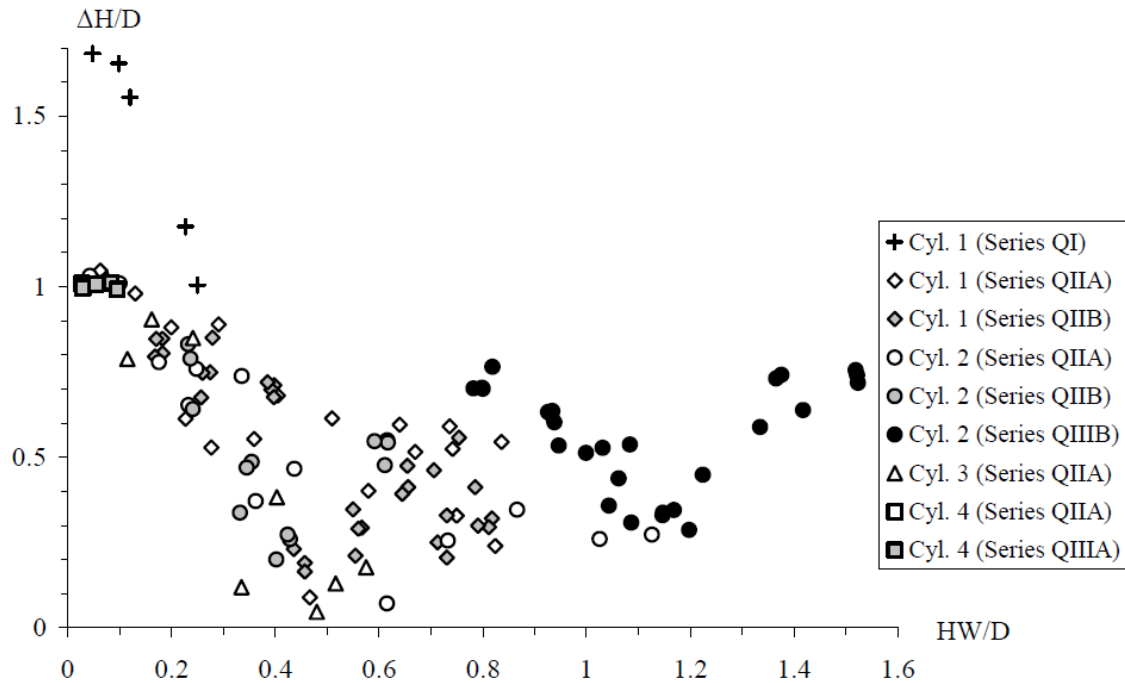


Figure 2.51 Energy loss over weir crest Chanson (1998)

2.5.7 Energy dissipation and jump length on the downstream of weir

The hydraulic jump in effect is the instantaneous raise in the water levels with decrease in the flow velocity. This phenomenon occurs when water is abruptly stopped, slowed and undergoes a sudden change of depth. Figure 2.52 gives the definition of the hydraulic jump.

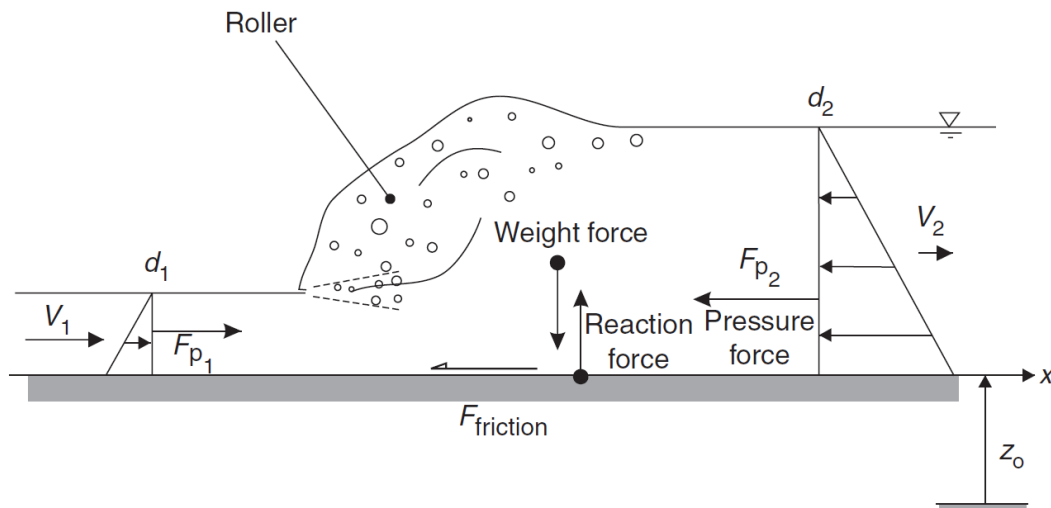


Figure 2.52 Hydraulic jump definition (Chanson, 2004)

When the speed of the flowing fluid is below critical no jump formation occurs, but the flow forms undulating waves. Increasing the flow speed of water will reach a point wherein the transition in

the fluid becomes abrupt and it curls up, forming a jump. When this takes place, air entrapment, eddy currents, violent turbulence and surface waves occur. In essence, the general use of a hydraulic jump is for the energy dissipation in water flowing over a hydraulic structure, in this instance, the weir.

In the occurrence of the hydraulic jump, there are three possibilities of its formation as seen in Figure 2.53:

1. The ideal case when $y_1' = y_2$;
2. When jump moves downstream such that $y_1' > y_2$ and;
3. When the jump moves upstream with $y_1' < y_2$.

Figure 2.53 illustrates the formation of a jump.

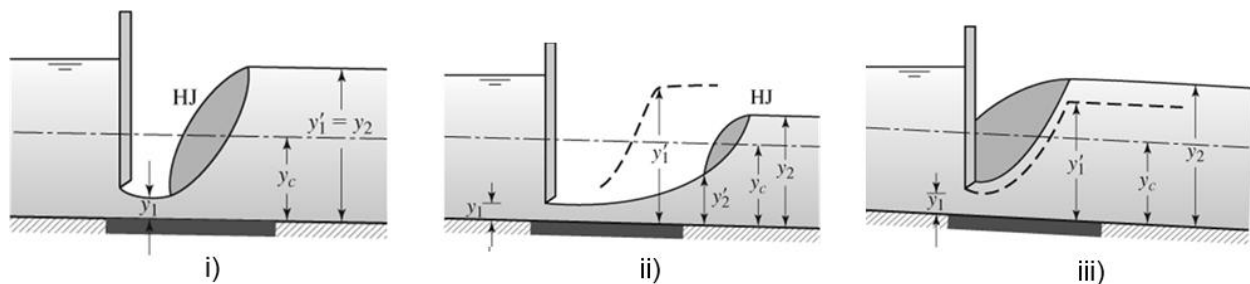


Figure 2.53 Cases of the formation of a hydraulic jump (Cruise, 2007)

Assuming negligible air entrainment, hydrostatic pressure distributions, and uniform velocity and applying the momentum equation, the Belanger equations for the sequent depth of a hydraulic jump can be used to describe the hydraulic jump. Figure 2.54 depicts the types of hydraulic jumps and tabulated in table 2.3 according to Finnemore (2002).

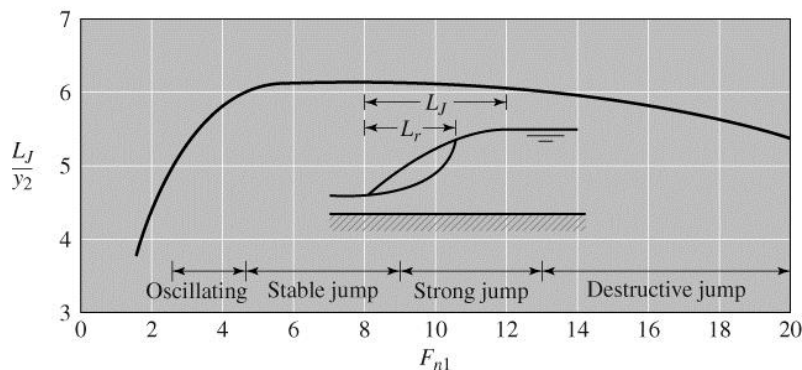
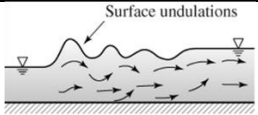
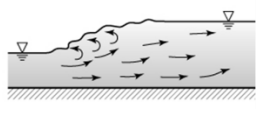
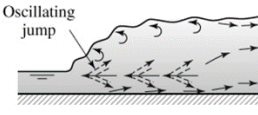
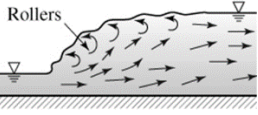
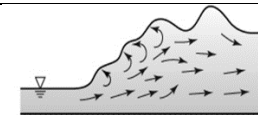


Figure 2.54 L_j/y_2 against Froude number (Cruise, 2007)

Table 2.3 Types of Hydraulic Jumps (Finnemore, 2002)

Name	Froude's Number	Energy dissipation	Characteristics
Undular Jump	1.0-1.7	<5%	Standing waves 
Weak Jump	1.7-2.5	5-15%	Smooth rise 
Oscillating Jump	2.5-4.5	15-45%	Unstable; avoid 
Steady Jump	4.5-9.0	45-70%	Best design range 
Strong Jump	> 9.0	70-85%	Choppy, intermittent 

The Belanger equation for the sequent depth of a hydraulic jump considers the conservation of the momentum in the upstream depth y_1 and downstream depth y_2 for a specific discharge. A relationship exists, in which the two are related as well as the Fr and critical depth y_c as expressed in equation 2.20, 2.21 and 2.22:

$$y_2 = \frac{y_1}{2} \left[-1 + \sqrt{1 + \frac{8q^2}{gy_1^3}} \right] \dots\dots\dots 2.20$$

$$y_2 = \frac{y_1}{2} \left[-1 + \sqrt{1 + 8Fr_{n1}^2} \right] \dots\dots\dots 2.21$$

$$y_2 = \frac{y_1}{2} \left[-1 + \sqrt{1 + 8 \left(\frac{y_c}{y_1} \right)^3} \right] \dots\dots\dots 2.22$$

The occurrence of a submerged jump, however, has little air entrapment as compared to the free hydraulic jump. In contrast, energy dissipation is less in a submerged jump as compared to the *free hydraulic jump*. Submerged jumps also introduce more pressure differentials in the downstream water since energy dissipation is little. The submerged jump often becomes a jet in

the water characterized by less noise and air bubbles. Because of poor energy dissipation, submerged jumps cannot be used as good energy dissipaters.

In the design of a weir, the energy of the fast flowing water over the dam body must be dissipated to prevent erosion of the downstream. The hydraulic jump formed normally occurs on the apron designed to endure hydraulic forces are formed and prevents cavitation and processes the accelerate erosion. In most cases of a hydraulic jump design 60-70% energy dissipation is achieved at the jump, reducing the structural damage and potential bed erosion. Though at this level of energy dissipation is recommended, there is a need to design for the uplift, cavitation, vibration and abrasion.

CHAPTER 3: METHODOLOGY FOR EXPERIMENTAL STUDY

3.1 Introduction

This chapter presents a description of the model schematization of the different stages of an inflatable weir, for example of weir which is deflated during a flood situation and describes the model setup in the laboratory and data collection/measurement. The methods of measurement (instrumentation, data acquisition and analysis) of discharge, water levels (stage), pressures on the downstream face of the weir from the crest and the downstream hydraulic jump are described. The accuracy of measurements during the experimental test conditions applied are also presented. Finally, a description of model scaling is presented to enable recorded data to be scaled up to prototype data of a 3m high inflatable weir.

3.2 Schematization of deflation stages of the inflatable weir

With regard to the nature of the flow profile over weirs, the cylindrical weirs are also classified as narrow-crested weirs (Lakshmana Rao, 1975) or short-crested weirs (Bos, 1989). For this type of weir, the curvature of the streamlines could be considerable. Cylindrical weirs were very much in use in the late 19th century and in the early 20th century before the use of the ogee shaped weirs. In the hope of improving the discharge coefficient of the weir in the 19th century, investigations led to the design of the circular weir. Inflatable dams became a new form of weir similar to the circular weir. Circular weirs were used as a close representation of the inflatable weir. However, in practice a partially deflated or deflating weir forms a broad crested weir of varying heights joined to a circular weir of respective varying sizes or rather a droplet squat/tear drop shape. Using a cylindrical weir would simplify the measurement of the discharge over the weir by maintaining stage for a fixed inflow. Similarly, in this study, successive sizes of circular weirs are used to analyze the hydraulic dynamics on an inflatable weir, though there is a possibility of having a deformed shape when pressure is reduced in a real life situation. Figure 3.1 shows the different stages of an inflatable weir which were tested in the laboratory. The largest weir model assumes the fully inflated weir, the intermediate weir assumes the partially deflated and the smallest the almost fully deflated state.

Cylindrical simulations (red dotted lines) of different stadia of an inflatable weir

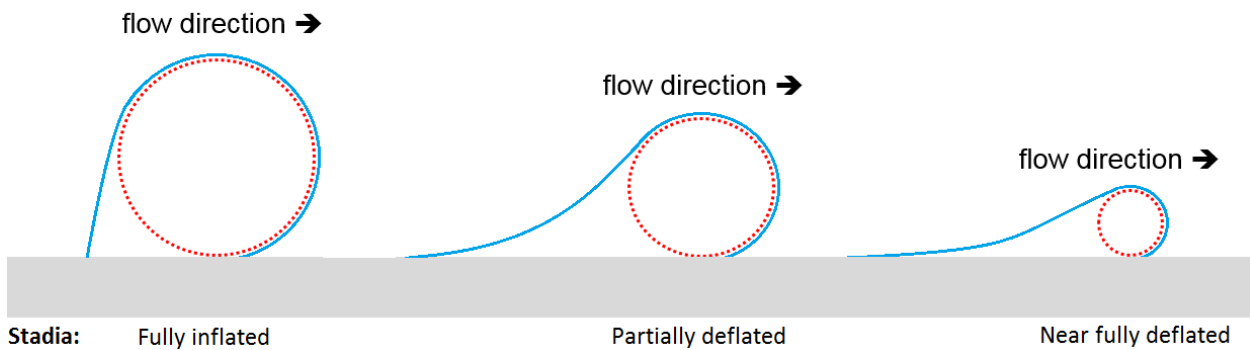


Figure 3.1 Simulation of different stages of the inflatable weir (viewed from US laboratory)

Inflow water to the test flume eventually impinged on the weir model before overflow occurs. The streamlines of flow due to the circular weir obstruction are however not shaped in the same way as with an inflatable weir obstruction, but this insignificantly alters the flow past the weir and is considered to have little effect on the weir performance as seen in literature studies on upstream arches in section 2.5.2. Building of a miniature model of the inflatable weir would have had a substantial cost, but it would have given a more accurate simulation of the hydraulics of the inflatable weir.

3.3 Experimental configuration and physical model construction

The equipment chosen to perform the experiment was a rectangular flume having a length of 10m, a 2m width and a height of 1m. The walls along the entire length of the flume were made of glass with a steel-frame, allowing for visual observation of the flow transition over the weir model. Figure 3.2 shows the schematic set up of the whole system used for the experiments.

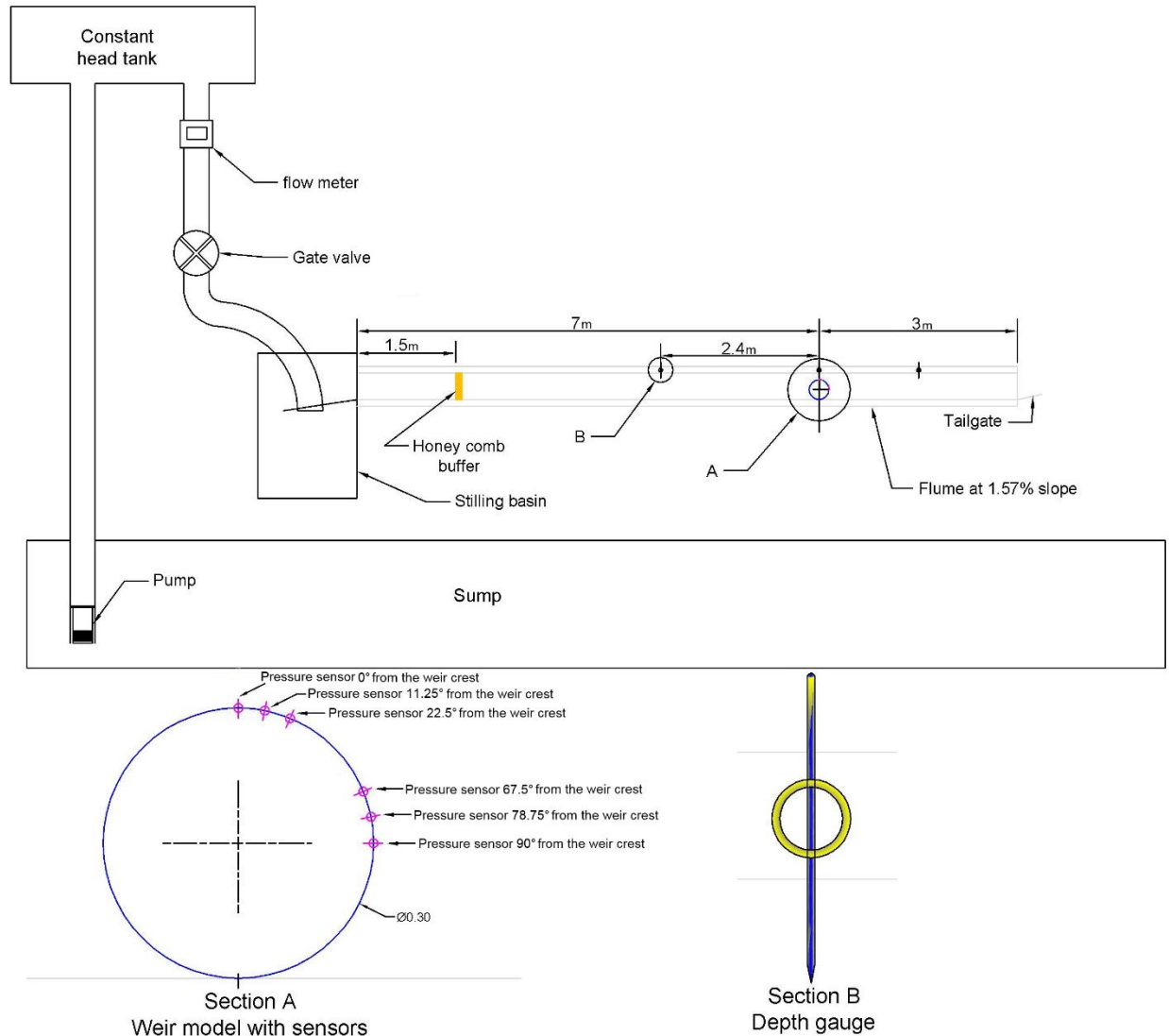


Figure 3.2 Schematic set up of the whole system used for the experiments (viewed from US laboratory)

Incoming water immediately went through a honey comb buffer with 40mm x 20mm openings to dissipate the energy at the inlet, thus suppressing any excessive turbulence from the supply water. This created more steady flow conditions for the experiment before the water was successfully passed over weir. In practice, the water entered the flume from a constant head tank, which was fed by centrifugal pumps with a maximum discharge of up to 150l/s. Figure 3.3 shows the experimental set up before water was allowed into the flume.

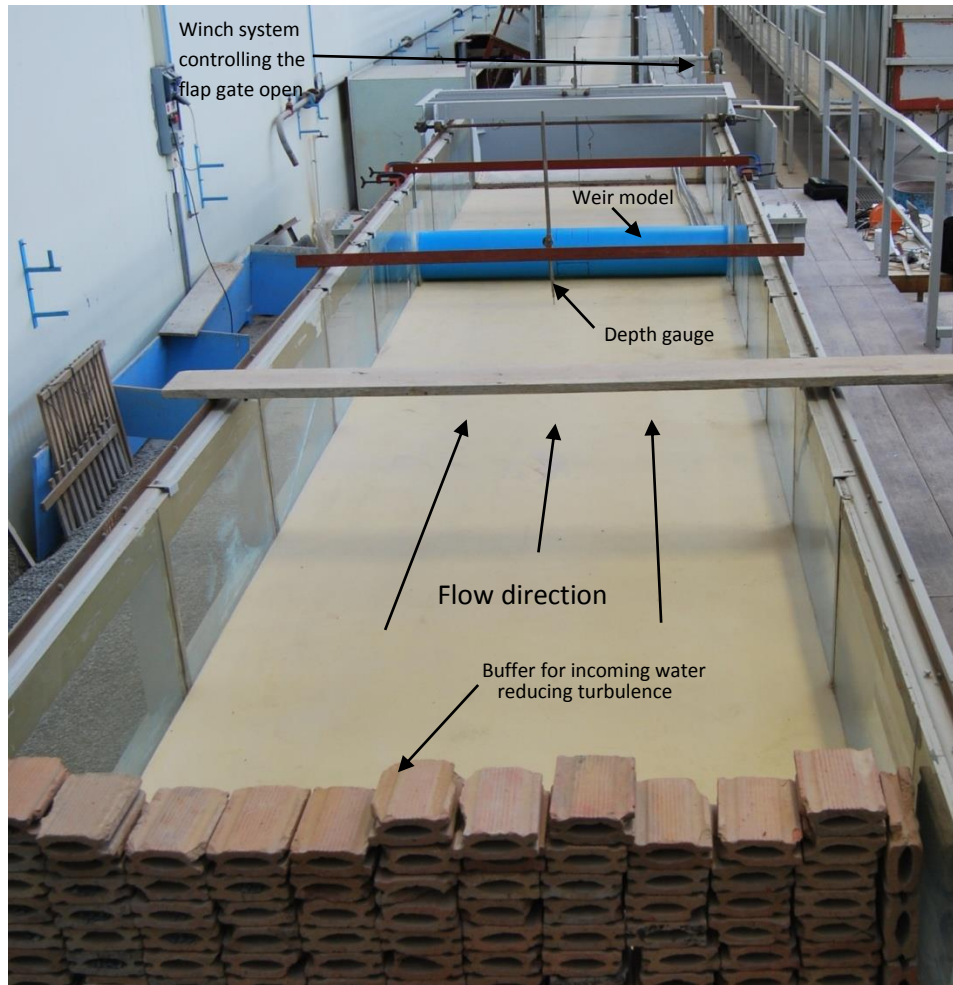


Figure 3.3 Flume with weir and measuring apparatus (viewed from US laboratory)

The weir models built into the flume were made from a 2m span of smooth uPVC pipes of three sizes. A 300mm, 250mm and a 100mm diameter pipe was put across the 2m wide flume for the three tests conducted. The large pipe (300mm) was used to simulate the conditions undergone in a fully inflated weir. The 250mm diameter pipe was for conditions of partial deflation and the 100mm pipe for the almost deflated weir as shown in Figure 3.1. Each weir was tested to simulate a stage undergone by the air/water inflated dam model, and the downstream faces of the cylinders used in each test were not ventilated in all the experiments.

With the cut pipe fitted across the flume (weir model) at a distance of 7m from the inlet, overflow conditions were reached with various discharges for each of the three pipe sizes, while measurement of upstream, nappe, jump and downstream depths were done. This simulated the conditions the inflatable weir is subjected to under normal flow conditions.

For the system, a recirculating discharge system was used with a constant head reservoir and an underground reservoir to retaining the water. The bottom of the flume provided a level drain area sloping at a slope of 1.57%, allowing the water from the flume to flow over the fixed weir model for each test. The tail water depth, which controlled the formation of a hydraulic jump, was controlled by a steel flap gate hinged at the downstream end of the flume, at the bottom, with an adjustable winch system. For pressure distribution over the weir models, a series of pressure sensors were put at intervals, and the use of tubing protected their electrical connection as seen in Figure 3.4.

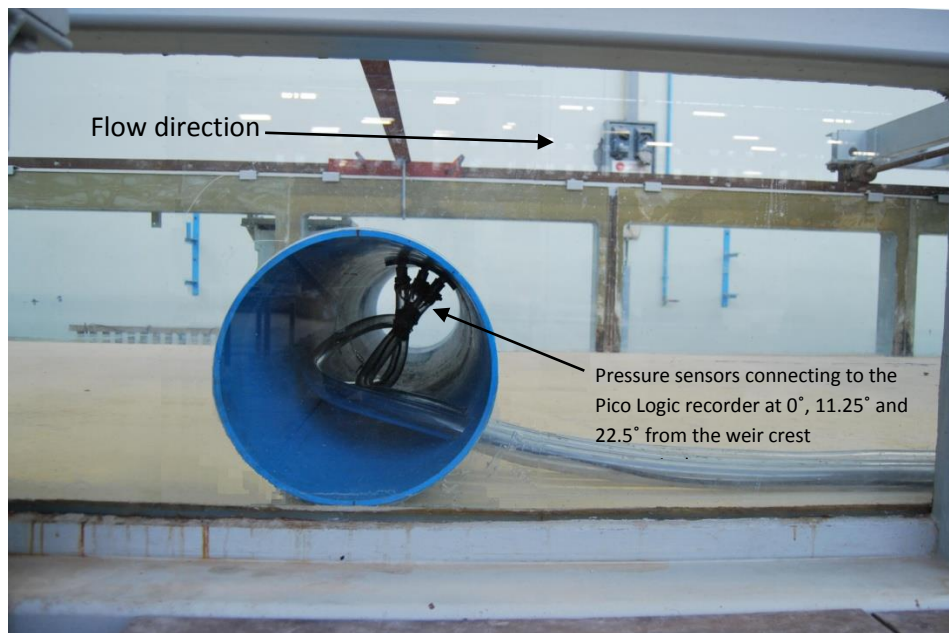


Figure 3.4 Side view of flume (viewed from US laboratory)

The pressure sensors measured the pressures at 0° , 11.25° and 22.5° from the weir crest in the downstream direction. Each sensor was in its own flow path with one in the center and the other two on the sides, spaced 100mm from the one in the center as seen in Figure 3.5.

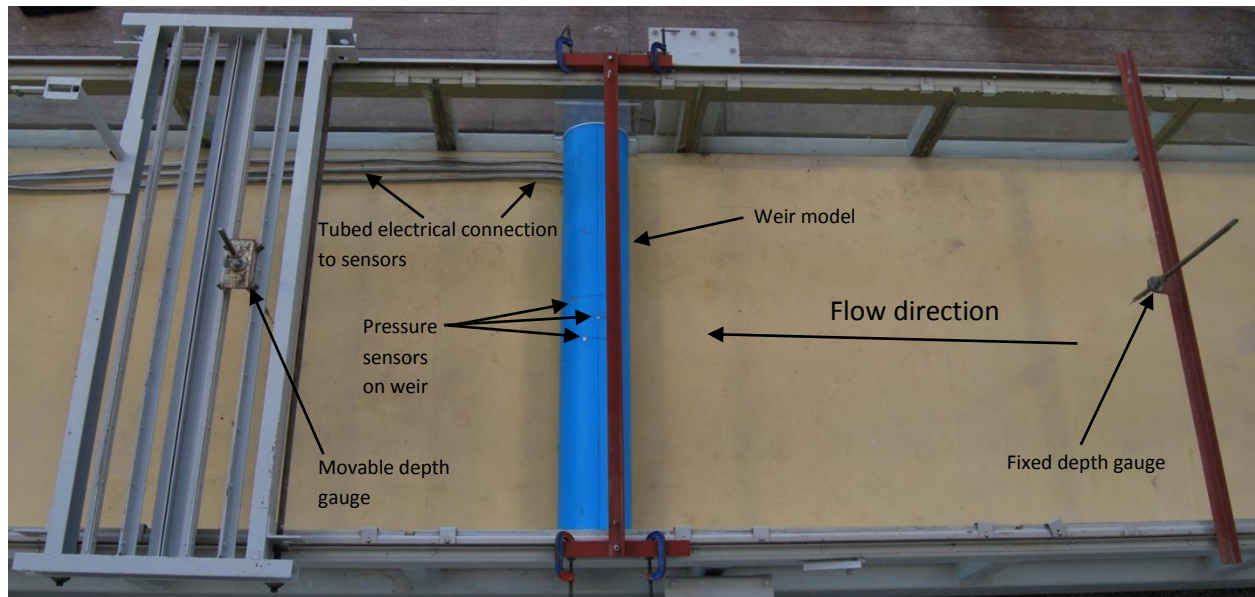


Figure 3.5 Measuring equipment in the middle of the flume (viewed from US laboratory)

The physical prototype model used was constructed in a period of one month to include the removal and placement of the various pipe sizes in the testing. The weir model was placed at a distance of 3m from the discharge end of the 10m flume (as seen in Figure 3.2) and measurements taken in the center of the flume. Measurement of the upstream and downstream depth was carried out by point gauges in the center of the flume as seen in Figure 3.5. The downstream gauge was, however, movable to allow the measurement at weir crest level and the hydraulic jump length, which was not stationary, together with the tail water after the jump.

As flow was introduced into the flume at the start of the experiment, it was observed that a submerged jump was formed when the flume was at a slope of 0.052%. At this bed slope, the submerged jump started at a minimum inflow of 53.028//s until it reached a maximum of 143.43//s which was available from the test apparatus. This inflow still produced a submerged jump even with a partially closed tail-gate of the flume (see Figure 3.6). The approach flow velocity at the jump was still at supercritical speed and air entrapment was small with a submerged jump.



Figure 3.6 Submerged jumps at 53.028 l/s (left) and 143.43 l/s (right) (viewed from US laboratory)

The submerged jump was pulsating and dynamic and this resulted in pressure build up that is normally avoided to prevent the jump becoming a less efficient energy dissipater. The bed slope was then increased for effective energy dissipation until a jump could be formed in the test flume. At the change of slope of the flume to 1.57%, it was then possible to introduce the flowing water, thus forming a hydraulic jump in the flume, and dissipating the excess energy in the process of the formation of a jump. Figure 3.7 shows the schematic diagram of the experiment set up during overflow with a controlled jump.

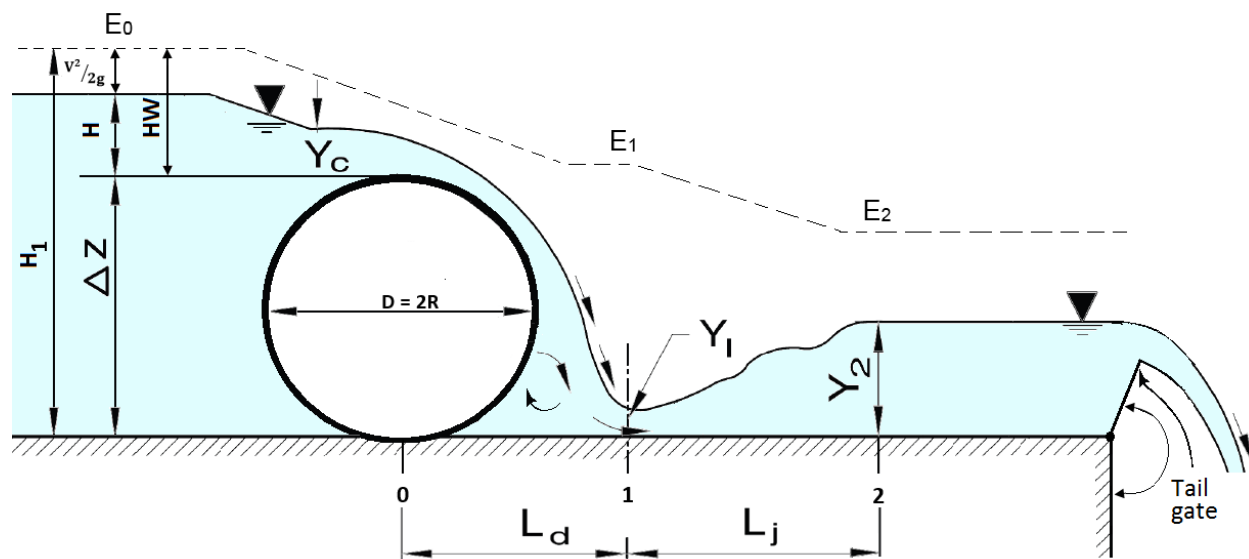


Figure 3.7 Schematic section through weir during overflow (viewed from US laboratory)

From the upstream side of the weir, the nappe was seen to accelerate until the attached free-falling nappe was projected downward before it impacted the floor of the flume. Separation of

the unventilated nappe was seen with one part recirculating before continuing with the flow. The surface flow continued to form the jump on collision with the slow moving water downstream. In the process, the depth of flow was forced to undergo a sudden change from supercritical to a subcritical depth, and the Froude number increased to values greater than 1.0. This flow condition is similar to the simulation of a real life weir in which high energy is often involved in the flowing water and energy dissipation is required. With visual observations, it was also seen that the jump was not formed until the tail-end gate was raised. The water levels upstream and downstream of the weir were only measured at the chosen slope with the least flow introduced into the flume until the highest possible flow with a steady jump formed. Careful measurement of the depth of the nappe above the crest and the corresponding depth at the recirculation pool down the weir were performed and comparisons of the weirs tests made with literature.

3.4 Instrumentation, data acquisition and analysis

Instruments used in the collection of data are described together with the way data was collected and analyzed.

3.4.1 Inflow measurement

A SAFMAG electromagnetic flow meter was used to measure the inflow into the flume as it was controlled by the gate valve immediately before the flume. Accuracy was within $\pm 0.5\%$ of the measured flow rate for velocities greater than 0.5m/s and $\pm 0.025\%$ for velocities less than 0.5m/s with an additional analog output error of $\pm 0.008\text{mA}$. Figure 3.8 shows the flow meter used.



Figure 3.8 SAFMAG electromagnetic flow meter

3.4.2 Depth gauge measurements

The depth gauge used was mounted on a beam and had an accuracy of $\pm 0.1\text{mm}$. Figure 3.9 shows a closer view of the depth gauge used.



Figure 3.9 Depth gauge (viewed from US laboratory)

When taking the readings, measurement of the depth of the flume bed and on the crest at the weir relative to the mounting of the gauge was done first. Successive measurement of the flow depths then gave the resultant, making the depth reading. If correction of the flume slope was to be applied in the depth gauge readings, decrease in the measured depth would be by a factor $\text{Cos } \theta = 0.999876777 \approx 1$ where $\text{tan } \theta = 1.57\%$. Figure 3.10 illustrate the insignificant decrease of the corrected depth relative to the accuracy of the depth gauge.

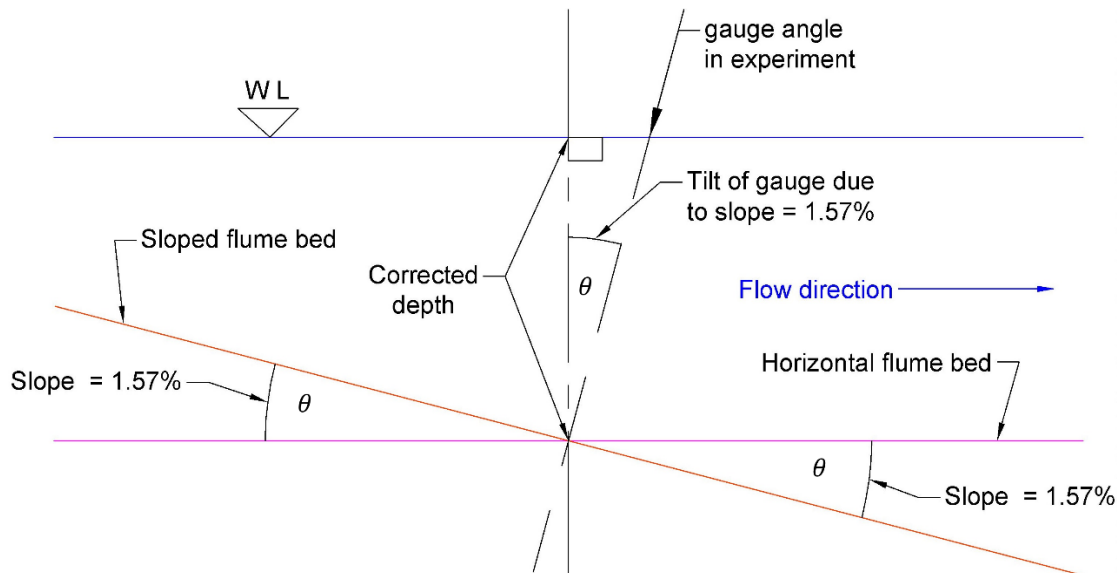


Figure 3.10 Corrected depth (viewed from US laboratory)

Depth, H , as used in the calculations, was measured 2.4m upstream of the weir crest. Gauge reading was first taken with no water on the bed of the flume, then measured again the depth of water behind the weir after filling up the upstream side flush with the weir. Successive readings of the water levels due to the respective increase in inflow were finally recorded. Measurement directly on top of the weir with a movable mounted depth gauge gave the successive readings of the crest depth. The depth gauge reading was also done with no water at the crest then flowed by the successive levels with increasing inflow. From the crest to the downstream side, depth y_1 and y_2 were also measured using the gauge mounted on the trolley and again the depth of flume bed without water followed by the successive rise in water levels for both y_1 and tail water depth y_2 were recorded.

3.4.3 Pressure measurement on weir model

Using the Pico-Log recorder unit and software, one was able to start and stop recording with a player that enabled one to go through the recorded test and also make comparison with other runs. For the output, a graphical interface showing the readings for single or multiple measurements over a period of time was made available. The graphical result was also available in a spreadsheet, showing a detailed summary of the recording. This software formed an interface, making it possible to collect, analyze and display data. The use of the Pico-Log recorder unit, together with the pressure sensors, enabled the reduction of error in the

measurement of pressure at the points indicated on the weir crest, but, inevitably, some error was involved due to vibrating equipment and water currents.

With the Pico-Log recorder unit and the use of pressure sensors, the pressure distribution at the top and downstream face of the weir models was measured electronically at various inflow conditions. Figure 3.11 shows the position of the pressure sensors on the upright weir model during each experimental set up. The PicoLog unit has a number of separate input channels, but one needs only to connect the necessary number of channels that one wishes to use, in this case, three were used at a time.

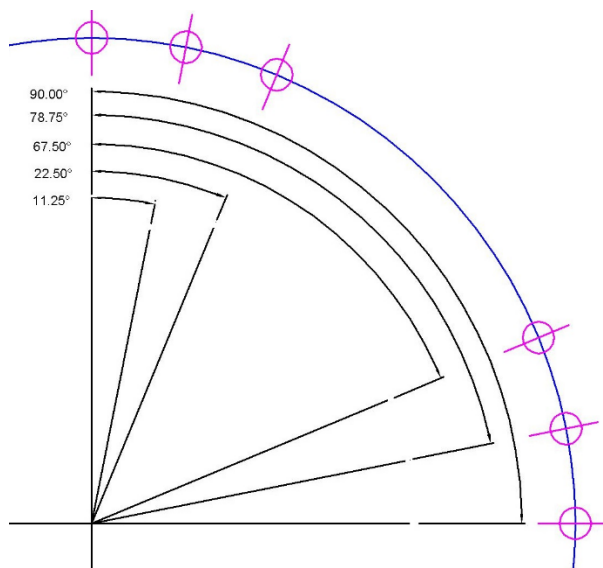


Figure 3.11 Position of the pressure sensors on a quadrant downstream of the weir model during the test (viewed from US laboratory)

The signal from the first three pressure sensors was then recorded with continuous logging in a computer using the PicoLog software. Measurement of the pressure from the continuous logging was done for 300s (5min) in each of the pressure sensors for the three weir sizes. Figure 3.12 and 3.13 show the data as record by the PicoLog unit from the software graphical plot, showing a section of the 300s recording of the pressure sensors from crest respectively.

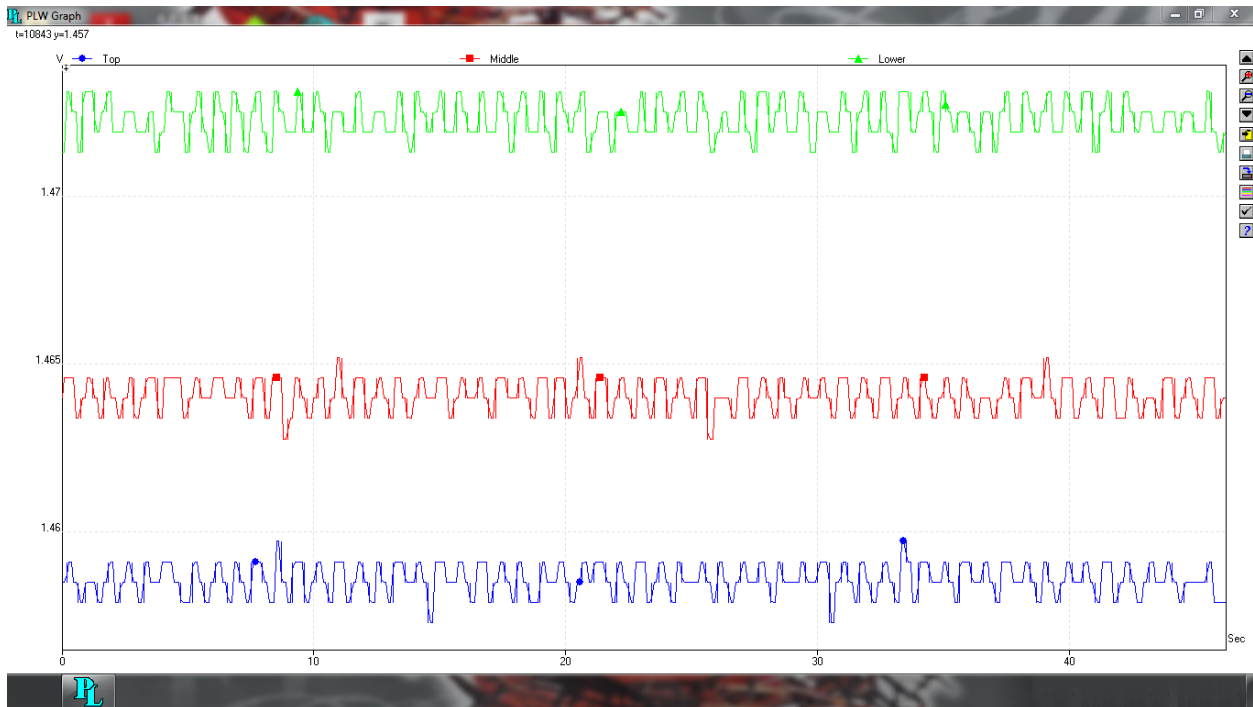


Figure 3.12 Zero flow measurement of pressure by the first three pressure sensors during test of the R = 0.15m weir model (Viewed in US laboratory)

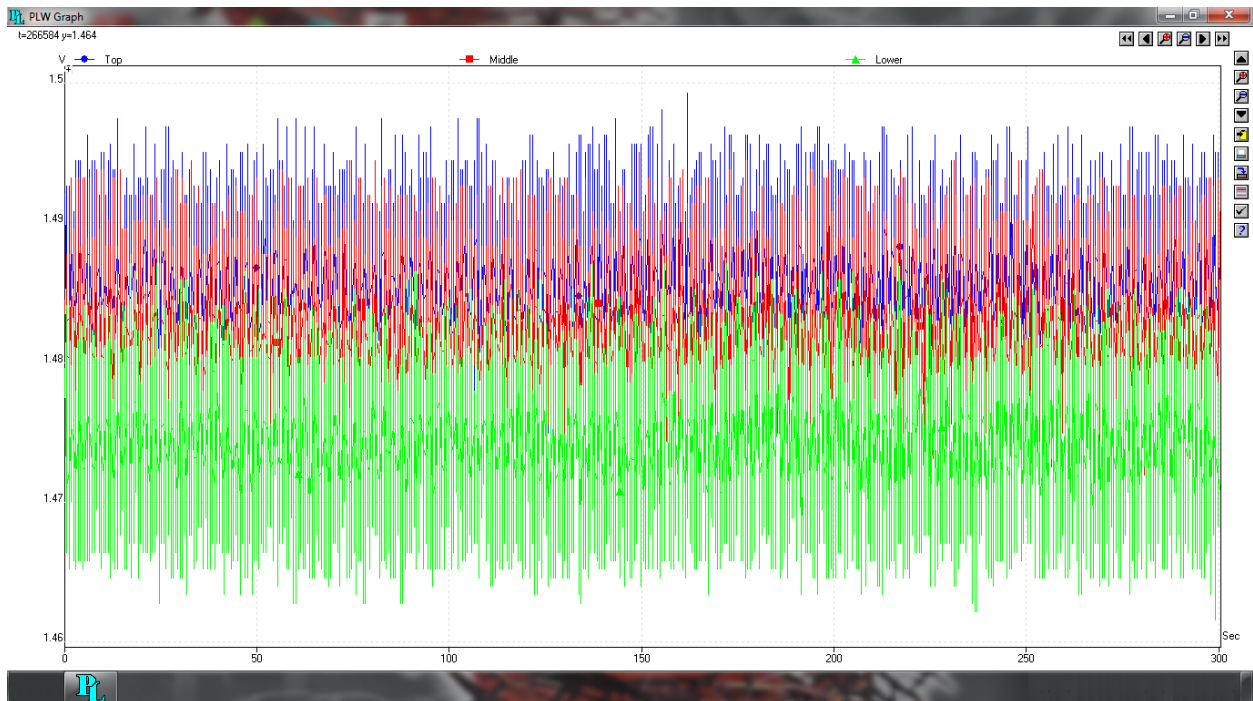


Figure 3.13 Pressure reading at 0.0236 m³/s during test of the R = 0.15m weir model (Viewed in US laboratory)

The first recording in each of the tests conducted on each weir model was used as a correction on the pressure gauge reading as inflow was introduced into the flume. However the data available from the spread sheet was imported to Excel to capture the whole 300s logging undertaken / cycle. Conversion of the electric signal to give the equivalent pressures from the tests was done to achieve the final pressure and enable analysis of the data. For conversion a formula applied such that:

$$Pressure = \frac{2}{16} \times \frac{V_s}{120} \times 1000 - 1.5$$

Where V_s is the voltage recorded by the pressure sensor. Figure 3.14 shows the graphical plot from the spread sheet data for 0.0394 m³/s inflow to the flume.

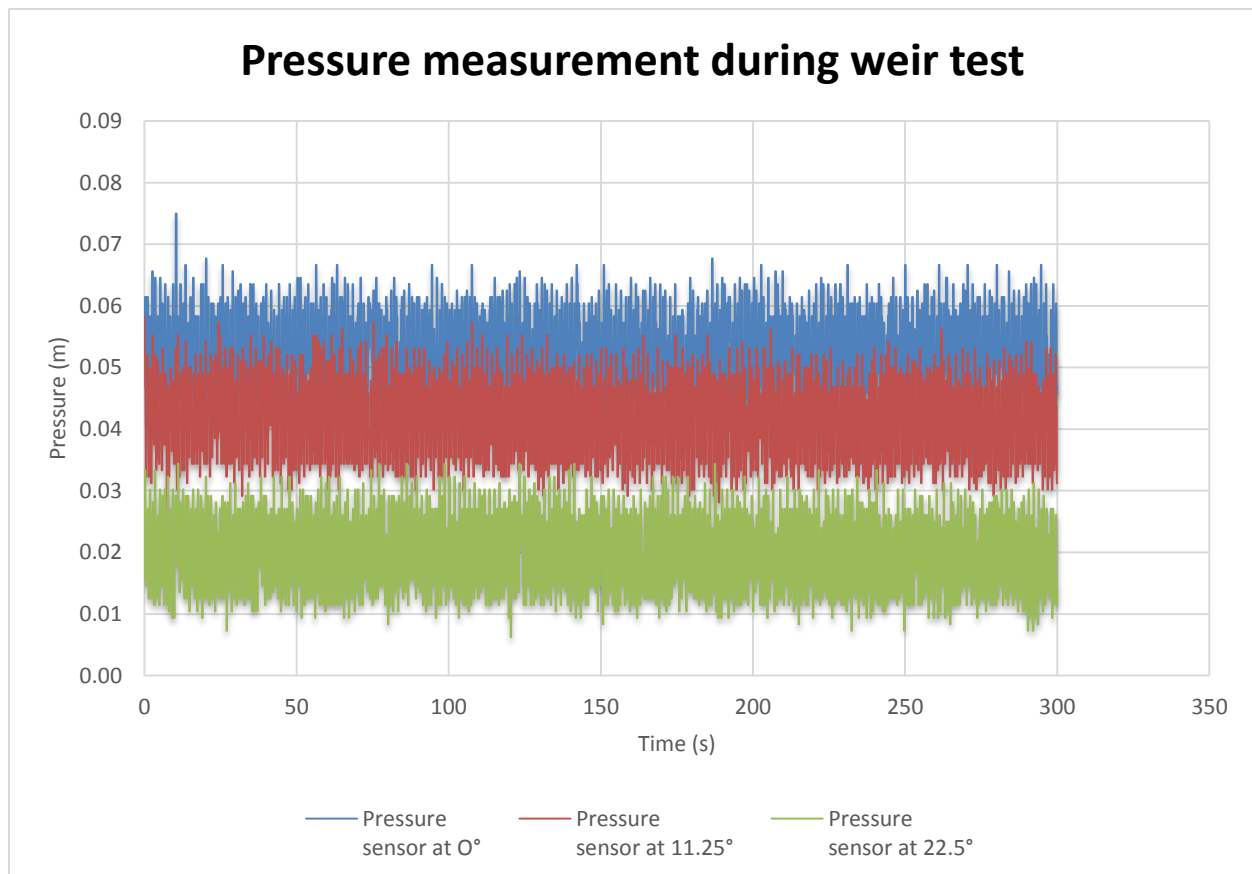
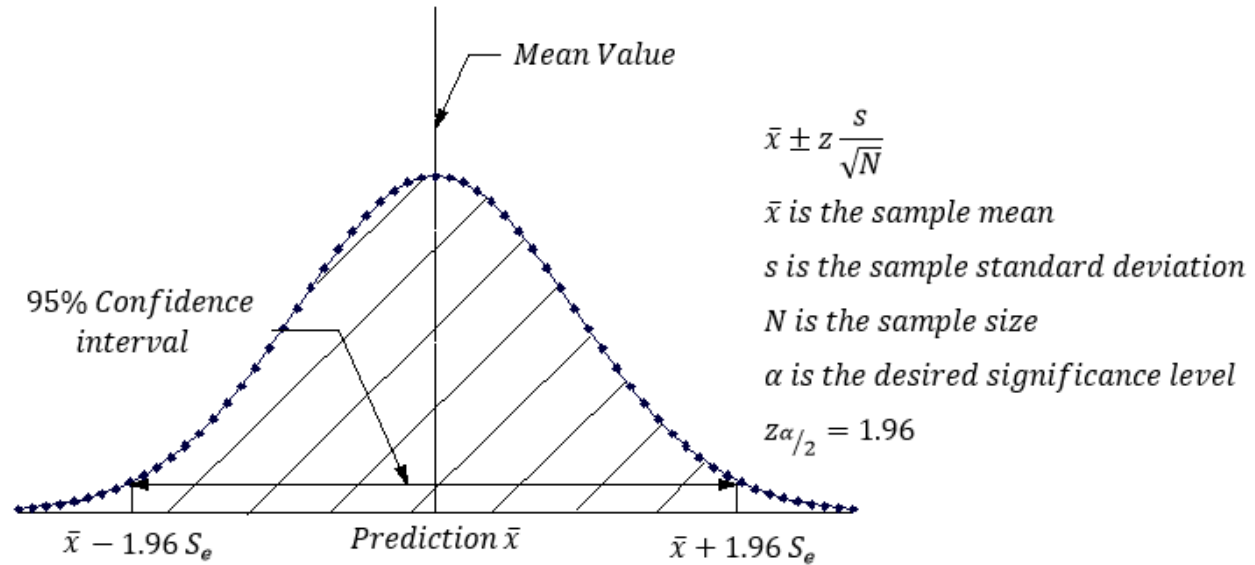


Figure 3.14 Pressure at 0.039389 m³/s during test of the R = 0.15m weir model (Viewed in US laboratory)

The average pressure (\bar{x}) and lower 95% pressure ($\bar{x} - z \frac{s}{\sqrt{N}}$) measured was then taken into consideration for each pressure recording at 0° , 11.25° and 22.5° on the downstream side of the weir crest.



Additionally a single test was done using the 0.15m radius weir again with three pressure sensors at the downstream face at 67.5° , 78.75° and 90° from weir crest. The 0.15m weir was turned 67.5° in the downstream direction positioning the first pressure sensor at 67.5° , the second at 78.75° and the last at 90° from the weir crest.

3.4.4 Jump length

Photographs and the use of a tape measure were used when recording the jump length (L_j). See Figure 3.15



Figure 3.15 Measurement of the jump length (Viewed in US laboratory)

A digital camera was used to capture the flow patterns over each circular weir tested. It was also used to produce photos that showed the state of flow in the whole model. These photographs were used for close observation of the jump formation and to check the jump lengths against the measured result.

3.5 Accuracy of measurements during experiment

The depth of water in the flume configuration shown (Figure 3.7) is often measured by the use of a depth or dial gauge. The dial gauge, made up of a vernier caliper mounted on a stand is not different from the standard vernier caliper and the principle of operation is the same. The same applies to the measurement of pressure by the sensors, which includes the measurement accuracy and capabilities. When in use, there are inaccuracies that arise in instruments when they are not properly mounted and due to observation with the dial gauge. In some instances, poor contact is made between the weir surface, the moving anvil and the floor of flume (Alan, 2001).

Accuracy and precision are important characteristics of any flow measurement device (Evan, 2010; Alan, 2001). Accuracy, in this case, is the ability of the measuring device to indicate the true depth/pressure without a systematic bias above or below the true value. The precision of the instrument being its ability to reproduce similar measurements. Figure 3.16 illustrates the aspect of accuracy and precision.

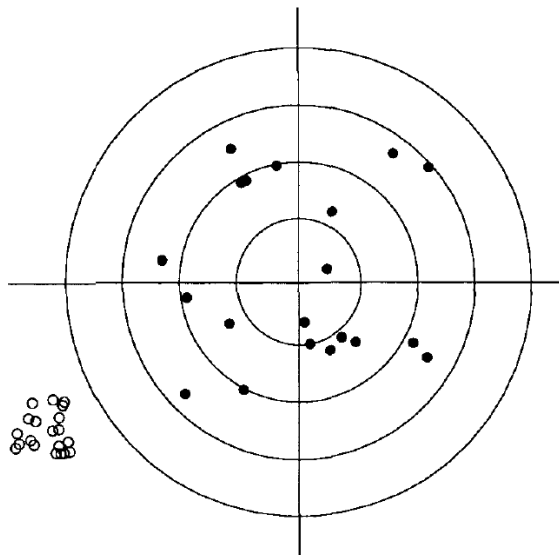


Figure 3.16 Accuracy versus precision (Rothman, 1998)

The set of solid points in Figure 3.16, exhibits good accuracy, but low precision, while the set of open points have poor accuracy and high precision (Rothman, 1998). Quite often, the precision and accuracy of the water level and pressure measurement by the measuring device, would affect the precision and accuracy of the complete measured quantities. Sources of error or uncertainty in individual measurements, classified as either random or systematic are both systematic; that is, they have a bias that affects repeated measurements in a similar manner and random, averaging to zero over the course of many measurements (Rothman, 1998). Even if all systematic biases are eliminated, the accuracy with which a single depth measurement and pressure could be made is limited by the precision with which a measurement could be reproduced. From a statistical point of view, a random error could also be envisaged as sampling variability. Systematic error, or bias, is the difference between an observed value and the true value due to all causes other than sampling variability (Victor, 2000).

Spurious errors in the measurements occur and introduce false data into the measurement procedures for the pressure and water levels. They are unpredictable in their occurrence, magnitude, and distribution, and invalidate the measurements taken. Human error or obstructions to normal flow also contribute largely to the spurious errors. These could sometimes be detected by comparing flow measurements at different times or at different locations within the flume.

To add to the possible error of actual reference setting, there is a possibility of error as a result of the unstable foundation, causing a drift in the zero reading. The reading error of a staff gauge is largely influenced by the distance between the gauge and the observer, the angle at which the gauge is read, the turbulence of the water, and also the graduation units of the gauge. Inevitably, in the experiment, the staff-gauge readings and pressure become inaccurate owing to the systematic error associated with turbulent flow.

3.6 Effects of viscosity and surface tension and model scaling

In general, it has been seen that tests on the weir models largely differ compared to the real life situation performance of the weir, owing to the viscosity and surface tension. The more significant of the two is the surface tension increases as stream line free surface curvature increase (Sarginson, 1972). Its effect is more evident in the case of the sharp crested weir where both sides of the nappe are affected and C_d is decreased until such a time when the increase in head water has negligible effects on C_d . With the circular weir, effect of surface tension is on the upper surface of the nappe and the lower which is in contact with the weir, making the large circular weir less affected by surface tension than a smaller weir. It has been seen that the phenomenon of surface tension, as seen in the Rehbock empirical formula for a weir, is applicable for 6mm diameter weirs and larger and heads of 6mm up to 150mm. Sarginson (1972) obtained this comparison with the theoretical Rehbock empirical formula and found a good agreement with the measured results. At crest radii larger than 50mm and head over 30mm, the effect of surface tension is observed to be negligible, but is considered as head waters decrease with the same weir crest radii. As aeration on the nappe is introduced, a critical point where the surface tension no longer applies on the nappe, develops. The situation is more of a trajectory, and gravitational forces and viscosity would mainly be at work. The critical corresponding head required for the circular weir is larger for a large weir as compared to the smaller weir.

Scale effects on circular crested weirs mainly accounts for the surface tension and the viscosity of the water. Orgaz *et al.* (2014) in his study, obtained an analytical solution for the scale effects by using very small weirs. The study shows that, for a circular weir, a minimum overflow head of 0.04m for a weir radius, $0.01\text{m} < R < 0.30\text{m}$, maintains the discharge curve unaffected by scale effects. For accurate reproduction of the important hydraulic gradual changes through a series of states in the hydraulic model, it was realized that the geometric and dynamic similarity

between the prototype weir and model weir must be fulfilled when determining the model scales (Abdelazim, 2010). For a large model that has free surface flow, the inertia and gravitation forces are dominant. Simulation of the model is based on Froude number equality with the prototype. The Froude number represents ratio between gravitational and inertial forces, given by the equation below:

$$F_r = \frac{V}{\sqrt{gh}} \quad \text{Where} \quad F_r = \text{Froude number,}$$

$$V = \text{average flow velocity, (m/s)}$$

h = characteristic depth, (m)

g = gravitational acceleration, (m/s²).

From the condition when the Froude Number in the prototype and model are equal, the velocity scale ratio could be determined from which the other scale ratios could be derived from the below mentioned equations:

$$\text{Velocity (v) scale ratio} = n_v = (n_h)^{0.5},$$

$$\text{Discharge (Q) scale ratio} = n_Q = n_l n_h n_v = n_l (n_h)^{1.5}, \text{ and}$$

$$\text{Time (t) scale ratio} = n_t = n_l / n_v = n_l / (n_h)^{0.5} \quad (\text{Abdelazim, 2010})$$

$$\text{Pressure (p) scale ratio} = n_p = n_l = n_h$$

Where:

l = length

h = depth

n = (prototype parameter)/(model parameter)

n_v = (prototype v)/(model v)

In this study, undertaken if the undistorted geometric scale of 0.3:3 i.e. 1:10 is selected, consequently, the ratios for the other quantities would be as stated below from the above mentioned equations:

Horizontal length scale	$n_h = 10;$
Velocity scale	$n_v = (10)^{0.5} = 3.162;$
Discharge scale	$n_Q = (10)^{2.5} = 316.228;$
Time scale	$n_t = (10)^{0.5} = 3.162$ and;
Pressure (ρ) scale	$n_p = 10$

CHAPTER 4: RESULTS AND DISCUSSION

4.1 Introduction

This chapter presents and discusses the stage-discharge relationships, pressures, crest depth, energy loss over crest, energy losses downstream of weir and jump lengths found from the experimental work undertaken. Analysis of results was done by comparing all experimental data with literature studies experimental data, empirical and theoretical equations. This gave an understanding of the inflatable weir hydraulics using the circular weirs.

4.2 Stage-discharge relationships of the weir models

Stage discharge relationships over the weir consists of the inflow water depth above the crest and its effect on weir discharge, the relationship between the coefficient of discharge, C_d with the total head, H_w above the crest and the weir radii, R tested.

4.2.1 Relationship between unit discharge (q) and stage (H)

From the successive measurements of the water depth at 2.4m upstream of the weir, an experimental relationship between unit discharge (q) and stage (H) was found. Unit discharge, q , increased with an increase in head, H , as seen with Abdul-latif (2010), this is seen in the graphical plot in Figure 4.1.

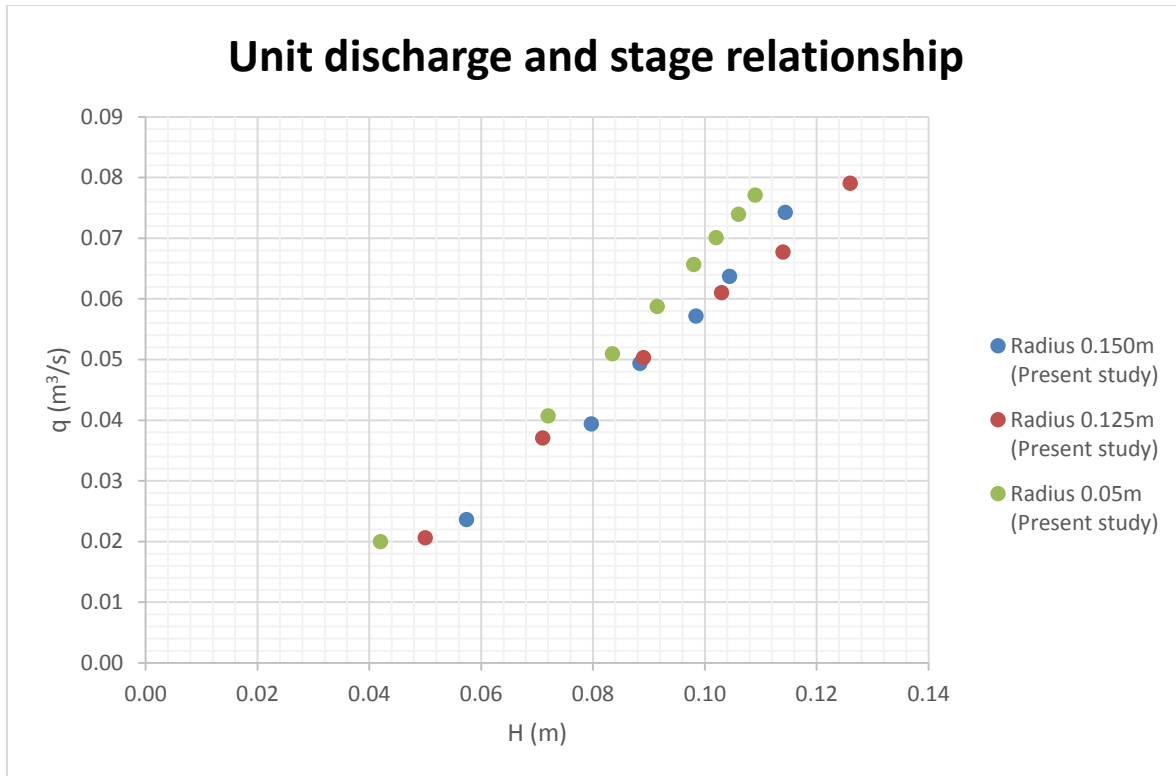


Figure 4.1 Relationship between unit discharge and stage

The experimental data from the study conducted also shows that there is variability for the individual model tests as seen by Abdul-latif (2010) experimental data. Consistence in the experimental data was archived in studies by Emad (2012) by performing repeated experiments with a weir model to reduce possible error in a single test. Unit discharge and head relationship is varied because of the accuracy and precision in the measured depths.

4.2.2 Relationship between coefficient of discharge, C_d with total head, H_w and radius of curvature, R

Using the broad crested weir formula $\left(Q = C_d b \sqrt{g} \left(\frac{2}{3} H_w \right)^{\frac{2}{3}} \right)$ where the width of the flume, b is 2m, a graphical plot of the C_d versus $\frac{H_w}{R}$ was done for the various inflows during each test and are shown in Figure 4.2.

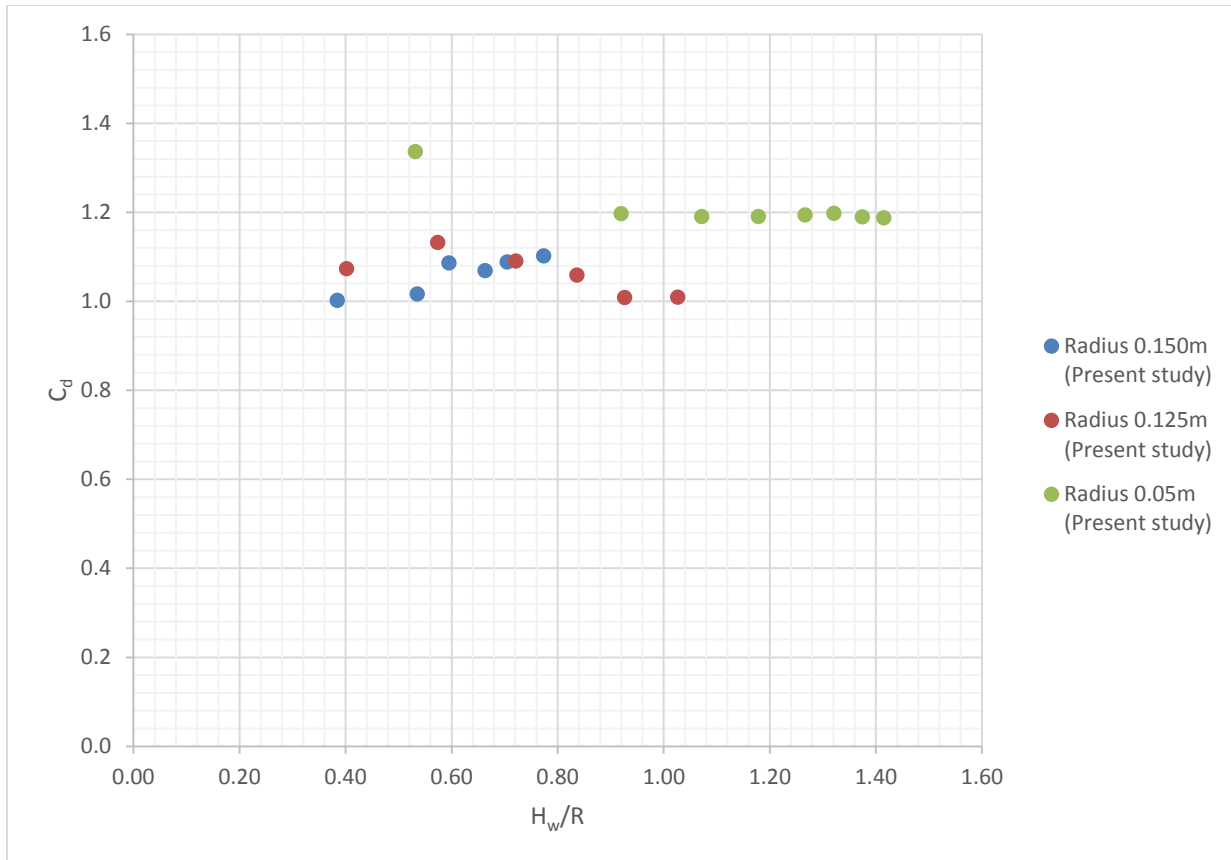


Figure 4.2 Relationship between C_d with H_w/R

Experimental data on Figure 4.2 shows that the C_d values are within a range; $1.0 < C_d < 1.3$. From the experimental data, generally as the weir radius is reduced, the unit discharge decreases and the large weir radius allows more discharge per unit width of the weir. This is the case as with the oblique weirs studied by Emad (2012), wherein the oblique weir radius gives a larger length of flow. The experimental data also revealed that the coefficient of discharge, C_d , slightly increased initially, but generally decreased as the H_w/R ratio increased. This shows that despite C_d being affected by a change in the head, H , being the only changing variable during each test scenario and the weir radius, R being constant, C_d is proportional to the weir head, H_w and inversely proportional to the radius of curvature, R . Using the results of this study and literature based on the broad crested weir formula, a combined plot shows the relative accuracy of the experimental study as seen in Figure 4.3. Data from converging literature studies was only considered for clear comparison and the other studies were included in the appendices. These are:

1. Bos (1978) Experimental;

2. Chanson (2008) Empirical fully developed inflow;
3. Heidarpour (2010) Empirical equation;
4. Haghiabi (2012) Theoretical equation and;
5. Shabanlou (2013) Empirical equation.

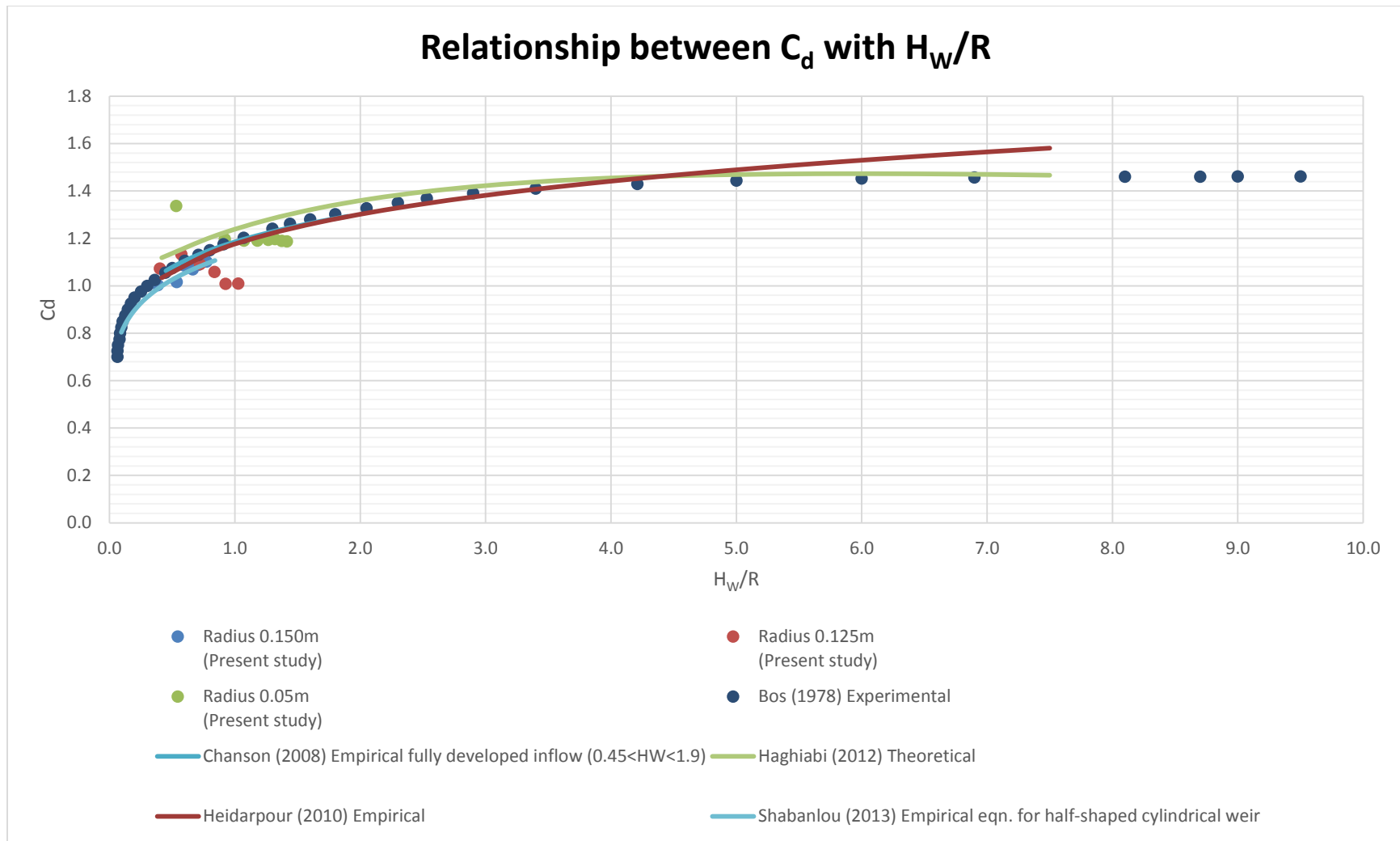


Figure 4.3 Relationship between C_d with H_w/R for the measured results and literature studies

From the comparison of the experimental data to literature, the variation of the flume bed slope did not affect the C_d because of the rounded weir crest. The results from the 0.05m, 0.125m and 0.15m weir radius compare reasonably well with those from literature. Bos (1976) concluded that the weir radius can affect its discharge as it either renders a weir sharp-, short-, or broad-crested, depending on the weir radius. The graphical representation of the three weirs also shows that the discharge coefficient becomes constant in relation to (H_w/R) as $R \rightarrow \infty$. The graph illustrates that the discharge coefficient is largely influenced by the upstream head, H_w , over the crest over the calibrated range with the flow over the weir also independent of the downstream water levels.

4.3 Pressure distribution over the weir

Pressure at the start of the test of weir model $R = 0.15\text{m}$ generally decreased as the overflow increased. Using the lower 95% of the recorded pressure gave more negative pressure with the measured values compared to the average pressures. Similarly, in each test for the other weir models, the pressure continued to drop successively on each of the three sensors on the downstream weir face. Pressure drop was more significant on the sensor located at the lower end of the weir crest. Pressure measured also gave a good prediction of the pressure of the intermediate weir sizes as undergone by the inflatable weir. Figure 4.4, 4.5 and 4.6 gives a graphical picture of the increasingly low measured pressures as measured on each test model.

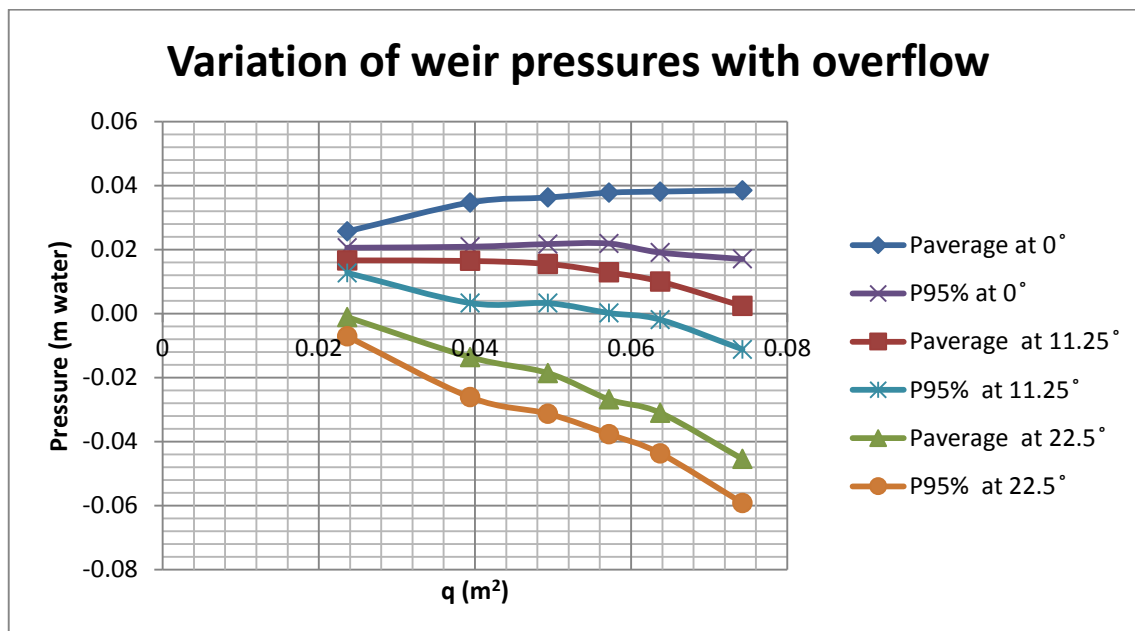


Figure 4.4 Pressures on surface of weir 1: R 0.15m

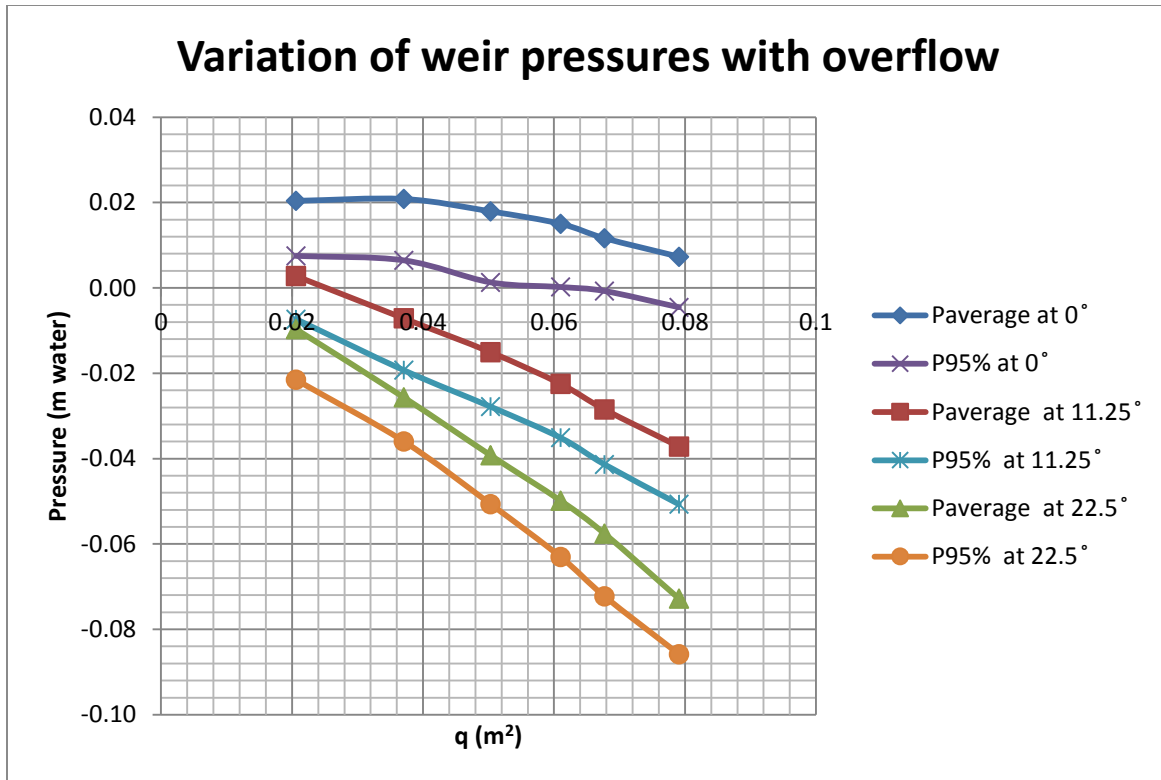


Figure 4.5 Pressures on surface of weir 2: R 0.125m

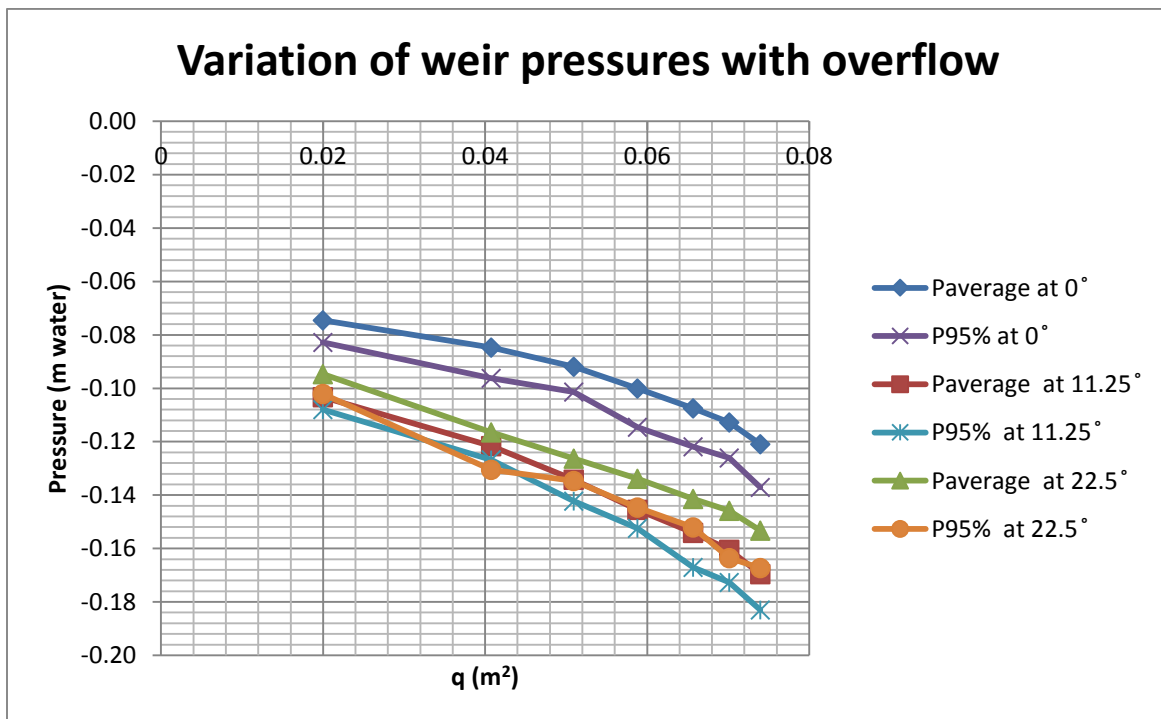


Figure 4.6 Pressures on surface of weir 3: R 0.05m

The $R = 0.15\text{m}$ weir model was tested again, after turning it through 67.5° in the downstream flow direction, for the first five inflows with the three pressure sensors now at 67.5° , 78.75° and 90° from the weir crest to span the assessment of pressure over the weir. The pressure also decreased as the inflow into the flume increased. Again the lower 95% of the pressure gave more negative pressure variation as compared to the average pressure. The pressure sensor at 90° from the weir crest showed that the pressure got to a point when it suddenly became high positive and negative, and started undulating as a result of the nappe pulsating. This was also confirmed by the pulsation of the nappe as seen visually during the tests with a fixed inflow. Figure 4.7 show the variation of pressure with increasing inflow.

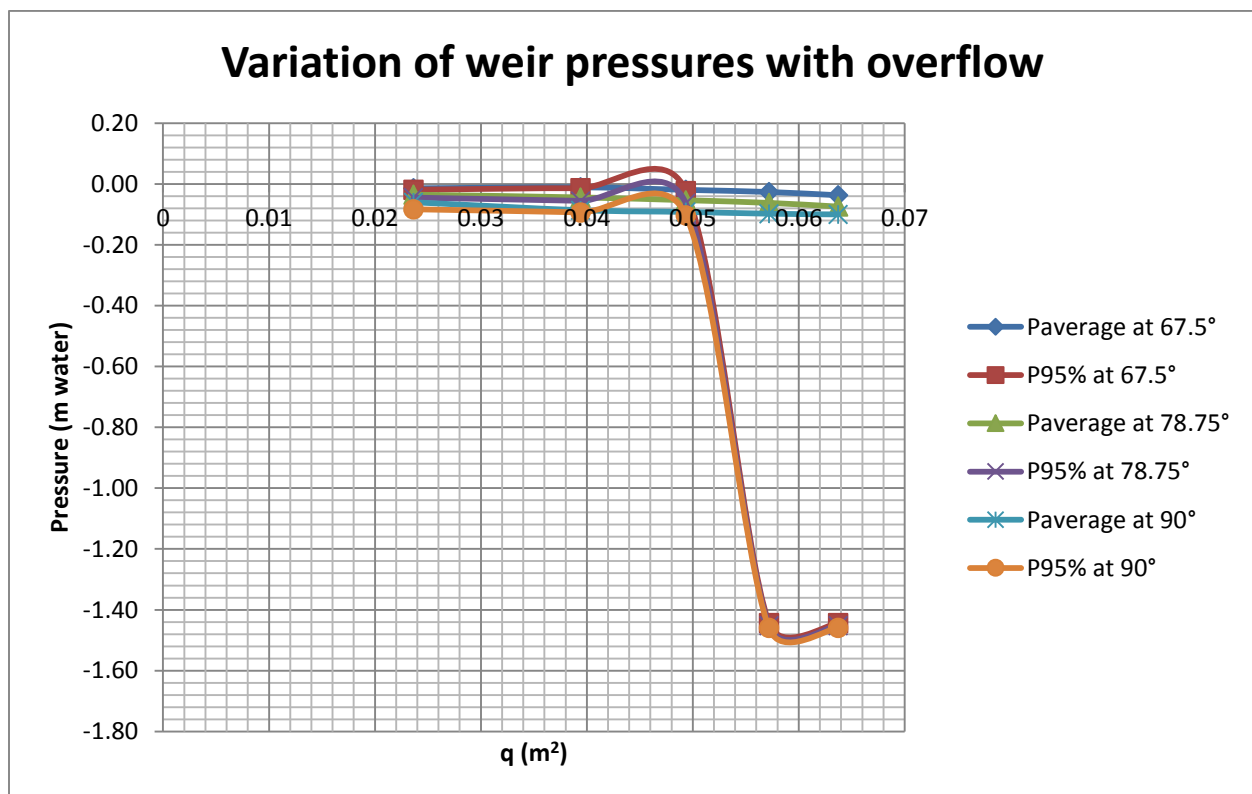


Figure 4.7 Pressures on surface of weir 1: R 0.15m

The pressure was also plotted as $P/(\rho_w g)$ against θ for the mean pressures for the first three pressure sensors on all weir models, and lastly the three pressure sensors on the $R = 0.15\text{m}$ weir model turned through 67.5° . Generally there was a decrease in pressure as the angle, θ , from the weir crest increased. However, as the weir radii decreased the pressure became more and more negative. Figures 4.8, 4.9 and 4.10 show the variation in pressure for the first three

sensor and Figure 4.11 shows the pressure for the last three sensors after turning the R = 0.15m weir by 67.5° in the downstream direction for the various inflows tested.

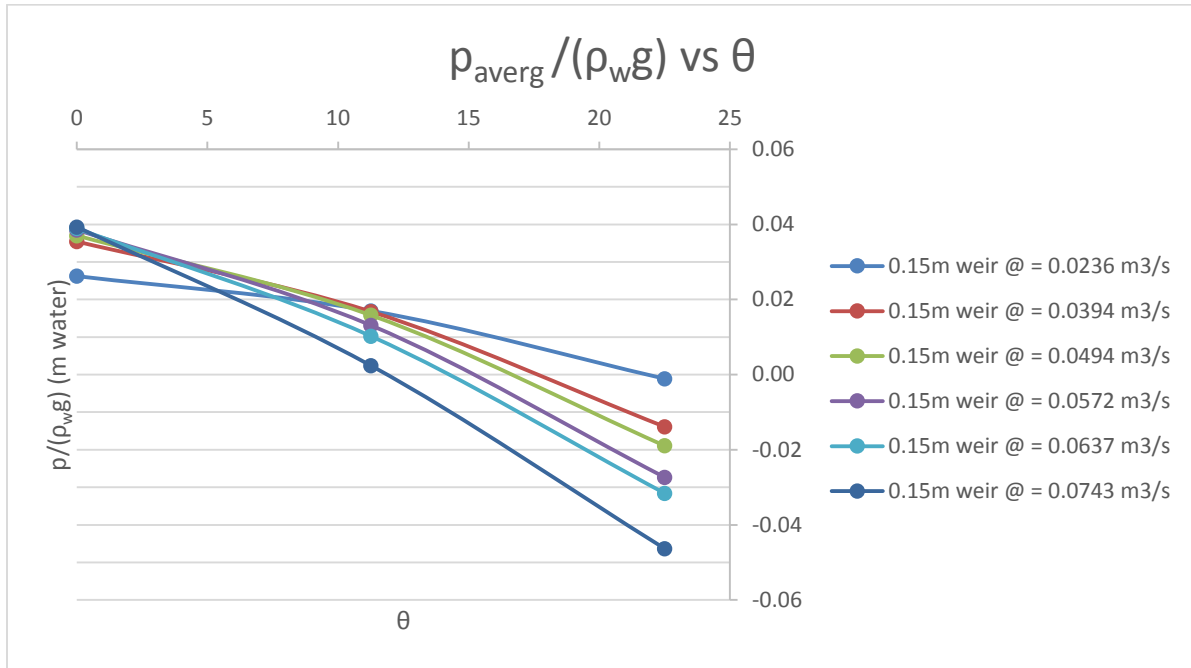


Figure 4.8 Measured average pressure against angle from weir crest for the R = 0.15m weir at 0°, 11.25° and 22.5° for different flows

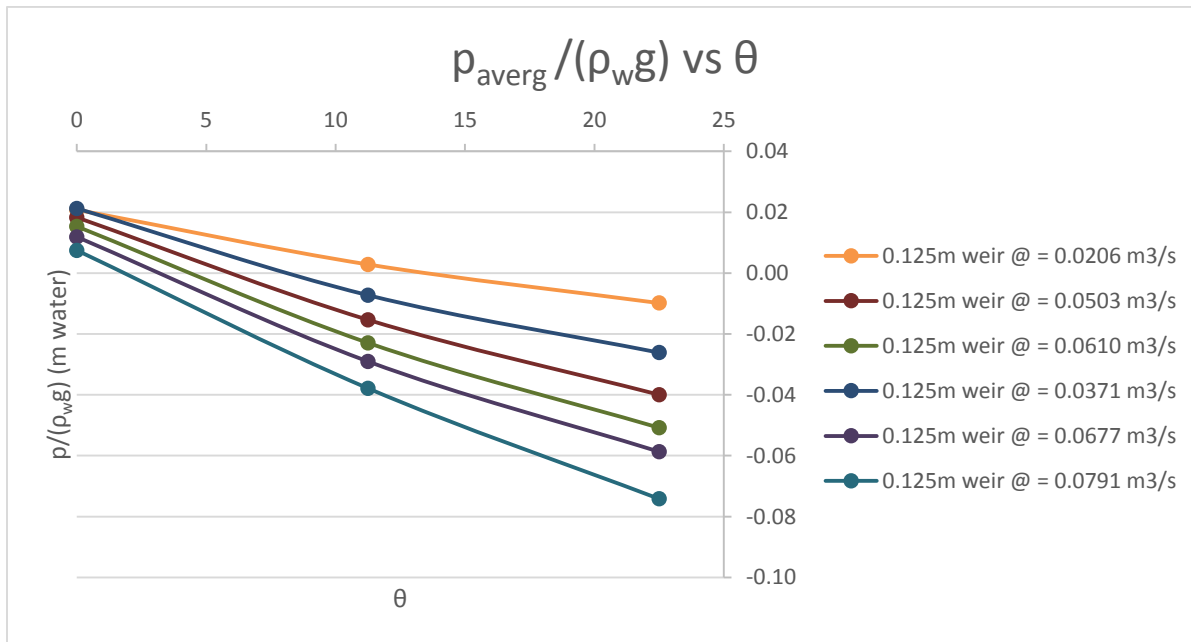


Figure 4.9 Measured average pressure against angle from weir crest for the R = 0.125m weir at 0°, 11.25° and 22.5° for different flows

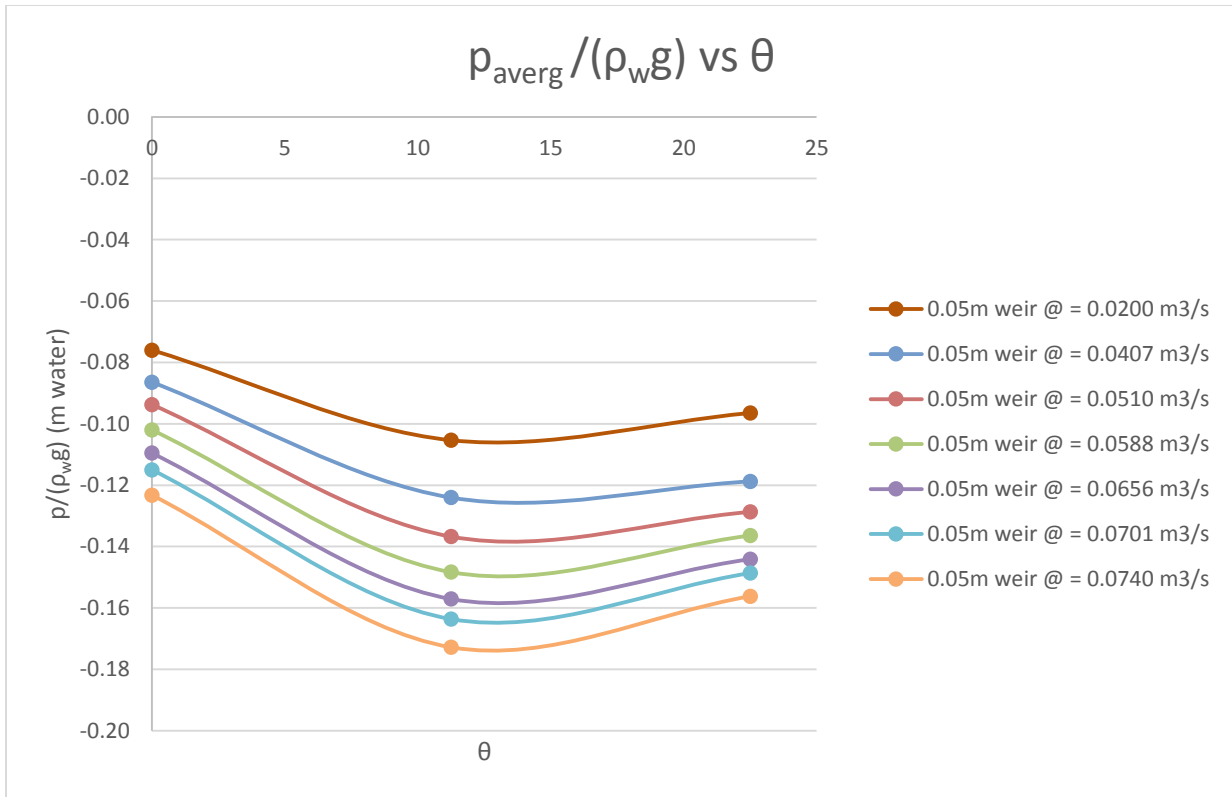


Figure 4.10 Measured average pressure against angle from weir crest for the R = 0.05m weir at 0°, 11.25° and 22.5° for different flows

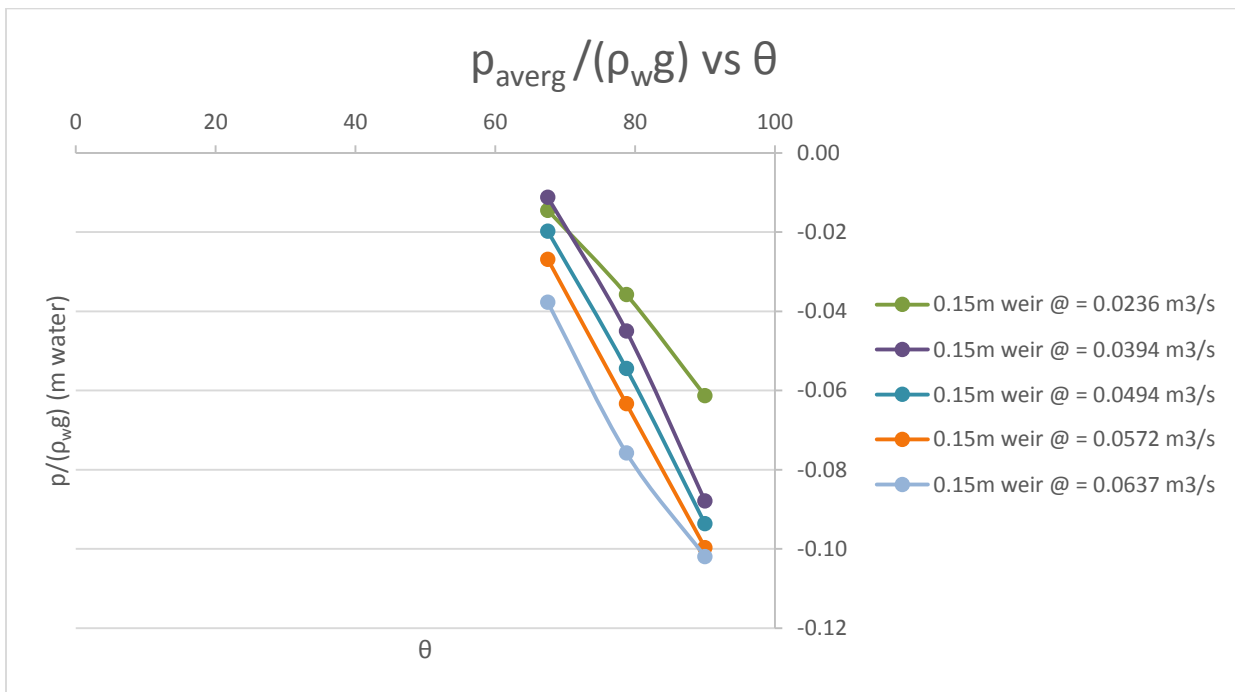


Figure 4.11 Pressure against angle for the R = 0.15 weir at different flows for the lower three pressure sensors after turning the R = 0.15m model

Experimental data shows that on the crest of the weir, 0° , pressure is mostly due to the water above the weir crest for a specific flow with a corresponding depth. As water moves to the downstream of the weir face, the centrifugal forces due to the curvature of the weir gradually increase, lowering the pressure on the face of the weir. Experimental data from all the weir test models was also compared with the motion equation 2.15 as derived by Chanson (1997) for the different Froude numbers at the corresponding inflow during the tests. Chanson's theoretical equation shows that the pressure should have been less negative as the weir radius decreases. The difference between the experimental data and equation 2.15 is due to the fact that the motion equation looks at an idea flow situation. Below is Figure 4.12, 4.13 and 4.15 showing the comparison of the theoretical equation for Chanson (1997) to the experimental data for the corresponding flows tested.

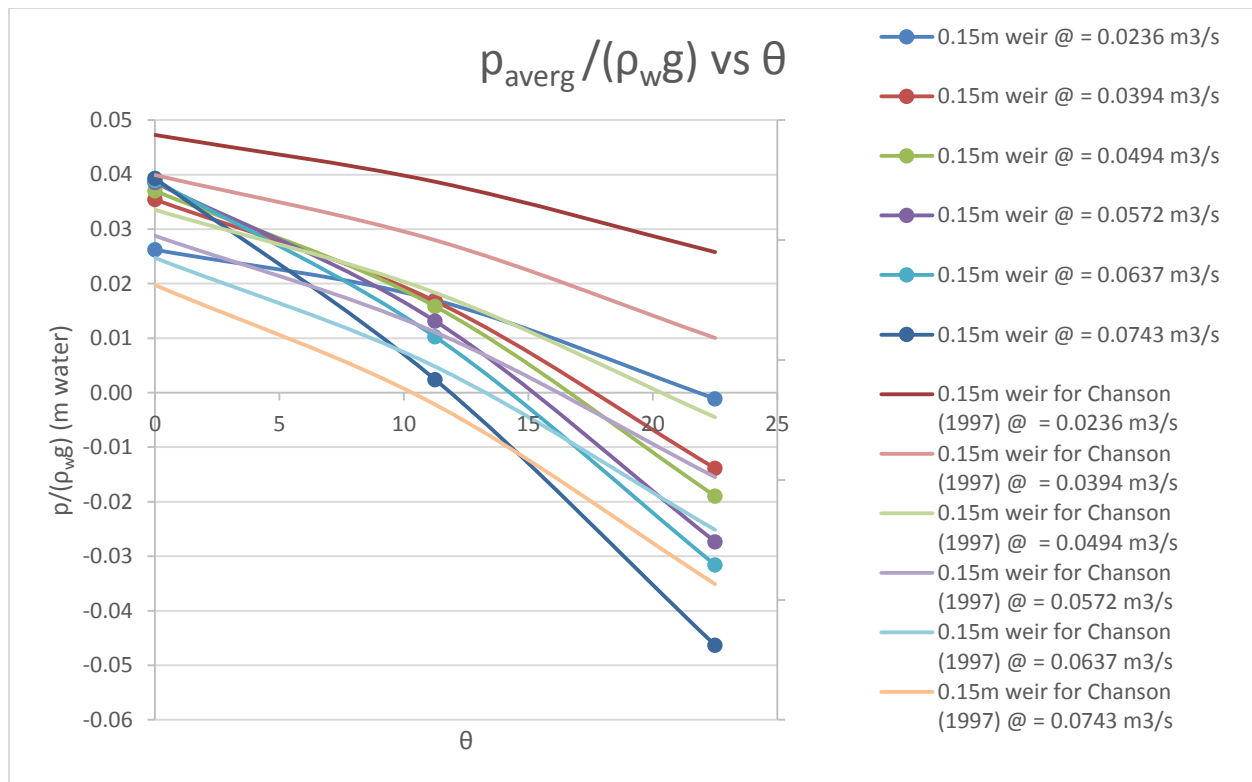


Figure 4.12 Comparison of Chanson (1997) motion equation and the first pressures at 0° , 11.25° and 22.5° on the $R=0.15\text{m}$

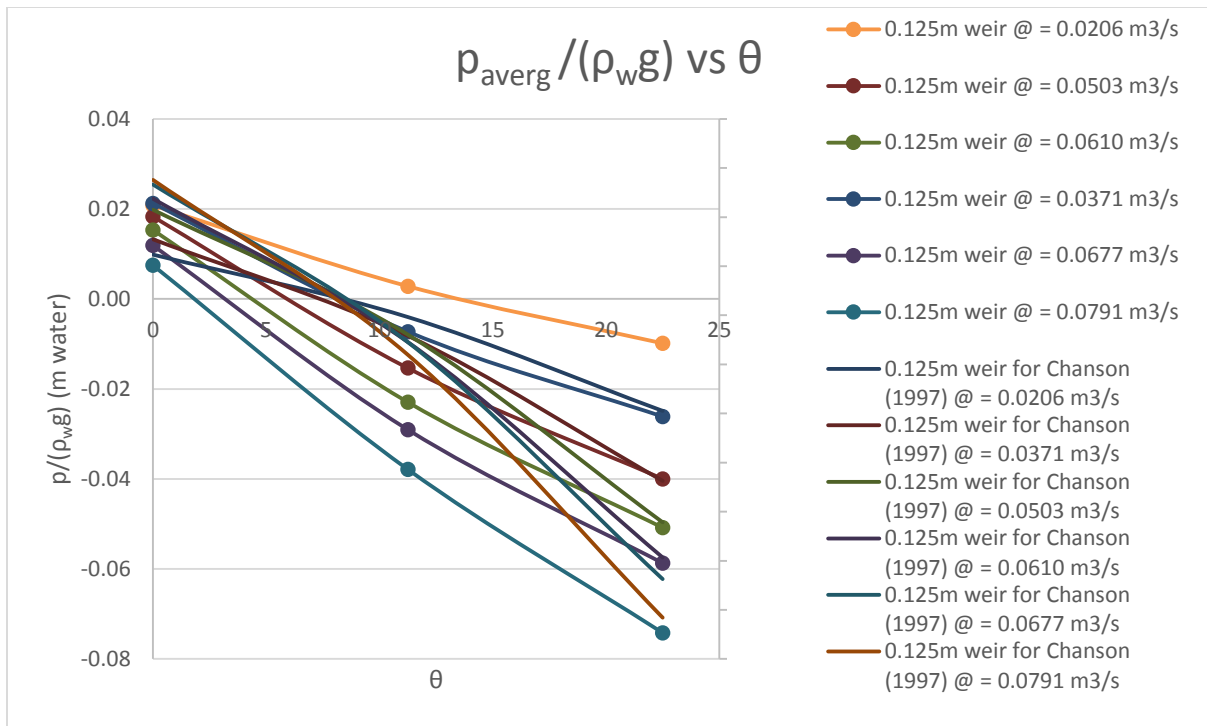


Figure 4.13 Comparison of Chanson (1997) motion equation and the first pressures at 0°, 11.25° and 22.5° on the R=0.125m

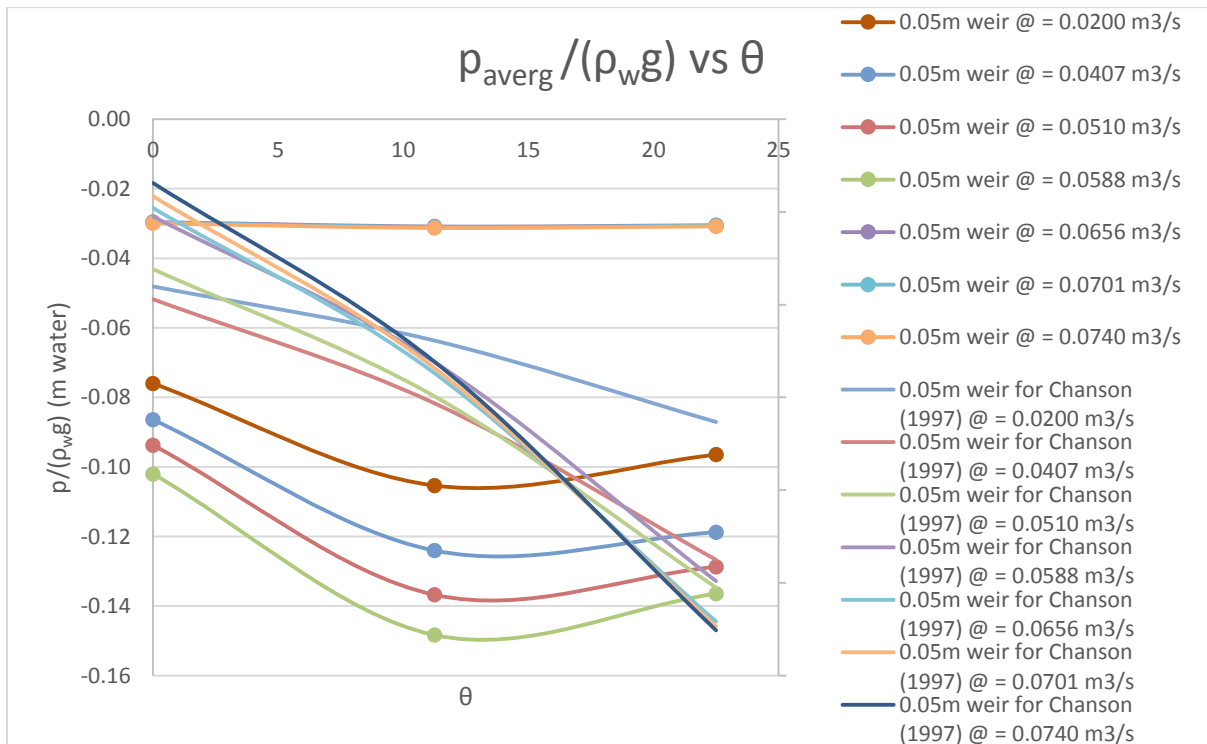


Figure 4.14 Comparison of Chanson (1997) motion equation and the first pressures at 0°, 11.25° and 22.5° on the R=0.05m

The $R = 0.05\text{m}$ weir, experimental data showed that the measured pressure continues to be negative. Figure 4.15 shows the comparison of the experimental data to Chanson's theoretical equation with pressure sensors at 67.5° , 78.75° and 90° for the respective Froude numbers due to the respective inflow.

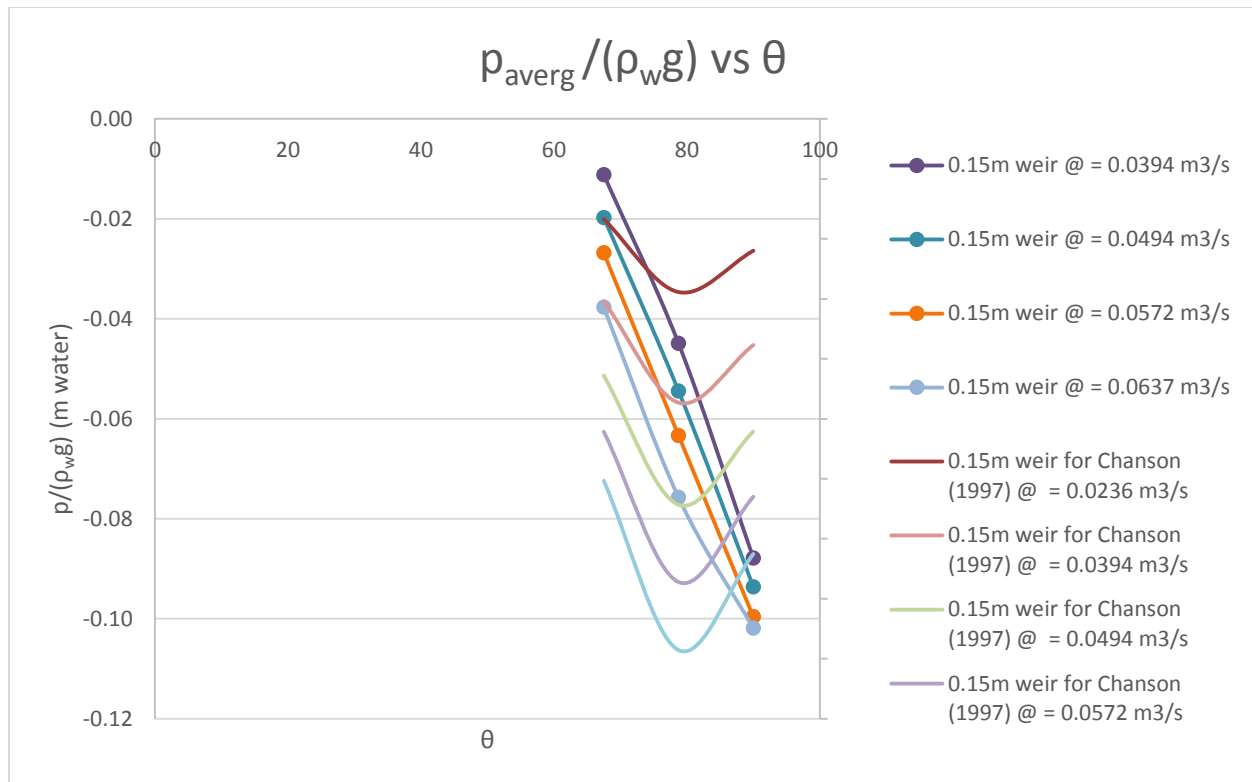


Figure 4.15 Comparison of Chanson (1997) motion equation and the experimental data after turning the $R = 0.15\text{m}$ model

As the nappe passed over the weir crest it adhered to the weir surface due to lack of aeration, a process called the Coanda effect (Coanda, 1932). With the almost uniform velocity and non-hydrostatic pressure distributions, a series of pressure changes were noticeable for each of the sensors. The reduction in pressure was a result of the curvature that caused the centrifugal force, at the same time introducing negative pressure on the wall of the weir (Abdul-latif, 2010). The centrifugal force, in effect, contributed to the negative pressures as seen above for all weir sizes. As the inflow water to the flume increased, the unit discharges over the weirs increased, resulting in an increase in the stage 'H.' Higher negative pressures occurred as the size of the weir reduced and could result in the bursting of the weir in the real life situation. On the lower

quadrant of the weir, the nappe also adhered to the wall due to lack of aeration, irrespective of the gravitational force. Separation occurred before the nappe impinged on the ground.

4.4 Crest depth and critical flow at crest

Experimental data shows that d_{crest}/d_c is fairly constant for each weir model tested in the study. The C_d is maximum when $d_{crest}/d_c = 1$. For d_{crest}/d_c less than one for on the test conducted shows that overflow on the circular weirs was at supercritical flow and critical flow conditions upstream of the weir crest. Figure 4.16 shows the relationship between d_{crest}/d_c with H_w/R .

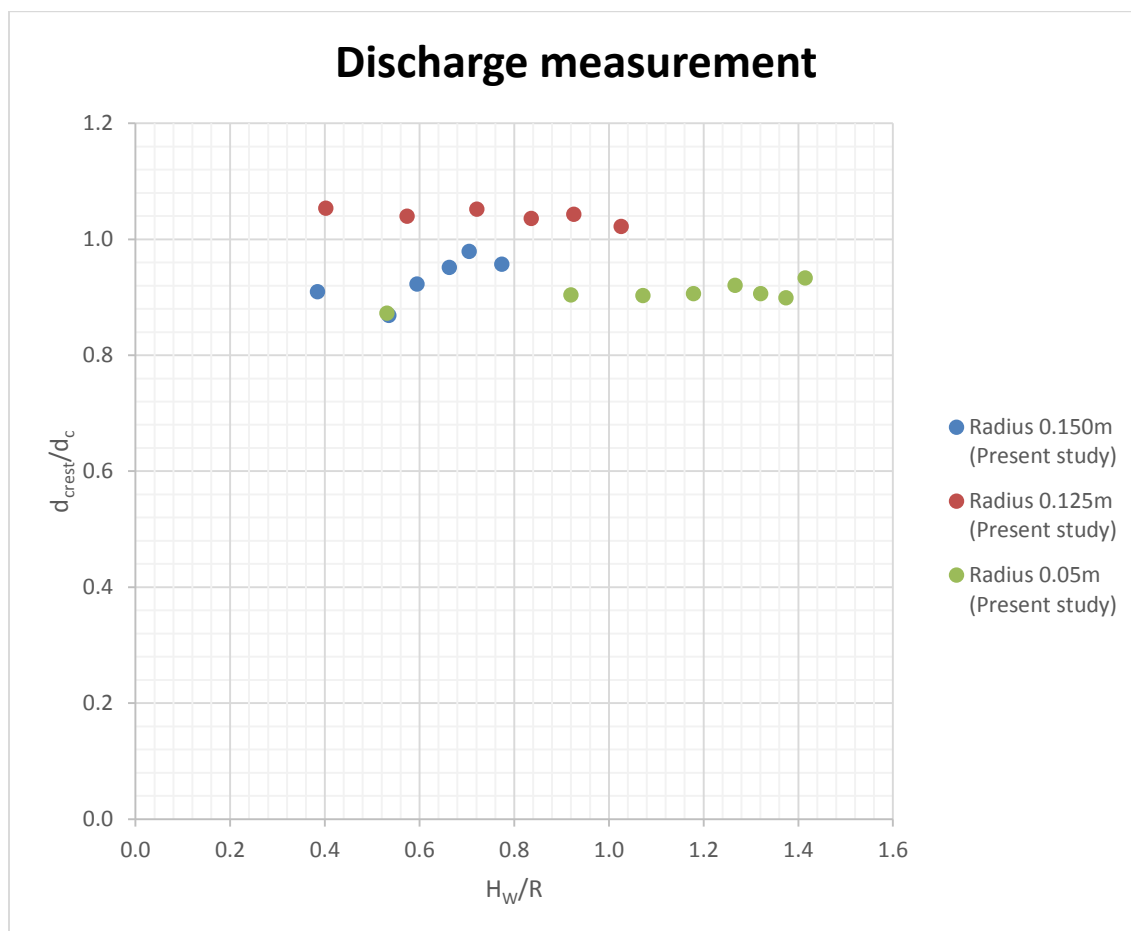


Figure 4.16 d_{crest}/d_c against H_w/R , a measure of discharge

d_{crest}/d_c values are close to 1 for the larger weir models, showing that the larger weirs (fully inflated weir) are capable of giving more discharge compared the smaller weir (slightly deflated weir). As q increases, d_{crest}/d_c is almost constant even as seen in literature studies by Chanson

(1998), with $d_{crest}/d_c \approx 0.85$ to 0.95 . The difference observed is mainly attributed to by the differences in the inflow condition (Chanson, 1998). For $H_w/R > 1$, d_{crest}/H_w was seen to be constant by many studies and the results from this study also showed that $d_{crest}/H_w \approx 0.7$ and is fairly constant throughout the tests conducted as inflow increased. Figure 4.17 shows the relationship of crest depth and H_w/R .

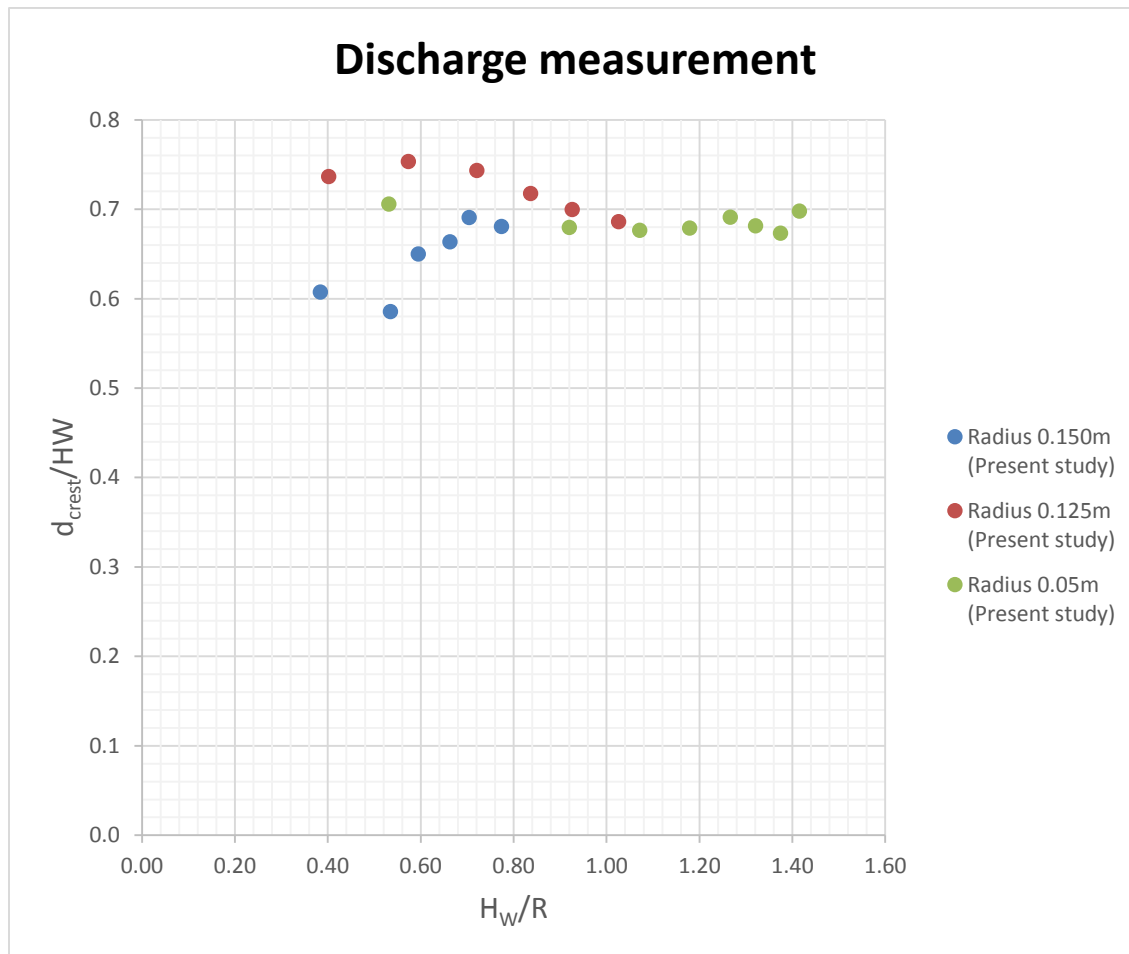


Figure 4.17 d_{crest} against q , a measure of discharge

4.5 Energy dissipation over of weir

As the inflow went over the weir and eventually forming a jump, energy was lost. Figure 4.18 shows the energy losses as realized with the measured values in the study.

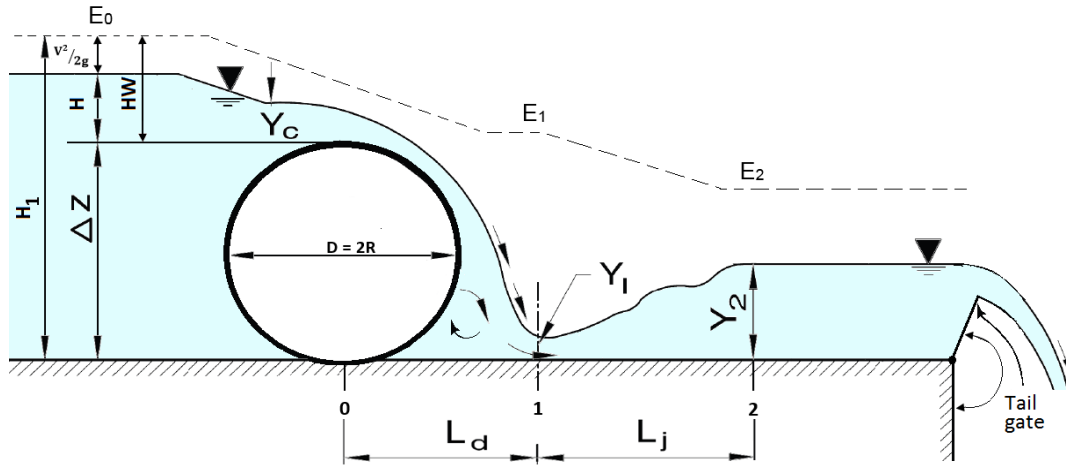


Figure 4.18 Energy line over weir and hydraulic jump (Viewed in the US laboratory)

From the results it is evident that energy is lost as overflow goes past the weir models. The energy loss ($E_0 - E_1$) is greater over the large weir and reduces as the weir radius, R , decrease. For a fixed weir radius, as the overflow increases, the energy loss is also reduced. Figure 4.19 and 4.20 show the energy dissipation over the weirs.

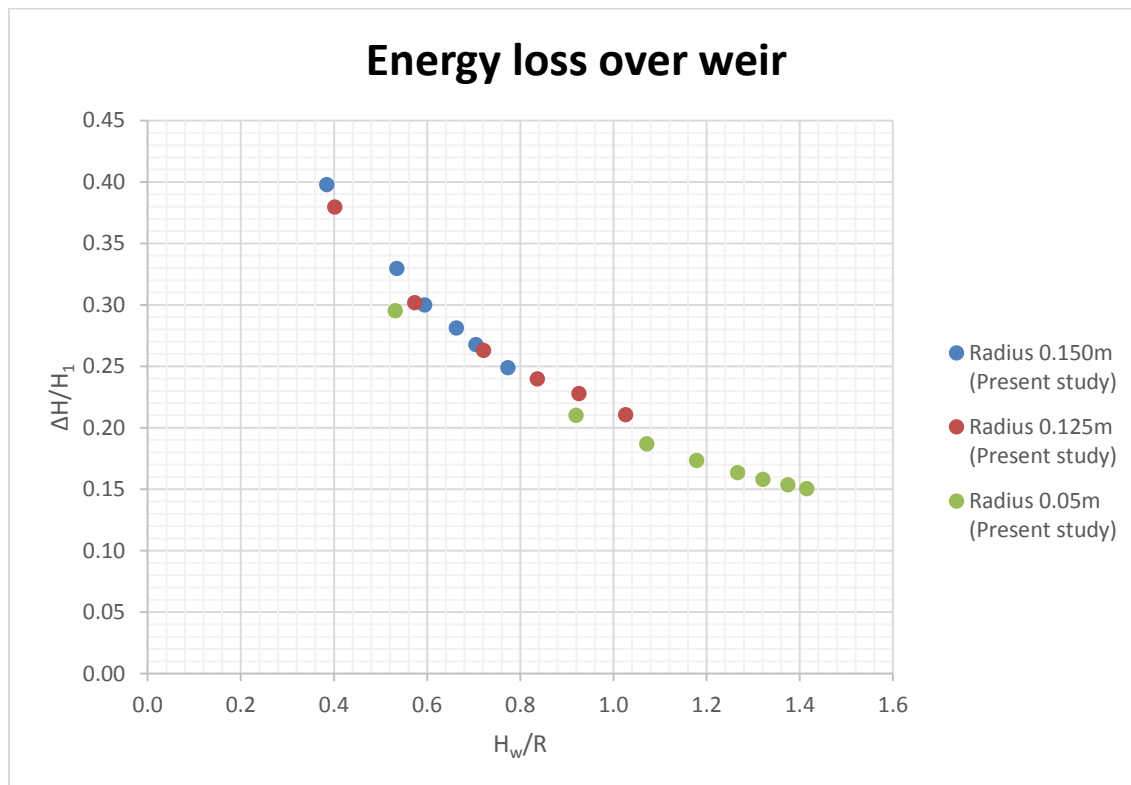


Figure 4.19 $\Delta H/H_1$ versus H_w/R a, measure of energy loss over weir

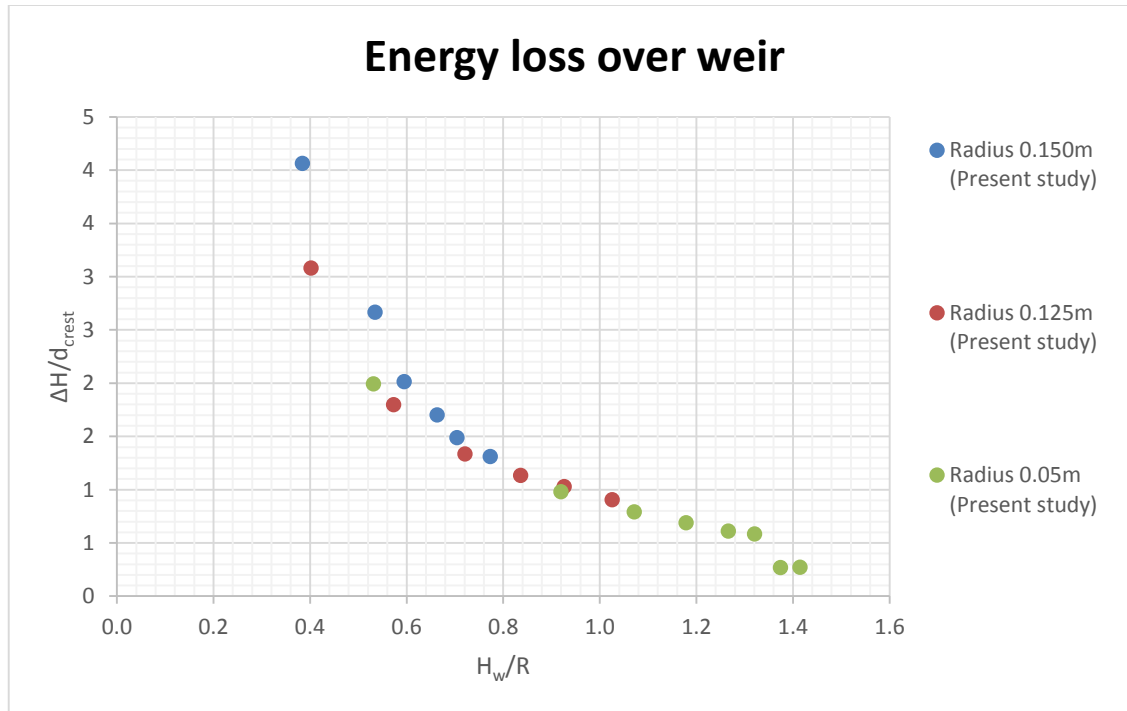


Figure 4.20 $\Delta H/d_{crest}$ versus, a measure of energy loss over weir

4.5 Energy dissipation downstream of weir

Energy dissipation downstream of the weir was due to the formation of a hydraulic jump. Experimental data shows that the energy loss due to an induced jump is varied. In most cases the introduction of a step at the bottom of hydraulic structure is put in place to control the formation of the hydraulic jump. Figure 4.21 shows the energy dissipation due to the hydraulic jump. Variation in the energy dissipation is a result of the oscillating jump and varying tailgate height.

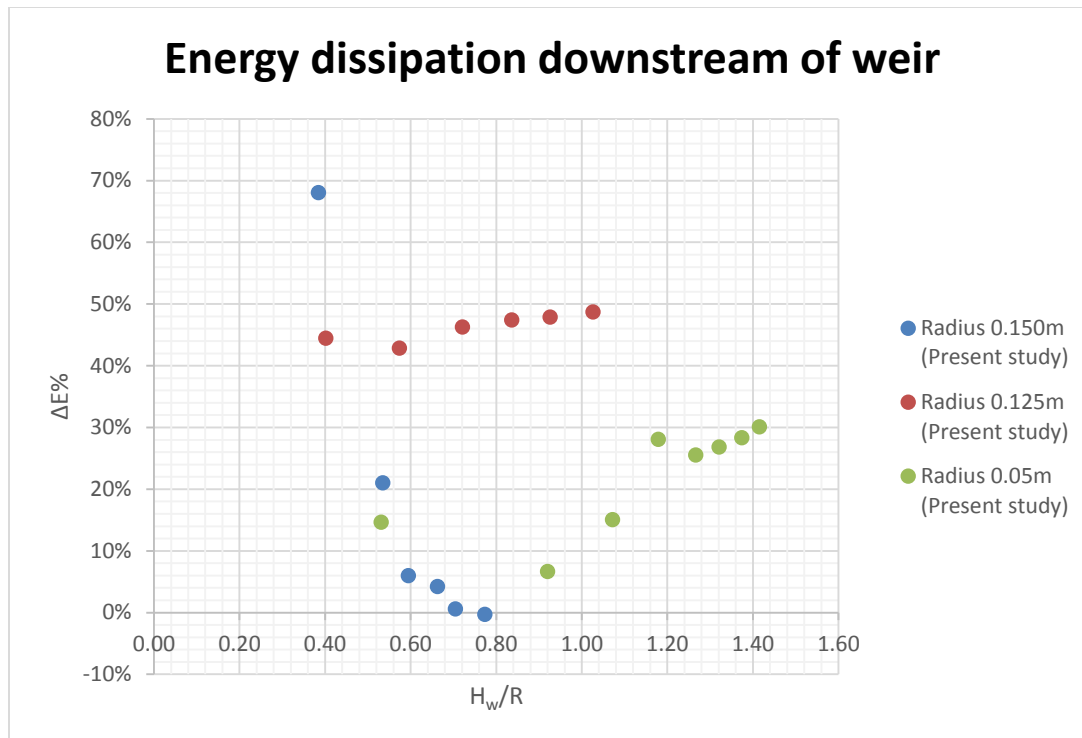


Figure 4.21 Variation of energy dissipation

4.6 Hydraulic jump length

Generally, the Froude number indicated that the flow downstream of the weir was at super critical, fast rapid flow. The jump was more stable with the smallest circular weir and could be more accurately determined in the case of a small weir. This is seen in Figure 4.22. Comparing the measured results with the USBR (1987) Shabanlou et al. (2013) relation of Froude number to dimensionless jump length shows that it was difficult to measure the jump length with the larger weir model as opposed to the small weir. This was mainly due to the oscillating jump length.

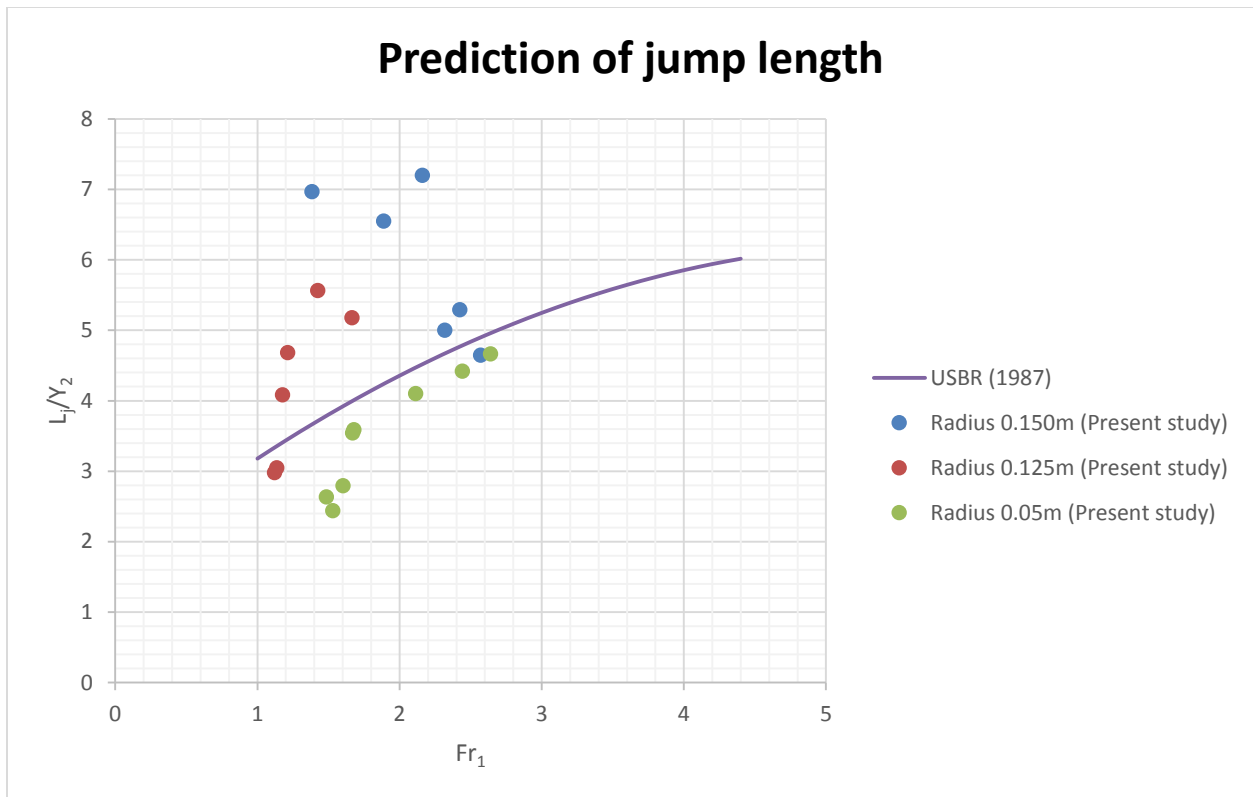


Figure 4.22 Relationship between L_j/Y_2 and Froude number

The pulsating jump length shows that there is more likelihood of having wave erosion in the fully inflated weir in the real life situation and this would reduce as it deflates.

CHAPTER 5: CONCLUSIONS AND RECOMMENDATIONS

This chapter summarizes the performance of the inflatable weir base on the circular weir findings on the discharge coefficient, head, total head, radius of curvature and nappe adherence and pressure distribution on the weir in the light of the hydraulics of the inflatable weir. As a conclusion to the study, the effect of the weir size and pressure in the three tests developed the hydraulics of the inflatable weir. Within the limits of the experimental data observed, assuming the deflation of an inflatable weir behaves as simulated by the circular weir, conclusions could be arrived at:

1. Based on literature by Chanson and Montes (1998), Shabanlou et al. (2013), Schmocker et al. (2011) and Bahzad et al. (2010), upstream arches have insignificant influence on the performance of the inflatable weir. There is rather reduced afflux due to the shape of the upstream of the weir from the Bernoulli's equation. This shape of the upstream of the weir also contributes to the transport of sediments Gebhardt et al. (2012).
2. Investigation of the discharge coefficients vary between 1.0 to 1.3 for the radii tested and general conclusions are:
 - As the weir radius is reduced during the deflation, the unit discharge over each weir increased with increase in head above the crest.
 - Discharge coefficient of the inflatable weir increases with the increase in head, and is inversely proportional to the radius of curvature.
3. Investigation of the pressures on the downstream face of the weir models showed that:
 - As the weir radius decreases during deflation, the suction/negative pressure acting on the downstream face of the weir became more negative with increasing H/R values.
 - Pulsation of the nappe occurred 90° from the weir crest as nappe detached from the weir.

Pressures ranges measured during the experimental study on the test models are tabulated in table 5.1 and table 5.2 shows an example of a prototype weir 3m high. Negative

pressures lower than -10m water in Table 5.2 indicate locations on the weir surface where cavitation is expected to occur.

Table 5.1 Range of pressure measured from weir face during experiments on weir models

Pressure from weir crest	Range measured of experimental data (m water)	Pressure from weir crest	Range measured of experimental data (m water)
P_{average} at 0°	0.026 to -0.121	P_{average} at 67.5°	-0.014 to -0.0370
$P_{95\%}$ at 0°	0.021 to -0.137	P_{average} at 78.75°	-0.035 to -0.074
P_{average} at 11.25°	0.017 to -0.170	P_{average} at 90°	-0.060 to -0.100
$P_{95\%}$ at 11.25°	0.013 to -0.183	$P_{95\%}$ at 67.5°	-0.0187 to -1.444
P_{average} at 22.5°	-0.001 to -0.153	$P_{95\%}$ at 78.75°	-0.045 to -1.452
$P_{95\%}$ at 22.5°	-0.007 to -0.167	$P_{95\%}$ at 90°	-0.083 to -1.459

Table 5.2 Range of pressure weir face on a prototype weir 3m high

Pressure from weir crest	Range measured of experimental data (m water)	Pressure from weir crest	Range measured of experimental data (m water)
P_{average} at 0°	0.26 to -1.21	P_{average} at 67.5°	-0.14 to -0.370
$P_{95\%}$ at 0°	0.21 to -1.37	P_{average} at 78.75°	-0.35 to -0.74
P_{average} at 11.25°	0.17 to -1.70	P_{average} at 90°	-0.60 to -1.00
$P_{95\%}$ at 11.25°	0.13 to -1.83	$P_{95\%}$ at 67.5°	-0.187 to -14.44
P_{average} at 22.5°	-0.01 to -1.53	$P_{95\%}$ at 78.75°	-0.45 to -14.52
$P_{95\%}$ at 22.5°	-0.07 to -1.67	$P_{95\%}$ at 90°	-0.83 to -14.59

4. Investigation of energy dissipation over the weir; and characteristics of the downstream hydraulic jump:

- Energy dissipation over the weir decreases with the decrease in the weir radius.

In general, the jump is more stable with the smallest circular weir and could be more accurately determined in the case of a small weir.

Recommendation

Future research on inflatable weirs should aim to monitor the negative pressures further downstream of the weir, because larger negative pressure is expected to occur lower down from the 90° angle used in this study.

REFERENCE LIST

1. Abdelazim M. Ali, Ahmed El-Belasy, Mohamed Roushdy, Mohamed Bahgat, Abdelhamid Abdelhaq, Karima Attia, Medhat Aziz, Mohamed Ali Hamed, Heba El Sersawi, Sonia El-Serafy, Peter Ryad, Mohamed El-Zeir, Moahmed Sobeih, Essam El-Din. (2010). "A Hybrid Approach to Improve the Design of Stilling Basin": Coordinated by Dr. Ahmed Sayed Mohamed Ahmed Hydraulics Research Institute NBCBN Egypt Node Hydraulics Research Institute Country Coordinator Prof. Dr. Fathi El-Gamel
2. Alan S. Morris. (2001). "Measurement and Instrumentation Principles. Third edition".
3. Anwar H. O. (1967). "Inflatable dams: J. Hydraulics Division", ASCE 93 (1967) 99-119.
4. Alhamati A.A. (2002). "Investigation and analysis of inflatable dams", [M.Sc. thesis]: Building and Construction Department, University of Technology, Baghdad, Iraq, p. 117.
5. Al-Shami A. (1983). "Theory and design of inflatable structures", [Ph.D. thesis].
6. Alwan, A.D. (1979). "The analysis and design of inflatable dams", [Ph.D. thesis]: University of Sheffield, Sheffield, United Kingdom, p. 195.
7. Andrew Chadwick, John Morfett, Martin Borthwick (2004). "Hydraulics in Civil and Environmental Engineering." Chapter 5
8. Arcon-aquapro. (2013) <http://www.arcon-aquapro.com/>
9. Sara Bagheri & Manouchehr Heidarpour (2010). "Overflow characteristics of circular-crested weirs", Journal of Hydraulic Research, 48:4, 515-520
10. Benyamin Naghavi , Kazem Esmaili , Jafar Yazdi and Fatemeh Koorosh Vahid (2011). "An experimental and numerical study on hydraulic characteristics and theoretical equations of circular weirs." Canadian Journal of Civil Engineering. 38.12 (Dec. 2011): p1327
11. Bhowmik G. (2003). "Hydraulic Jump Type Stilling Basins for Froude Number 2.5 to 4.5."
12. Bridgestone Corporation. (1994). "Questions and answers about the Bridgestone rubber dam": Tokyo, Japan.
13. Bridgestone Corporation (1997a). "Rubber dam inflatable rubber weir": Tokyo, Japan'.
14. Brussels, January (2006). "INCOM WG26 Report: Design of Movable Weirs and Storm Surge Barriers", Publ. PIANC.
15. Bos M.G. (1989). "Discharge Measuring Structures": Oxford & IBH Publishing Co., New Delhi, India.

16. Charles R, Rodney D, Jeremy P. (2004). "River Weirs – Good Practice Guide." Guide - Section B3. R&D Publication W5B-023/HQP: Research Contractor, Mott MacDonald Ltd and University of Hertfordshire.
17. Cruise, Singh and Sherif (2007). "Elementary Hydraulics, International Edition ISBN10": 0-495-08239-2 ISBN13: 978-0-495-08239-2'
18. Bos, M. G. (1978). "Discharge measurement structures." Wageningen, The Netherlands: Int. Institute for Land Reclamation and Improvement.
19. Chanson H. and Montes, J.S. (1998). "Overflow Characteristics of Circular Weirs: Effect of Inflow Conditions." *Jl of Irrigation and Drainage Engrg.*, ASCE, Vol. 124, No. 3, pp. 152-162 (ISSN 0733-9437).
20. Chanson H. (1998). "Hydraulics of rubber dam overflow": A simple design approach 13th, Australasian Fluid Mechanics Conference, pp.255-258.
21. Chanson H. (1996). "Some Hydraulic Aspects during Overflow above Inflatable Flexible Membrane Dam": Report CH47/96, Dept. of Civil Engineering, University of Queensland, Australia, May, 60 pages (ISBN 0 86776 644 1).
22. Chanson H. (1997). "A Review of the overflow of inflatable flexible membrane dams": *Australian Civil/Structural Engineering Transactions*, Vol. CE39, No.2 & 3, pp.107-116.
23. Chanson H. (2004). "Environmental Hydraulics of Open Channel Flows." ME, ENSHM Grenoble, INSTN, PhD (Cant), DEng (Qld) Eur Ing, MIEAust, MIAHR 13th Arthur Ippen awardee (IAHR) Reader in Environmental Fluid Mechanics and Water Engineering The University of Queensland, Australi E-mail: h.chanson@uq.edu.au
24. Chanson H. (2005). "Some hydraulic aspects during overflow above inflatable flexible membrane dam": Department of civil Engineering, The University of Queensland Brisbane QLD 4072, Australia.
25. Chanson H. (2006). "Minimum Specific Energy and Critical Flow Conditions in Open Channels." *Jl of Irrigation and Drainage Engrg.*, ASCE, Vol. 132, No. 5, pp. 498-502 (ISSN 0733-9437).
26. Cheng P. (1997). "A review of the use of rubber dams in Hong Kong. M.Sc. dissertation": The University of Hong Kong, Hong Kong, China.
27. Chervet A. (1984). "Model-prototype comparison of the defective behaviour of an inflatable dam": *Symposium on Scale Effects in Modeling Hydraulic Structures*, S.1.16-1 bis 1.16-6.
28. Chow V.T. (1959). "Open Channel Hydraulics": International Student Edition. John Wiley & Sons, New York, p. 362-363.
29. Coanda H. (1932). "Procédé de Propulsion dans un Fluide." ('Propulsion Process in a Fluid') Brevet Invent. Gr. Cl. 2, No. 762688, France (in French).

30. Dr. Bahzad M.A. and Noori Mrs. Rondik Adil Jaafar (2010). "Crest Shape Effect on the Performance of Rectangular Side Weirs." Civil Engineering Dept. College of Engineering and Dept. of Water Resources, University of Duhok.
31. ec21(2013) http://cnfilter1.en.ec21.com/Rubber_Dam--3980865_3981619.html
32. Emad Abdul Gabbar, Adnan Abdul Wahab and Mohammad Akram (2011) "Overflow Characteristic of Cylindrical Shape Crest Weirs Over Horizontal Bed." Tikrit Journal of Engineering Sciences/Vol.18/No.4/December 2011, (92-39)
33. Emad Abdul Gabbar Al Babely (2012). "Behavior of the Discharge Coefficient for the Overflow Characteristics of Oblique Circular Weirs." Tikrit Journal of Engineering Sciences/Vol.19/No.4, (55-64)
34. Evan C; Karst S. (2010). "Generalized Monitoring Strategy."
35. Fawer C. (1937). "tude de quelques écoulements permanents à filets courbes." Thesis, Univ. de Lausanne, La Concorde, Lausanne, Switzerland (in French).
36. Finnemore, John E. and Joseph B. Franzini. (2002). "Fluid Mechanics with Engineering Applications". 10th ed. Boston: McGraw-Hill.
37. Gebhardt M. (2006). "On the causes of vibrations and the effects of Inflatable Dams": Federal Waterways Engineering and Research Institute Karlsruhe, Germany.
38. Gebhardt M. (2006). "Hydraulic and Structural Design of Inflatable Dams Dissertation": University Karlsruhe.
39. Gebhardt Michael Dr.-Ing. , Udo Pfrommer Dipl.-Ing. (FH) , Fabian Belzner M. Eng. & Norbert Eisenhauer (2012). "Backwater effects of Jambor weir sill", Journal of Hydraulic Research, 50:3, 344-349, DOI: 10.1080/00221686.2012.686712.
40. George R. and Stefan H. (2004). "Use of Inflatable Weir Structures Makes Water Resources Management More Efficient": Florida water resources journal.
41. Habibzadeh A., S.M.ASCE¹; S. Wu²; Ade³ F.; Rajaratnam N., F.ASCE⁴; and Loewen M. R.⁵ (2011). "Exploratory Study of Submerged Hydraulic Jumps with Blocks. "
42. Henderson, F. M. (1966). "Open channel flow", MacMillan, New York.
43. Heidarpour, M. and Chamani, M. R.(2010). "Velocity distribution over cylindrical weirs", Journal of Hydraulic Research, 44: 5, 708 — 711
44. Hager Willi H. (1985). "Critical flow condition in open channel hydraulics" Acta Mechanica, Vol.54(3), pp.157-179 [Peer Reviewed Journal].
45. Hager, W. H. (1994b). "Discussion of Momentum model for flow past weir", by A. S. Ramamurthy, N.-D. Vo., and G.Vera." J. Irrig. Drain Eng., 120(3), 684–685.

46. Haghiabi AH. (2012). "Department of Water Engineering, College of Agriculture", Lorestan University, Khorramabad 68149-84649, Iran
47. Honar, T. and Keshavarzi, A. (2008). "Effect of Rounded-Edge Entrance on Discharge Coefficient of Side Weir in Rectangular Channels", *Irrig. and Drain.* Published online in Wiley InterScience (www.interscience.wiley.com) DOI: 10.1002/ird.420
48. Jaeger C. (1956). "Engineering fluid mechanics", Blackie & Son, Glasgow,U.K.
49. Jahanshir Mohammadzadeh-Habili, Manouchehr Heidarpour (2013). "Department of Water Engineering", College of Agriculture, Isfahan University of Technology, Isfahan 84156-83111, Iran
50. Jambor, F. (1953). "Increase of fixed weir sill at identical hydraulic capacity". *Mitteilungsblatt der Bundesanstalt für Wasserbau* 1, 1–2 (in German).
51. Jambor, F. (1959). "Possible increase of fixed weir-sill and arrangement of the associated weir design, especially the sector gate". *Die Bautechnik* 36(6), 221–228; 36(8), 297–300 (in German).
52. Joongu Kang, Sungjoong Kim, Hongkoo Yeo, Namjoo Lee (2014). "Experimental Study on Flow Characteristic in Sloping Weir." Water Resource Research Department, Korea Institute of Construction Technology, Goyang, Korea Kyungsoong University, Busan, Korea
53. Abdullah Ali Nasser Alhamati, Thamer Ahmed Mohammed, Abdul Halim Ghazali, Jamalodin Norzaie and Karim Khalaf Al-Jumaily (2005). "Determination of coefficient of discharge for air-inflated dam using physical model": *Suranaree J. Sci. Technol.* Vol. 12 No. 1.
54. Lakshmana Rao . N.S. (1975). "Theory of Weirs". In: Chow, V.T. (ed.), *Advances in Hydroscience*, Vol. 10. Academic Press, NewYork, pp. 309–406.
55. Matthew G. D. (1991). "Higher order one dimensional equations of potential flow in open channels." *Proc.-Inst. Civ. Eng.*, 91, 187–201.
56. Markus M.R., Thompson C.A. and Ulukaya M. (1995). "Aquifer recharge enhanced with rubber dam installations": *Water Engineering and Management*, 142(1): 37–40.
57. Minor H.E. (1975). "Schwingungen überströmter Wehre und ihre Beseitigung": *Universität Stuttgart, Mitteilungen Nr. 35.*
58. Montes, J. S. (1970). "Flow over round crested weirs." *L'Energia Elettrica*, 47(3), 155–164.
59. Bruce R. Munson, Theodore H. Okiishi, Wade W. Huebsch and Alric P. (2013). "Fundamentals of fluid mechanics"
60. Charles Rickard, Rodney Day, Jeremy Purseglove (2005). "River Weirs – Good Practice Guide: R&D Publication W5B-023/HQP", Mott MacDonald Ltd and University of Hertfordshire.

-
61. Ogihara K. and Muramatsu T. (1985). "Rubber dam, causes of vibrations of rubber dams and counter measures": 21st IAHR Congress, Melbourne, Australia, pp.601-604.
 62. Oscar Castro-Orgaz & Willi H. Hager (2014). "Scale effects of round-crested weir flow, Journal of Hydraulic Research", DOI: 10.1080/00221686.2014.910277
 63. Papoutsis-Psychoudaki S. and Sutton P. (1988). "Details of the flow and bottom pressure downstream of a thin-plate weir": Agric. Water Manage, 13: 369-382.
 64. Plaut R.H., Liapis S.I., and Telionis D.P. (1998). "When the levee inflates". ASCE, Vol. 68, No. 1.
 65. Rooseboom A. and Jordaan J. M. (2011). "Hydraulic structures, equipment and water data acquisition systems": Wells Bloomington, IN 47405, USA.
 66. Rothman and Greenland (1998). "Principles and Quantitative Methods Modern Epidemiology": Epidemiologic Research Chapters 7, 8. Kleinbaum, Kupper and Morgenstern. Chapter 10, Introduction to Validity.
 67. Rand. W (1955). "Flow geometry at straight spillways. Proc. ASCE, 81 (791) 1-13.
 68. Rouve, g., and Indlekofer, H. (1974). "Discharge over Straight Weirs with Semi cylindrical Crest." Vol. 49, No. 7, pp. 250-256 (in German)
 69. Saeid Shabanlou, Eghbal Khorami , Ahmad Rajabi (2013). "The effects of various upstream arches of crest of the circular crested weir on hydraulic parameters". www.elsevier.com/locate/flowmeasinst
 70. Sarginson E. J. (1972). "The influence of surface tension on weir flow, Journal of Hydraulic Research", 10:4, 431-446
 71. Schmocker Lukas, Berglind R. Halldórsdóttir and Hager Willi H. (2011). "Effect of Weir Face Angles on Circular-Crested Weir Flow DO": 10.1061/(ASCE)HY.1943-7900.0000346. American Society of Civil Engineers
 72. Shabanlou, S., and Khorami, E. (2013). "Study of the hydraulic properties of the cylindrical crested weirs." J. Flow Meas. Instrum., 33, 153–159.
 73. Stuart W. (2012). "Long crested weir design": Cal Poly Irrigation Training and Research Center www.itrc.org.
 74. Sumitomo (1985). "Technical description of Sumigate inflatable rubber dams": Osaka, Japan.
 75. Tam P.W.M. (1994). "River improvement work in Hong Kong. In Proceedings of the 9th IWSA–ASPAC Regional Conference and Exhibition": Philippine Water Works Association, Inc., Manila, The Philippines. pp. A30–A39.

-
76. Tam P.W.M. (1997). "Use of rubber dams for flood mitigation in Hong Kong": ASCE Journal of Irrigation and Drainage Engineering, 123(2): 73–78.
 77. Thabet M. Abdul-latif * & Mohammed Sharif Abdul-Mohsen. (2010). "Calibrating the Discharge Coefficient of Semicircular Crested Weir". Eng. &Tech. Journal, Vol. 28, No. 24, 2010.
 78. Thornton Christopher I., Anthony M. Meneghetti, Kent Collins, Steven R. Abt, and S. Michael Scurlock (2011). "Stage-Discharge Relationships for U-, A-, and W-Weirs in Un-submerged Flow Conditions": Journal of the American Water Resources Association (JAWRA) 47(1):169-178. DOI: 10.1111/j.1752-1688.2010.00501.x.
 79. U.S. Army (2011). "Cold Regions Research and Engineering Laboratory", Hanover, New Hampshire.
 80. Victor J. Schoenbach and Wayne D. Rosamond (2000). "Understanding the Fundamentals of Epidemiology an evolving text": Ph.D. Department of Epidemiology School of Public Health University of North Carolina at Chapel Hill Fall 2000 Edition
 81. Water Supplies Department. (1976). "Plover Cove: Government Printer, Hong Kong, China."
 82. Zhang X.Q., Tam P.W.M., and Zheng W. (2002). "Construction, operation, and maintenance of rubber dams."
 83. William W. (2006). "Inflatable weir fish passage systems and methods US 7670083 B2". Online <http://www.google.com/patents/US7670083>
 84. Wittler JR (2004). "Upper Gila River fluvial geomorphology study". Final report Arizona US Department of The Interior Bureau Of Reclamation.
 85. <http://www.savatech.eu/environmental-protection-and-rescue/rubber-dam/water-and-air-filled-rubber-dams.html>
 86. http://en.wikipedia.org/wiki/Hydraulic_jump
 87. http://en.wikipedia.org/wiki/Inflatable_rubber_dam
 88. wikipedia.org (2013). http://en.wikipedia.org/wiki/Hydraulic_jump
 89. <http://books.google.co.za/books?id=TxLtWJwYY8oC&pg=PA67&lpg=PA67&dq=submerged+jump&source=bl&ots=QFZDYF1tpj&sig=h7ONqK4xY9g5JjKqTR-9YpibZfc&hl=en&sa=X&ei=-x6cU87rPMKBPebkgfgE&ved=0CFIQ6AEwDA#v=onepage&q&f=true>

APPENDIX A: Over flow over weir models

Weir 1



Hydraulic jump at 98.709l/s over a 0.3m diameter weir

Weir 2



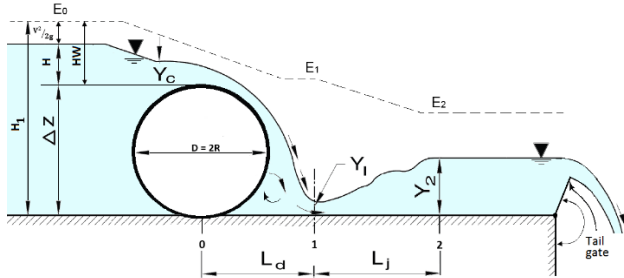
Hydraulic jump at 41.208l/s over a 0.25m diameter weir

Weir 3



Hydraulic jump at 101.9l/s over a 0.1m diameter weir

APPENDIX B: Experimental data on discharge measurement



Radius 0.150m (Present study)

Test	Q (m^3/s)	q (m^2/s)	g (ms^{-2})	$\Delta Z = D$ (m)	H (m)	H_w	H_w / R	d_{crest} (m)	C_d	d_{crest} / H_w	d_c	d_{crest}/d_c	Y_1 (m)
A1	0.0473	0.0236	9.81	0.3	0.0574	0.0576	0.3842	0.035	1.0024	0.6074	0.0385	0.9096	0.031
A2	0.0788	0.0394	9.81	0.3	0.0797	0.0802	0.5350	0.047	1.0163	0.5857	0.0541	0.8691	0.035
A3	0.0987	0.0494	9.81	0.3	0.0884	0.0892	0.5948	0.058	1.0861	0.6501	0.0628	0.9228	0.038
A4	0.1144	0.0572	9.81	0.3	0.0984	0.0994	0.6630	0.066	1.0694	0.6637	0.0693	0.9519	0.040
A5	0.1275	0.0637	9.81	0.3	0.1044	0.1057	0.7044	0.073	1.0882	0.6909	0.0745	0.9795	0.041
A6	0.1485	0.0743	9.81	0.3	0.1144	0.1160	0.7736	0.079	1.1020	0.6808	0.0825	0.9572	0.044

Radius 0.150m (Present study) continued

V_1 (ms^{-2})	Fr_1	Y_2 (m)	Y_2/R	L_d (m)	L_j (m)	L_j/Y_2	E_0	E_1	$\Delta E\%$	ΔH	$\Delta H / H_w$	$\Delta H/d_{crest}$
0.7625	1.3828	0.099	0.660	0.160	0.690	6.970	0.3660	0.0606	31%	0.1423	0.3978	4.0651
1.1127	1.8881	0.113	0.753	0.210	0.740	6.549	0.3921	0.0985	29%	0.1253	0.3296	2.6662
1.3125	2.1611	0.125	0.833	0.225	0.900	7.200	0.4043	0.1254	28%	0.1168	0.3000	2.0135
1.4439	2.3167	0.144	0.960	0.230	0.720	5.000	0.4156	0.1459	27%	0.1123	0.2812	1.7020
1.5430	2.4241	0.155	1.033	0.243	0.820	5.290	0.4234	0.1626	26%	0.1086	0.2677	1.4874
1.6878	2.5690	0.170	1.133	0.250	0.790	4.647	0.4359	0.1892	25%	0.1036	0.2490	1.3114

Radius 0.125m(Present study)

Test	Q (m ³ /s)	q (m ² /s)	g (ms ⁻²)	ΔZ = D (m)	H (m)	H _w	H _w /R	d _{crest} (m)	C _d	d _{crest} / H _w	d _c	d _{crest} /d _c	Y ₁ (m)
B1	0.0412	0.0206	9.81	0.25	0.0500	0.0502	0.4019	0.037	1.0732	0.7365	0.0351	1.0539	0.025
B2	0.0741	0.0371	9.81	0.25	0.0710	0.0717	0.5734	0.054	1.1326	0.7534	0.0519	1.0400	0.041
B3	0.1006	0.0503	9.81	0.25	0.0890	0.0901	0.7210	0.067	1.0907	0.7434	0.0637	1.0524	0.056
B4	0.1220	0.0610	9.81	0.25	0.1030	0.1045	0.8362	0.075	1.0590	0.7175	0.0724	1.0360	0.065
B5	0.1354	0.0677	9.81	0.25	0.1140	0.1158	0.9261	0.081	1.0085	0.6997	0.0776	1.0437	0.072
B6	0.1581	0.0791	9.81	0.25	0.1260	0.1283	1.0260	0.088	1.0096	0.6861	0.0860	1.0227	0.079

Radius 0.125m(Present study) continued

V ₁ (ms ⁻²)	Fr ₁	Y ₂ (m)	Y ₂ /R	L _d (m)	L _j (m)	L _j /Y ₂	E ₀	E ₁	$\Delta E\%$	ΔH	$\Delta H / H_w$	$\Delta H / d_{crest}$
0.8242	1.6642	0.083	0.664	0.160	0.430	5.181	0.3087	0.0596	25%	0.1140	0.3796	3.0802
0.9038	1.4251	0.113	0.900	0.164	0.626	5.564	0.3349	0.0826	25%	0.0971	0.3017	1.7974
0.8984	1.2121	0.135	1.080	0.168	0.632	4.681	0.3553	0.0971	26%	0.0895	0.2631	1.3356
0.9386	1.1754	0.154	1.232	0.171	0.629	4.084	0.3709	0.1099	26%	0.0851	0.2399	1.1341
0.9406	1.1191	0.165	1.316	0.170	0.490	2.979	0.3820	0.1171	26%	0.0833	0.2279	1.0290
1.0008	1.1368	0.184	1.472	0.179	0.561	3.049	0.3961	0.1300	27%	0.0797	0.2107	0.9057

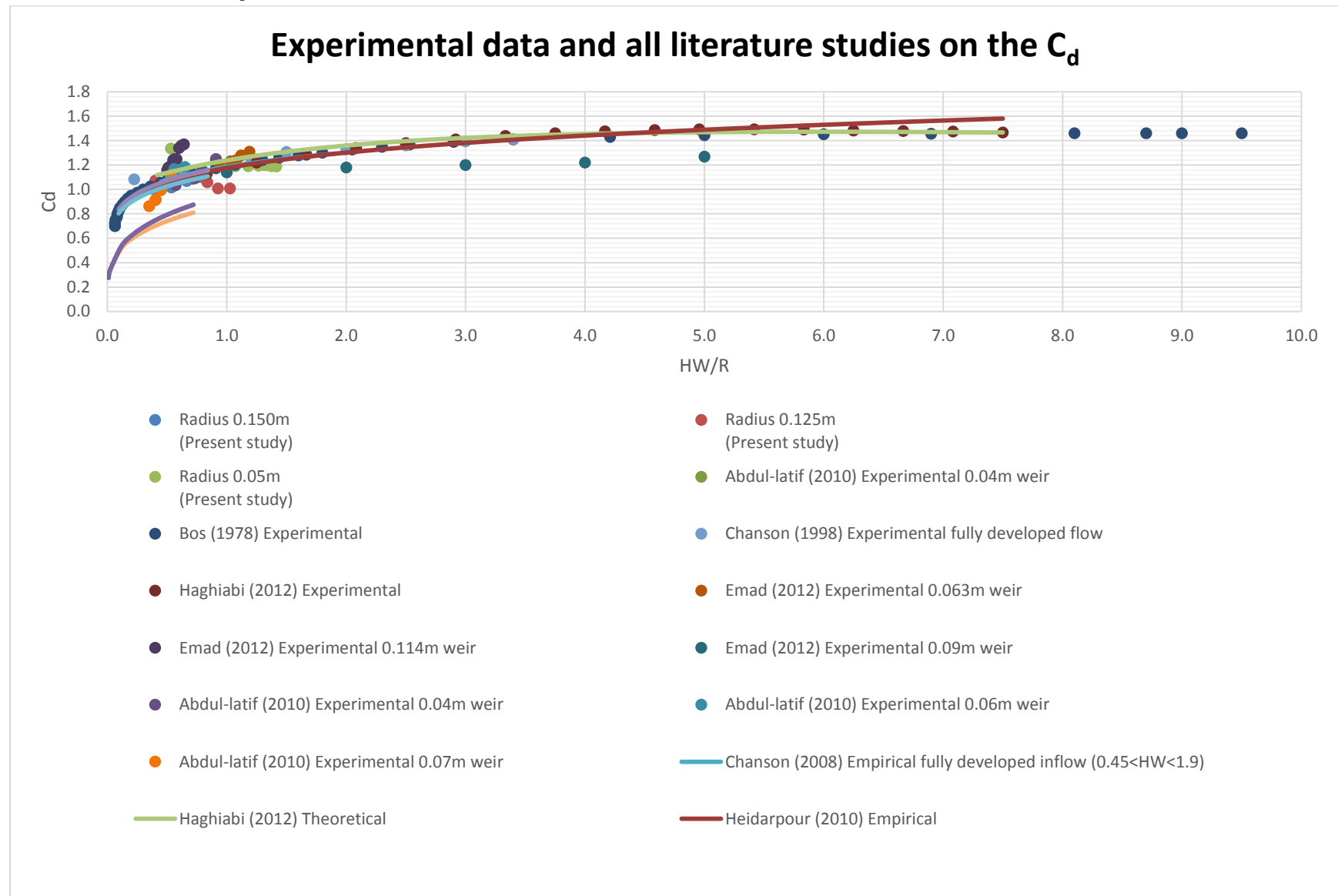
Radius 0.05m (Present study)

Test	Q (m ³ /s)	q (m ² /s)	g (ms ⁻²)	ΔZ = D (m)	H (m)	H _w	H _w /R	d _{crest} (m)	C _d	d _{crest} / H _w	d _c	d _{crest} /d _c	Y ₁ (m)
C1	0.0399	0.0200	9.81	0.16	0.0420	0.0425	0.5312	0.03	1.3367	0.7059	0.0344	0.8726	0.018
C2	0.0815	0.0407	9.81	0.16	0.0720	0.0736	0.9196	0.05	1.1972	0.6796	0.0553	0.9042	0.031
C3	0.1019	0.0510	9.81	0.16	0.0835	0.0857	1.0716	0.058	1.1905	0.6765	0.0642	0.9034	0.039
C4	0.1176	0.0588	9.81	0.16	0.0915	0.0943	1.1785	0.064	1.1908	0.6788	0.0706	0.9063	0.050
C5	0.1313	0.0656	9.81	0.16	0.0980	0.1013	1.2662	0.07	1.1942	0.6910	0.0760	0.9208	0.054
C6	0.1402	0.0701	9.81	0.16	0.1020	0.1057	1.3206	0.072	1.1976	0.6815	0.0794	0.9065	0.058
C7	0.1479	0.0740	9.81	0.16	0.1060	0.1099	1.3742	0.074	1.1899	0.6731	0.0823	0.8991	0.062
C8	0.1542	0.0771	9.81	0.16	0.1090	0.1132	1.4148	0.079	1.1875	0.6980	0.0846	0.9336	0.065

Radius 0.05m (Present study) continued

V ₁ (ms ⁻²)	Fr ₁	Y ₂ (m)	Y ₂ /R	L _d (m)	L _j (m)	L _j /Y ₂	E ₀	E ₁	$\Delta E\%$	ΔH	$\Delta H / H_w$	$\Delta H / d_{crest}$
1.1092	2.6395	0.090	1.125	0.150	0.420	4.667	0.2135	0.0807	13%	0.0598	0.2952	1.9923
1.3354	2.4413	0.124	1.550	0.152	0.548	4.419	0.2483	0.1214	13%	0.0491	0.2100	0.9812
1.3064	2.1121	0.138	1.725	0.154	0.566	4.101	0.2625	0.1260	14%	0.0459	0.1870	0.7922
1.1755	1.6784	0.146	1.825	0.156	0.524	3.589	0.2725	0.1204	15%	0.0441	0.1734	0.6891
1.2156	1.6702	0.153	1.913	0.158	0.543	3.546	0.2809	0.1293	15%	0.0428	0.1636	0.6108
1.2089	1.6026	0.158	1.975	0.159	0.441	2.794	0.2861	0.1325	15%	0.0420	0.1581	0.5832
1.1927	1.5294	0.162	2.025	0.160	0.396	2.441	0.2908	0.1345	16%	0.0415	0.1537	0.2699
1.1861	1.4854	0.167	2.088	0.160	0.440	2.635	0.2945	0.1367	16%	0.0411	0.1504	0.2732

APPENDIX C: Experimental data and literature studies on C_d



APPENDIX D: Experimental data on pressures in meters

Pressure results [colour shaded from lower (green) to higher (red) negative pressures]

Test	q (m ²)	P _{average} at 0°	P _{95%} at 0°	P _{average} at 11.25°	P _{95%} at 11.25°	P _{average} at 22.5°	P _{95%} at 22.5°	P _{average} at 67.5°	P _{average} at 78.75°	P _{average} at 90°	P _{95%} at 67.5°	P _{95%} at 78.75°	P _{95%} at 90°	d _{crest} (m)	F _r	R
0.15m weir @ = 0.0236 m ³ /s	0.0236	0.026	0.021	0.017	0.013	-0.001	-0.007	-0.014	-0.035	-0.060	-0.019	-0.045	-0.083	0.035	1.383	0.150
0.15m weir @ = 0.0394 m ³ /s	0.0394	0.035	0.021	0.016	0.003	-0.014	-0.026	-0.011	-0.044	-0.086	-0.014	-0.055	-0.093	0.047	1.888	0.150
0.15m weir @ = 0.0494 m ³ /s	0.0494	0.036	0.022	0.016	0.003	-0.019	-0.031	-0.019	-0.053	-0.092	-0.023	-0.064	-0.103	0.058	2.161	0.150
0.15m weir @ = 0.0572 m ³ /s	0.0572	0.038	0.022	0.013	0.000	-0.027	-0.038	-0.026	-0.062	-0.098	-1.444	-1.452	-1.460	0.066	2.317	0.150
0.15m weir @ = 0.0637 m ³ /s	0.0637	0.038	0.019	0.010	-0.002	-0.031	-0.044	-0.037	-0.074	-0.100	-1.444	-1.452	-1.459	0.073	2.424	0.150
0.15m weir @ = 0.0743 m ³ /s	0.0743	0.039	0.017	0.002	-0.011	-0.045	-0.059	-	-	-	-	-	-	0.079	2.569	0.150
0.125m weir @ = 0.0206 m ³ /s	0.0206	0.020	0.008	0.003	-0.007	-0.010	-0.022	-	-	-	-	-	-	0.037	1.664	0.125
0.125m weir @ = 0.0371 m ³ /s	0.0371	0.021	0.006	-0.007	-0.019	-0.026	-0.036	-	-	-	-	-	-	0.054	1.425	0.125
0.125m weir @ = 0.0503 m ³ /s	0.0503	0.018	0.001	-0.015	-0.028	-0.039	-0.051	-	-	-	-	-	-	0.067	1.212	0.125
0.125m weir @ = 0.0610 m ³ /s	0.0610	0.015	0.000	-0.022	-0.035	-0.050	-0.063	-	-	-	-	-	-	0.075	1.175	0.125
0.125m weir @ = 0.0677 m ³ /s	0.0677	0.012	-0.001	-0.028	-0.041	-0.058	-0.072	-	-	-	-	-	-	0.081	1.119	0.125
0.125m weir @ = 0.0791 m ³ /s	0.0791	0.007	-0.005	-0.037	-0.051	-0.073	-0.086	-	-	-	-	-	-	0.088	1.137	0.125
0.05m weir @ = 0.0200 m ³ /s	0.0200	-0.075	-0.083	-0.103	-0.108	-0.095	-0.102	-	-	-	-	-	-	0.030	2.640	0.050
0.05m weir @ = 0.0407 m ³ /s	0.0407	-0.085	-0.096	-0.122	-0.127	-0.117	-0.131	-	-	-	-	-	-	0.050	2.441	0.050
0.05m weir @ = 0.0510 m ³ /s	0.0510	-0.092	-0.101	-0.134	-0.142	-0.126	-0.135	-	-	-	-	-	-	0.058	2.112	0.050
0.05m weir @ = 0.0588 m ³ /s	0.0588	-0.100	-0.115	-0.146	-0.152	-0.134	-0.145	-	-	-	-	-	-	0.064	1.678	0.050
0.05m weir @ = 0.0656 m ³ /s	0.0656	-0.107	-0.122	-0.154	-0.167	-0.141	-0.152	-	-	-	-	-	-	0.070	1.670	0.050
0.05m weir @ = 0.0701 m ³ /s	0.0701	-0.113	-0.126	-0.161	-0.173	-0.146	-0.164	-	-	-	-	-	-	0.072	1.603	0.050
0.05m weir @ = 0.0740 m ³ /s	0.0740	-0.121	-0.137	-0.170	-0.183	-0.153	-0.167	-	-	-	-	-	-	0.074	1.529	0.050

Test	Chanson (1997)						$p/(\rho_w g)_{Average}$ vs θ					
	0	11.25	22.5	67.5	78.75	90	0	11.25	22.5	67.5	78.75	90
0.15m weir @ = 0.0236 m ³ /s	-0.062	-0.257	-0.550	-0.334	-0.577	-0.439	0.026	0.017	-0.001	-0.014	-0.036	-0.061
0.15m weir @ = 0.0394 m ³ /s	-0.229	-0.500	-0.908	-0.608	-0.946	-0.754	0.035	0.017	-0.014	-0.011	-0.045	-0.088
0.15m weir @ = 0.0494 m ³ /s	-0.374	-0.719	-1.239	-0.856	-1.287	-1.042	0.037	0.016	-0.019	-0.020	-0.054	-0.094
0.15m weir @ = 0.0572 m ³ /s	-0.483	-0.884	-1.488	-1.043	-1.544	-1.260	0.039	0.013	-0.027	-0.027	-0.063	-0.100
0.15m weir @ = 0.0637 m ³ /s	-0.575	-1.027	-1.708	-1.206	-1.772	-1.451	0.039	0.010	-0.032	-0.038	-0.076	-0.102
0.15m weir @ = 0.0743 m ³ /s	-0.688	-1.186	-1.934	-	-	-	0.039	0.002	-0.046	-	-	-
0.125m weir @ = 0.0206 m ³ /s	-0.153	-0.407	-0.789	-	-	-	0.021	0.003	-0.010	-	-	-
0.125m weir @ = 0.0371 m ³ /s	-0.090	-0.483	-1.074	-	-	-	0.021	-0.007	-0.026	-	-	-
0.125m weir @ = 0.0503 m ³ /s	0.030	-0.479	-1.243	-	-	-	0.018	-0.015	-0.040	-	-	-
0.125m weir @ = 0.0610 m ³ /s	0.075	-0.509	-1.386	-	-	-	0.015	-0.023	-0.051	-	-	-
0.125m weir @ = 0.0677 m ³ /s	0.133	-0.509	-1.474	-	-	-	0.012	-0.029	-0.059	-	-	-
0.125m weir @ = 0.0791 m ³ /s	0.152	-0.561	-1.632	-	-	-	0.007	-0.038	-0.074	-	-	-
0.05m weir @ = 0.0200 m ³ /s	-0.804	-1.387	-2.265	-	-	-	-0.076	-0.105	-0.096	-	-	-
0.05m weir @ = 0.0407 m ³ /s	-0.941	-2.064	-3.751	-	-	-	-0.086	-0.124	-0.119	-	-	-
0.05m weir @ = 0.0510 m ³ /s	-0.617	-1.989	-4.051	-	-	-	-0.094	-0.137	-0.129	-	-	-
0.05m weir @ = 0.0588 m ³ /s	-0.049	-1.620	-3.982	-	-	-	-0.102	-0.148	-0.136	-	-	-
0.05m weir @ = 0.0656 m ³ /s	0.042	-1.739	-4.417	-	-	-	-0.110	-0.157	-0.144	-	-	-
0.05m weir @ = 0.0701 m ³ /s	0.169	-1.684	-4.471	-	-	-	-0.115	-0.164	-0.149	-	-	-
0.05m weir @ = 0.0740 m ³ /s	0.312	-1.615	-4.512	-	-	-	-0.123	-0.173	-0.156	-	-	-

APPENDIX D: Real life inflatable weir



<http://www.huachenrubber.com/en/products.asp?id=65>